# CHAOS CONTROL OF AN OPEN SHEAR FLOW: A NOVEL CONTROL STRATEGY AND ITS EXPERIMENTAL DEMONSTRATION IN AN AXISYMMETRIC JET

A Dissertation

Presented to

the Faculty of the Department of Mechanical Engineering

Cullen College of Engineering

University of Houston

In Partial Fulfillment

of the Requirements for the Degree

Doctor of Philosophy

by

Satish Narayanan

May 2013

# CHAOS CONTROL OF AN OPEN SHEAR FLOW: A NOVEL CONTROL STRATEGY AND ITS EXPERIMENTAL DEMONSTRATION IN AN AXISYMMETRIC JET

---

Satish Narayanan

Approved:

Chairman of the Committee
Stanley J. Kleis, Associate Professor
Mechanical Engineering

Committee Members:

Ralph Metcalfe, Professor
Mechanical Engineering

Pradeep Sharma, Professor
Mechanical Engineering

Gemunu Gunaratne, Professor
Physics

Dong Liu, Assistant Professor
Mechanical Engineering

Suresh K. Khator, Associate Dean
Cullen College of Engineering

Pradeep Sharma, Chairman
Mechanical Engineering

# ACKNOWLEDGEMENTS

I am very thankful to many for their support, guidance and interactions over these years of my degree pursuit. I am most thankful to Dr. George Broze for mentoring and help which were instrumental to my development and research. I want to thank Prof. Gemunu Gunaratne for his active interest and frequent informal interactions at a very technical level, helping me frame and formulate much of what went into my research. I will always be grateful for the extra efforts of Professors Pradeep Sharma, Ken White and Stan Kleis to help bring closure to my dissertation work. Prof. Fazle Hussain, who served as an advisor for much of my research and offered me the opportunity to conduct interesting research among an admirable group of colleagues.

My colleagues Hyder Husain, Davinder Virk, Shashi Menon, and Nick Albanis made my working environment enjoyable and I learnt much from them. A special thanks to Sukesh Roy and Dhoorjaty Pradeep, who I was acquainted with much later but who were of tremendous help as I worked to complete my degree. I am also thankful to Frank and Jim at the machine shop for their patient and cheerful efforts at machining various sections of my experimental facilities.

Finally, few words could not summarize my gratitude to members of my family. My mother has been a sustained source of inspiration. My wife Saras has been an unfaltering source of support and encouragement as I worked to complete my degree well after departure from University of Houston. Last but not certainly the least, I dedicate this body of work to my late and dear brother Prakash Narayanan whose own academic aspirations were unexpectedly cut short.

# CHAOS CONTROL OF AN OPEN SHEAR FLOW: A NOVEL CONTROL STRATEGY AND ITS EXPERIMENTAL DEMONSTRATION IN AN AXISYMMETRIC JET

An Abstract

of a

Dissertation

Presented to

the Faculty of the Department of Mechanical Engineering

Cullen College of Engineering

University of Houston

In Partial Fulfillment

of the Requirements for the Degree

Doctor of Philosophy

by

Satish Narayanan

May 2013

# Abstract

A nonlinear dynamical systems approach to control the coherent structure dynamics and turbulence in the near field of an axisymmetric jet is presented. Experiments were performed in an initially laminar, top-hat profile, circular jet at a Reynolds number of 2.5 x $10^4$, housed in a low-noise anechoic chamber. Acoustic excitation was used to inject axisymmetric velocity perturbations into the jet shear layer at the nozzle exit plane for control. Periodic flow states involving various sequences of vortex ring formation and their pairings were achieved using open-loop (requiring no feedback) and closed-loop control methods. In contrast to conventional, linear, control approaches that use brute-force high-amplitude excitation, a systematic nonlinear control method is presented. Furthermore, flow states, which are inaccessible using prior control methods, are achieved with small changes to control parameters. Measurements of velocity traces at several locations show the ability to achieve effective control of periodic states over a region extending beyond the end of the jet potential core and transitional region. Control is also demonstrated using flow visualization and measurements of the mean flow and turbulence intensity, and of the two-point spatial correlation. Measurements reveal effective amplification and suppression of nonlinear instabilities associated with the controlled vortex dynamics.

Single- and two-point velocity measurements were used to describe the low dimensional (chaotic) jet flow dynamics, which have inherently periodic (but unstable) flow states, and to determine the control perturbations. Due to its susceptibility to external disturbances and modeling errors, the open-loop method did not achieve control of some

periodic states. A closed-loop method using feedback from a downstream sensor was used to control the flow for cases when the open-loop method failed, showing potential for "robust" control. Furthermore, potential benefits from the jet control were assessed revealing turbulence enhancement (having nearly 20% jet spread increase) and turbulence suppression (having up to 70% turbulence intensity decrease). Finally, in an attempt to address the applicability and extension of the control approach to other open shear flows, the control method presented here was also demonstrated in a plane mixing layer, suggesting potential extension to other open shear flows.

# TABLE OF CONTENTS

# LIST OF FIGURES

# LIST OF TABLES

# NOMENCLATURE

**English Symbols**

$a_f$ non-dimensional forcing amplitude; $\equiv u'_f/U_e$

C(r) Grassberger-Procaccia correlation integral

d dimension of a geometric object

D jet diameter (m)

f fundamental frequency (Hz)

$f_{ex}$ excitation frequency (Hz)

$f_{unf}$ peak of the broadband in the unforced flow (Hz)

h time between recording successive samples

I mutual information

L linear transfer function

m embedding dimension

$p_i$ probability in the ith bin of a discrete probability density function

q quarter harmonic component (f/4) (Hz)

Q quadratic transfer function

r separation in phase-space

$R_{xy}$ cross-correlation

Re Reynolds number

s subharmonic component (f/2) (Hz)

$St_D$ Strouhal number based on jet diameter; $\equiv f_{ex}\, D/U_e$

$St_{\theta e}$ Strouhal number based on mixing layer exit momentum thickness; $\equiv f_{ex}\, \theta_e/U_e$

t time (sec)

u streamwise velocity component (m/s)

u' root-mean-square value of u (m/s)

$U_c$ centerline velocity (m/s)

$U_e$ mixing layer exit velocity (m/s)

w exit slit width (m)

x streamwise coordinate (m)

X fourier transform of variable x

y transverse corrdinate (m)

z spanwise coordinate (m)

**Greek Symbols**

$\beta$ cross-bicoherence

$\delta^*$ displacement thickness (m)

$\varepsilon$ rms-integrated amplitude; contribution from higher order terms

$\gamma$ coherence

$\theta_e$ exit momentum thickness (m)

$\tau$ time delay for attractor reconstruction

$\lambda_f$ fundamental instability wavelength

$\lambda$ largest Lyapunov exponent (bits/sec)

$\nu$ correlation dimension

$\phi$ relative phase angle

$\rho$ cross-correlation coefficient

$\xi$ correlation length

# CHAPTER 1

# INTRODUCTION

The dynamically significant role of large-scale vortical structures – *coherent structures* (CS) – in transitional and turbulent shear flows (Brown & Roshko 1974, Hussain 1983) is well known, as is their role in turbulence phenomena such as mixing, aerodynamic noise and drag. It is now generally agreed upon that flow control is not meaningful, perhaps unachievable, in the absence of deterministic features such as CS, i.e., *no CS no control*. However, no systematic approach to the control of these large-scale structures exists and most flow control methods rely on passive approaches or active but "brute force" open-loop forcing methods (such as steady and unsteady blowing/suction). On the other hand, the dominant role of spatiotemporally organized CS in shear flows suggests that the dynamics of several technologically relevant flows, such as mixing layers, wakes, boundary layers and jets, may be low dimensional. This implies that reduced-order flow models capturing the essential and controllable large-scale structure dynamics can be developed, thereby avoiding computationally expensive and high-dimensional simulations for evaluating flow control strategies. Using such models intelligent and feasible strategies for active flow control (e.g., closed-loop control) can be proposed (e.g., see suggested application to a jet by Corke et al. 1994), which do not require (impractical) full flow field information and large control energy input.

It is the goal of this dissertation to demonstrate a novel approach to the control of the near field of a circular jet utilizing the inherent low-dimensional dynamics of the (orga-

nized) large-scale CS. Circular jets themselves have been a focus of significant research in the past three decades, beginning with the studies of (organized) coherent structures, their evolution and interactions (see early works such as Brown & Roshko 1974, and detailed review in Hussain 1986). More recent studies have focused on methods to identify controllable dynamics of these open shear flows.

In the following section, a detailed review of prior research aimed at understanding the physics and dynamics of jet flows, particularly their coherent structure dynamics, is provided. As referred to earlier, a coherent structure-based approach should form the foundation of any rational framework for modeling and control of these flows. This is followed, in the next section, by a discussion of several known approaches to the control of shear flows, particularly of jet control methods, followed by a discussion of the recent advances in nonlinear control and dynamical systems theory and their implications for jet control.

### 1.1 Dynamics, Modeling and Control of Jets

Coherent structures have been the focus of numerous investigations in transitional and turbulent shear flows. This has provided a structural and dynamical framework for describing the transport of heat, mass and momentum in several turbulent shear flows of technological relevance (Hussain 1986, Adrian & Moin 1988, Aubry et al. 1988). A coherent structure has been defined as "a connected turbulent fluid mass with instantaneously phase-correlated vorticity over its spatial extent" (Hussain 1986). Early studies focused on qualitative identification of such organized motion (e.g., flow visualizations of a turbulent mixing layer reported in Brown & Roshko 1974). This was followed by more

quantitative (but often times subjective) coherent structure eduction, used to identify, describe and understand the dynamical significance of coherent structures in turbulent mixing layers, jets and boundary layers (see review in Hussain 1986). More recently, objective (but semi-empirical) methods for identifying and describing coherent structures and their dynamics in fully turbulent flows have become possible (Aubry et al. 1988 in boundary layers, Broze & Hussain (1994, 1996) and Ukeiley et al. 2001 in jets, and Narayanan & Hussain 1996 in a mixing layer). The use of proper orthogonal decomposition (POD) and the nonlinear dynamical systems theory are examples of approaches that have enabled such descriptions. While the large-scale (coherent) structures in the fully developed turbulent regions of shear flows remain buried (hence often masked) inside large-amplitude, random fluctuations, such organized motion is more evident in transitional flows, such as in the near fields of jets and mixing layers (Zaman & Hussain 1980) and in transitional boundary layers. Thus, a significant amount of attention has been focused on the near fields of flows such as mixing layers and jets. In the following, a review of the studies of coherent structure dynamics, approaches for their modeling and control in the context of jet flows is presented.

*Coherent structure dynamics in excited jets*. The earliest studies of coherent structures and their dynamics have been in excited flows, particularly in circular jets forced at a single frequency, where a periodic and organized flow behavior can be induced and studied in detail. Notable are the studies by Crow & Champagne (1971), Petersen et al. (1971), Browand & Laufer (1975), Moore (1977), Zaman & Hussain (1980), and Hussain & Zaman (1981), which studied the nature of coherent structures as well as implications of

controlling them on practically relevant phenomena such as mixing and aerodynamic sound generation.

The relevance of coherent structures in an excited jet to those in a naturally evolving jet is often contended. However, since all naturally evolving jets are in fact forced by external disturbances (albeit with a broadband spectrum), the issue becomes that of similarity of coherent structures in a flow with controlled and uncontrolled excitation. For cases with low levels of excitation employed, it is believed that only the most unstable (or naturally preferred) structures would be formed; the similarity of (educed) coherent structures in low-level excited jets and uncontrolled jets has been addressed in Hussain (1986). The earliest observations of orderly "vortical puffs" by Crow & Champagne (1971) in excited axisymmetric jets were associated with a "preferred mode" corresponding to a non-dimensional frequency ($St_D \sim 0.3$) having maximally amplified centerline fluctuation intensity. Zaman & Hussain (1980) found that the centerline turbulence intensity achieved was even higher for a jet excited at a non-dimensional frequency of $St_D \sim 0.85$, attributing the intense turbulence intensity levels to vortex pairings. Thus, the "preferred mode" was re-defined to be the frequency at which the fundamental (forcing frequency) amplitude attains the maximum amplification.

Petersen et al.'s (1977) study focused on turbulence intensity suppression as a result of jet excitation, while suggesting that jet noise was caused by vortex pairing. Moore (1977) studied the amplification of broadband jet noise by excitation of jets. Husain & Zaman (1981) showed that the non-dimensional frequency scaling of the "preferred mode" was independent of whether the jet exit conditions were laminar or turbulent,

mentioning that the gradual independence from initial conditions is achieved via successive restructuring of the shear layer, evolving into a "terminal structure" at the end of the jet potential core (discussed below). Vortex pairings, namely interactions between rolled up vortex rings in the transitional region of a jet, were also the subject of several investigations (e.g., Browand & Weidman 1976, Zaman & Hussain 1980) and are described later.

The formation of transitional coherent structures is believed to be the result of jet instabilities, particularly of initially laminar jet shear layers. The transitional jet region extends from the jet nozzle exit plane, where the nozzle boundary layer separates into a still ambient, and terminates where the unsteady, spatially growing jet shear layers collapse. A conical region is circumferentially encompassed by the spatially evolving shear layers and is typically referred to as the potential core of the jet. Linear instabilities of the jet shear layer (i.e., the Kelvin Helmholtz instability of a cylindrical vortex sheet) are responsible for the roll up and formation of the nominally axisymmetric vortex rings, which are typically followed by interactions of the vortex rings that result in mergers (also termed pairings) and tearing of structures. The role of three-dimensional vortex dynamics in the transitional jet region has not received much attention until recently (Corke & Kusek 1993, Broze & Hussain 1996). Tilted vortex rings and their partial pairings can also be found in jets where the levels of excitation are very low (almost an order of magnitude lower than for excited jets displaying axisymmetric vortex dynamics). The above-mentioned vortex dynamics are found to be prevalent in the near field of jets with initially turbulent shear layers as well, although the structures are less evident in instantaneous

and phased-averaged images (e.g., see studies of Hussain & Zaman 1985 in a turbulent mixing layer). For instance, pairing-like motions, not resulting in actual merger of vortices, are possible in fully turbulent flows with acceleration of vorticity-bearing fluid elements. Such dynamics are believed to play key roles in phenomena such as entrainment (precursor to mixing) and noise generation.

The circular jet, typically exiting from a contraction nozzle, has two distinct length scales, namely the exit boundary layer thickness and the jet diameter. There are two distinct modes of linear and nonlinear instability associated with these length scales, termed shear layer mode and jet column mode. The shear layer mode is seen to dominate the near-nozzle region of the jet flow, behaving similar to a plane mixing layer, with vortex roll up and pairings. Farther downstream in the jet, where the spatially evolving mixing layer thickness becomes comparable to the jet diameter, azimuthal curvature can no longer be ignored and the jet evolution is governed by a new length scale. New instabilities and vortex dynamics (namely, vortex ring formation and their interactions) result and are discussed later. Linear stability analysis of axisymmetric jets with thin initial shear layers (i.e., boundary layer much smaller than jet diameter), such as by Michalke (1971), Mattingly & Chang (1974) and Plaschko (1979), has predicted that the initial region of the jet is equally unstable to both axisymmetric and first helical modes. This has been confirmed in experiments of Strange & Crighton (1981) and Cohen & Wygnanski (1987a,b), among others. While the linear characteristics of the axisymmetric and helical modes are similar, their nonlinear evolutions are known to be different. Vortical interactions resulting in larger scale structures are more common in axisymmetric jets, while more effective trans-

fer to fine-scale turbulence is found for jets with helical modes (e.g., see Strange 1981, Corke & Kusek 1993).

A knowledge base exists for understanding, modeling and exciting axisymmetric jet dynamics of vortex ring roll up and their interactions. As noted previously, large augmentation of velocity fluctuations has been shown to be associated with axisymmetric vortex pairings in the jet (Zaman & Hussain 1980). Similarly suppression of turbulence intensity was also found for excitation at higher frequencies, although this result has been fraught with controversy and the phenomenon needs further investigation (Husain 1986). The spectral evolution of velocity fluctuations during vortex pairing, the conditions most favorable for vortex pairing, measurements of the Reynolds stress distributions, and the details of the coherent structure dynamics (substantiated by detailed phase-locked measurements) have been documented in Zaman & Hussain (1980). The occurrence of two successive stages of vortex ring pairing was also documented in Bridges (1990) and Broze & Hussain (1994), termed "stable double pairing" (see also Fig. 1.1). Measured velocity spectra in all studies show that the jet flows are periodic (or nearly periodic) at a frequency one-half or one-fourth of the forcing frequency, when excited at a single forcing frequency corresponding to the fundamental or primary instability frequency.

*Nonlinear instabilities in jets*. The saturation of the fundamental instabilities, corresponding to vortex ring formation, is followed by nonlinear instabilities involving interaction of the primary instabilities in the transitional jet. These are typically instabilities of the subharmonic and are of two kinds, namely "pairing" and "tearing" or "shredding."

Pairing is the interaction of two vortex rings, when their cores revolve around one

another, typically merging (through the action of viscosity) into a single core. Tearing or shredding occurs as a result of a relatively weak vortex trapped between the opposing induced-velocity fields of two stronger vortices, which shear the weaker vortex and merge with portions of the shredded vortex. Since these interactions result in coherent structures with half the frequency of the original flow (e.g., for a stationary probe sampling the vortex passage frequency), these are termed subharmonic instabilities.

Kelly (1967) had studied the nonlinear instability of a spatially periodic two-dimensional base flow (namely, a temporal mixing layer), showing that nonlinear resonance with the highest growth rate occurs between the fundamental wave number and a wave with half its wave number, while also noting that a threshold amplitude of the fundamental is required for the resonance. Monkewtiz (1988) studied this nonlinear subharmonic resonance in the context of a spatially evolving mixing layer (although only weakly inhomogenous in the streamwise direction) even further and found additional criteria requiring equal phase speeds for and precise phase differences between the fundamental and subharmonic waves.

Experiments in an axisymmetric mixing layer by Husain & Hussain (1995) confirmed most of the theoretical findings regarding subharmonic resonance and vortex pairing using two-frequency excitation. Detailed measurements of the mixing layer flow field were conducted, including flow visualizations, to explain the physics of subharmonic resonance and describe the corresponding vortex pairing and tearing dynamics. Similar analysis of the interactions between the fundamental and subharmonic waves for circular jets was performed by Mankbadi (1985) using energy methods, reaching similar conclu-

sions regarding sensitive dependence of nonlinear resonant growth rate on phase difference. Figure 1.1 schematically displays snapshots of a section of a transitional jet undergoing axisymmetric vortex ring formation (with no vortex pairings) and another having vortex pairings of rolled up vortex rings, prior to the turbulent breakdown of the jet potential core. The relative phase difference between the fundamental and subharmonic waves/frequencies is the controlling dynamical variable. Furthermore, near field flow events such as vortex formation and vortex pairings have also been shown, via simulations and experiments, to be responsible for feedback of perturbations to the upstream point of receptivity (Dimotakis & Brown 1976, Grinstein et al. 1991). The significance of such dynamical closure will be evident in the forthcoming discussions and will be quantified and utilized for modeling the dynamic system behavior and for control in later chapters of this dissertation.

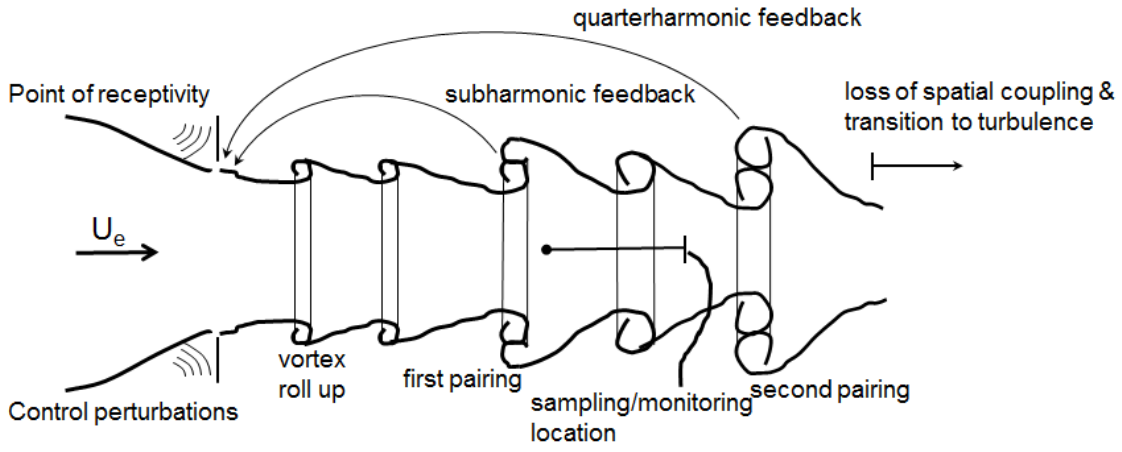


Figure 1.1 Schematic displaying the dynamics of a transitional axisymmetric jet, with vortex ring formation and their multiple pairings. Typically periodic excitation is used at the jet nozzle exit to control these types of vortex dynamics.

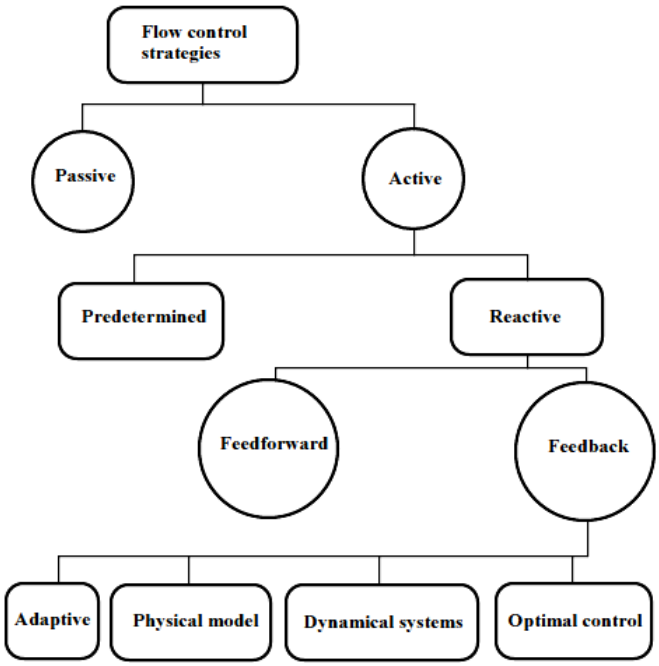


Figure 1.2 Classification of flow control techniques (from Gad-el-Hak 1996) displaying prior approaches (such as passive and predetermined active control) as well as recent and promising future approaches such as those based on the dynamical systems approach and optimal control (discussed in the next section).

*Dynamical approach to coherent structure dynamics in jets*. The theoretical and experimental evidence of subharmonic resonance and hydrodynamic feedback led Broze (1992) to hypothesize a conceptual dynamical system of transitional jets. From initial perturbations, the fundamental and the subharmonics grow independently in accordance with the linear theory at exponential rates determined by their frequencies (e.g., see Michalke 1965). The fundamental saturation (manifested as a vortex ring formation) is followed by a resonance involving the modification of the subharmonic growth rate, which if favorable results in the pairing of vortex rings and if unfavorable inhibits further vortex ring interactions. At some point, when the subharmonic amplitude reaches a threshold level, a second resonance is initiated with a quarterharmonic, which in turn triggers the second

vortex pairing of once-paired vortices. The vortex pairings in turn trigger a pressure perturbation that is fed back (almost instantaneously in an incompressible jet) to the nozzle exit plane, the only point of receptivity in the flow, thereby triggering future subharmonic and quarterharmonic perturbations, hence subsequent vortex pairings.

The nature of the vortex pairing dynamics, namely periodic or disordered (chaotic) was found to be dependant on the relative phase difference between the fundamental and subharmonic frequencies, also a crucial dynamical variable in subharmonic resonance. Thus, a self-sustained temporal dynamical system was proposed for the transitional jet, which was claimed to be capable of exhibiting low-dimensional global dynamics, thought to be unattainable for physically open flows such as jets (e.g., see Huerre & Monkewitz 1990). Thus, elements of linear stability, subharmonic resonance and feedback were combined to explain how global modes could occur in a locally convectively unstable jet flow. Excitation of the fundamental frequency was needed in these studies to control the primary instability, thereby limiting the degrees of freedom of the flow.

Temporal velocity measurements in the transitional jet region were used to describe the jet as a low-dimensional dynamical system with periodic and chaotic dynamics in a parameter space of the non-dimensional forcing frequency and amplitude (Broze & Hussain 1994, 1996). These dynamics were shown to be associated with nominally axisymmetric vortex dynamics of vortex formation and vortex pairings, prior to the jet breakdown to turbulence. Similar conclusions were reached for a plane mixing layer as well (Narayanan & Hussain 1996). These results are discussed further in later chapters as

well as in the Appendices. In summary, the near-field shear layer and far-field jet column mode dynamics of the jet may be thought to constitute a dynamical system whose coherent structure dynamics are low dimensional and deterministic, consistent with prior coherent structure eduction-based approach findings.

Reisenthel (1988) performed experiments in the near field of an axisymmetric jet to study the enhancement of organized coherent motion via a feedback loop of controllable strength. Similar to the above-mentioned studies, Reisenthel also attempted to study the transitional jet dynamics as a result of a global instability triggered by enhanced feedback, provided via electronic feedback of downstream velocity measurements in the shear layer to acoustic speakers at the jet exit plane. Model phenomenological equations utilizing linear stability theory were used to describe the dynamics of feedback and some of its nonlinear consequences. The externally induced feedback was used to better understand the self-excited nature of mixing layers and jets, whose natural pairing-driven feedback was speculated previously. A dual empirical and analytical approach, motivated by observations from the self-excited flow field was used to explain the origin of frequency selectivity (hence receptivity) and the existence of a critical Reynolds number in feedback systems. This study was also one of the first to attempt (linear) feedback-based control of free shear flows.

While such new approaches to describing the coherent structure dynamics in transitional jets has emerged, no systematic procedure for their control has emerged. Jet control techniques continue to rely on brute-force excitation of chosen linear instabilities in the near field (described in further detail in the following section). High-fidelity simulations

of the Navier Stokes equations (even of relatively low Reynolds number jets) is a daunting task and an expensive proposition. One of the reasons for the lack of systematic control strategies or algorithms is the lack of low order models to describe the coherent structure dynamics. Research over the past decade has focused on this subject and produced several promising results, described in the following.

*Low order modeling of jet dynamics*. The need for understanding the dynamics of large-scale flow organization and their role in ultimately controlling turbulent jet flows led to the creation of relatively simple dynamical models, comprised of a small system of coupled nonlinear ordinary differential equations, for an axisymmetric turbulent mixing layer typical of the very near field of a circular jet (e.g., see Rajaee et al. 1994, Delville et al. 1999, Ukeiley et al. 2001). A low order dynamical systems model was developed for the axisymmetric jet, albeit simpler and conceptual, by Glauser et al. (1989), utilizing eigenfunctions obtained from two-point velocity measurements in the near-field mixing layer of the jet. POD (introduced to turbulence research by Lumley 1967) provides an optimal basis set in terms of kinetic energy representation, providing eigenfunctions on to which the Navier Stokes equations with appropriate boundary conditions can be projected. The Galerkin projection provides a low-dimensional system with a relatively small number of equations for the leading order modes or eigenfunctions, depending on the level of truncation of the basis set. Recently, good comparisons between the experimentally acquired velocity spectra data and those predicted from a truncated POD-based model were demonstrated by Ukeiley et al. (2001). Such models have only recently been fine-tuned (using various closure schemes) to represent the essential physics correctly, and therefore

are providing promising avenues for developing control strategies. However, there is no guarantee that the POD modes are relevant for a forced, excited or controlled jet. New measurements or simulations would be needed to test the validity of the originally chosen basis set. The potential requirement of obtaining new eigenfunctions (POD modes) for a controlled jet flow field remains a concern and produces a significant hurdle in obtaining control-worthy models using such procedures.

### 1.2 Prior Flow Control Approaches

The use of free/wall-bounded shear flow control can produce significant energy savings through performance enhancement of several industrial devices involving turbulent flows, e.g., enhanced efficiency and decreased pollutant and acoustic emission for combustion in gas turbines and jet engines, enhanced commercial/military aircraft performance through skin-friction drag reduction, improved gas turbine efficiency through heat transfer enhancement (e.g., via blade cooling), improved aircraft maneuverability using separation control. The developments in flow control in the context of a wide variety of free and wall-bounded shear flows have been the subject of several review articles (e.g., Gad-el-Hak & Bushnell 1991, Moin & Bewley 1994, Gad-el-Hak 1996). A useful classification of flow control approaches used over several decades is illustrated in Fig. 1.2.

Passive flow control involving geometric modifications has been used extensively in the past in various practical settings. For instance, turbulence enhancement, for improved mass entrainment and mixing in mixing layer and jet flows can be achieved by generating energetic, organized three-dimensional large-scale structures (e.g., elliptic jets studied by Husain & Hussain 1983, lobed mixer studies by Lasheras & Choi 1988, and tab jets stud-

ied by Zaman 1996). The use of vortex generators for flow separation control and the use of riblets for skin friction drag reduction are other examples of successful passive flow control. These solutions can, however, be limiting in their applicability, e.g., not effective over a wide range of operating conditions, and can incur performance penalties (such as parasitic drag) during sustained deployment.

Active flow control has therefore become appealing and received much attention. Such control can be "predetermined" or "reactive". The former has been the most prevalent form of active control in the context of jet flows. Predetermined oscillatory forcing was used in jets and mixing layers, for enhancing mass entrainment and mixing (Zaman & Hussain 1980, Ho & Huang 1982, Ho & Huerre 1984, Freund & Moin 2000), for turbulence suppression (Zaman & Hussain 1981), and for broadband jet noise reduction (Bechert & Pfizenmaier 1975, Hussain & Hasan 1985). These methods capitalize on the ability to excite the linear (Kelvin Helmholtz) instabilities using low-amplitude perturbations at the point of receptivity (e.g., jet nozzle exit and mixing layer splitter plate lip), using periodic forcing.

The above open-loop forcing methods use single or multiple frequency excitation to induce a periodic flow response via excitation of the linear instabilities, but having uncontrolled nonlinear flow response. Typically large amplitudes of excitation have been necessary to produce significant gains; for instance, jet mixing enhancement using oscillatory forcing of axisymmetric and helical models of a jet by Freund & Moin (2000) required upwards of 25% modulation of the jet exit velocity. Other active flow control examples include the use of blowing and suction in boundary layers (Narasimha 1983, Choi

et al. 1994), and the use of (linear) feedback control (shear layer – Wiltse & Glezer 1993, boundary layer – Haritonidis et al. 1993).

Examples of reactive control are typically found in feedback control applications, although feedforward control methods are emerging. Linear feedback-based control of the global instabilities in the linear instability region of a circular jet was demonstrated by Reisenthel (1988) using a probe situated in the downstream shear layer of the jet to feedback velocity perturbations to acoustic speakers located at the nozzle exit plane; the downstream nonlinear flow response (prior to the end of the jet potential core) was however largely ignored and uncontrollable with the linear approach. Experimental and numerical investigations into the active control of the near-wall region of a turbulent boundary layer have also been attempted using a linear adaptive feedforward control algorithm (Rathnasingham & Breuer 1997), however, applications to jet flows is lacking. Note that, being linear approaches, these techniques are limited to only stable flow solutions and may need significant input of control energy.

Attempts to control the nonlinear dynamics of free shear flows have also relied on linear approaches for manipulating the linear instabilities (which dominate the initial flow region) using carefully chosen forcing frequencies and amplitudes and phase differences between the forcing frequency components (Arbey & Ffowcs-Williams 1984, Husain & Hussain 1995, Paschereit & Wygnanski 1995). The primary focus of these studies has been the subharmonic resonance phenomenon (Monkewitz 1988), which dictates the pairing interactions of large-scale vortices in mixing layers and jets. The sensitivity of the nonlinear evolution of the instabilities to control parameters such as the amplitude ratios

and phase differences between the forcing frequency components was the subject of theoretical (Monkewitz 1988) and experimental investigations (Husain & Hussain 1995). However, due to differences in the excitation methods and facility background disturbance spectrum, these parameters can vary widely between facilities and flows. To obtain a desirable flow response using these control methods, i.e., for controlling the interaction of vortices, studies have therefore been performed to probe the parameter space of several forcing frequencies, their amplitudes and relative phase differences among them (e.g., Arbey & Ffowcs-Williams 1984, Paschereit & Wygnanski 1995).

The proper combination of axial and helical excitation of a jet at different frequencies has also been shown to generate a unique class of flows known as "bifurcating" and "blooming" jets (Lee & Reynolds 1985, Parekh et al. 1987). While the axial forcing caused the jet shear layer to roll up into distinct vortex rings, the helical excitation produced small eccentricity in the ring alignment (which was amplified by the jet evolution) by radially perturbing the vortex rings. Substantial jet spread via jet bifurcation was observed experimentally by varying the excitation frequency amplitude ratios and phase differences. The excitation needed to generate periodic response is therefore typically predetermined experimentally. Moreover, each new desired flow response requires the parametric search-driven identification of a new set of control parameters. In some cases, the need to achieve a periodic flow response can also demand unduly large forcing amplitudes (e.g., see Arbey & Ffowcs-Williams 1984).

In summary, reactive control approaches involving feedforward and feedback techniques have not been explored in any detail for jet flows, while some applications in wall-

bounded shear flows have been emerging (discussed below). Such control strategies have promising directions including adaptive and optimal control, using physical and dynamical systems models (as pointed out in Fig. 1.2). In the following, some recent advances in the description and control of nonlinear dynamics in transitional and turbulent shear flows are presented. Further details of the dynamical systems approach and associated nonlinear control concepts are presented in Appendix A.

### 1.3 Recent Advances in Modeling and Control of Nonlinear Flow Systems

The development of nonlinear flow control approaches hinges on the availability of methods and tools to describe and model the complex flows as low-dimensional systems (Keefe 1993, Glauser et al. 1990, Ukeiley et al. 2001). Some modeling approaches for the coherent structure dynamics of jet flows were discussed in the previous section. The recent use of optimal control theory to explore advanced flow control approaches is promising (Bewley et al. 2001, Lee et al. 2001), but even the most recent successes have been limited to simple computational settings such as the streamwise periodic transitional and turbulent channel flows. Adjoint-based optimization strategies for controlling mixing and noise in low Reynolds number jet flows is only now becoming computationally feasible, and even so is limited to a few computational iterations of the flow solution (J. Freund, private communication). Advanced methods for parameter optimization have been recently attempted to develop evolution strategies (based on genetic algorithms) to optimize mixing in direct numerical simulations of jets (Koumoustsakos et al. 1998). The requirement of "full flow field information" and prohibitive computational expense in such numerical simulation-based studies makes its practical implementation challenging. The

feasibility of the use of more practical, "partial" flow field information for feedback control is a subject of ongoing research. Since the control of nonlinear systems remains a research topic, there is no general framework to obtain a desired controller. A very complicated and detailed model, simulations of the full Navier Stokes equations, might generate overly complex controller or make the derivation of the controller impossible. On the other hand, an over-simplified or linear model facilitates the controller design but it might be unable to achieve the desired control objective. A reasonable compromise is a reduced model able to capture the dynamic and controllable flow features; for instance, see the Cortelezzi (1996) application using a system of point vortices to model and control the wake behind a flat plate. Typically, the reduced model is a low-dimensional nonlinear system governed by a set of ordinary differential equations (such as those derived by Aubry et al. 1988 and Ukeiley et al. 2001), while the real flow is infinite dimensional.

An alternative approach to the low order modeling and control of organized structures in complex flow systems has been the use of the nonlinear dynamical systems (DS) approach. The use of this approach to describe and control seemingly disordered (high-dimensional) phenomena as low-dimensional systems has been very successful in closed hydrodynamic flows, e.g., Rayleigh-Bénard convection (Dubois 1982), Taylor-Couette flow (Brandstäter et al. 1983). However, the prediction and control of technologically significant *open flows* remains a major challenge despite several promising recent attempts in wakes (Sreenivasan 1985, Van Atta & Gharib 1987), jets (Bonetti & Boon 1989, Broze & Hussain 1994, 1996), mixing layers (Narayanan & Hussain 1996), and boundary layers (Healy 1993). The most problematic issue in the application of the DS

approach to open flows is that the intrinsic *convective instabilities* in these flows make them extremely sensitive to external perturbations (Huerre & Monkewitz 1990). This makes it very difficult to differentiate intrinsic (deterministic) dynamics from extrinsic ("noise-driven") dynamics (Huerre 1987). This "open flow problem" is discussed further in Chapter 3. Recent studies (Broze & Hussain (1994, 1996), Narayanan & Hussain 1996, Broze et al. 1997) also address the above-mentioned issues in detail.

*Chaos control* is a recent development in nonlinear control that uses the DS approach. This control concept has found applications in diverse fields such as chemical reaction, electronic communication, and lasers (Chen & Dong 1993). The control goal is to track periodic states embedded in a chaotic system typically requiring "small" parameter changes; the approach is particularly appealing because of its ability to target (potentially useful) unstable states, unattainable by conventional (linear) control methods.

Recent findings of low-dimensional chaos in open flows, such as cylinder wakes (Van Atta & Gharib 1987), a plane mixing layer (Narayanan & Hussain 1996), axisymmetric jets (Broze & Hussain 1994), and a transitional boundary layer (Healey 1993) suggest that technologically significant turbulence phenomena can also be manipulated via chaos control. However, prior chaos control methods have been applied to simple temporal dynamical systems of a few coupled ordinary differential equations, one-/two--dimensional maps, or closed flows (Ott et al. 1990). Virtually all practical flows are, however, spatiotemporal. Chaos control was shown via simulations of the spatially homogeneous Ginzburg-Landau equation, but necessitates full spatiotemporal velocity field information (Keefe 1993). Techniques have also been evaluated to control chaotic dy-

namics in direct numerical simulations of two-dimensional turbulence governed by the incompressible Navier–Stokes equations (Guan et al. 2003). Global and local feedback strategies were used to monitor the targeted periodic states and to provide control input to track the desired state, demonstrating control of periodic states in the model system. However, as for Keefe (1993), control required a network of spatially distributed sensing and actuation, making it difficult to realize in practice. In fact, an experimental demonstration of chaos control in an open flow is still lacking. Preliminary efforts in applying such control in low Reynolds number turbulent boundary layer simulations are reviewed in Lumley & Blossey (1998). A more detailed treatment of selected recent efforts aimed at realizing chaos control and other forms of modern flow control techniques for various applications, some of which are referenced above, is provided in Chapter 7.

A chaos control-based approach for controlling the transitional jet dynamics is developed in this study; details of the approach are presented in Appendix A. Briefly, the low-dimensional dynamics of the jet flow are studied and intrinsic flow states are stabilized via control. Control perturbations are provided to maintain an inherent periodic (albeit unstable) flow state. Consequently, the forcing levels to obtain a selected "goal state" are much less than those for brute-force control methods described above.

The choice of the axisymmetric jet near field is motivated by its simple geometry and technological relevance. The linear and nonlinear instabilities and the transitional CS dynamics of this shear flow have been well documented (Hussain 1986). A plane mixing layer is also studied to demonstrate the new control method in a prototypical open shear flow. Recent findings of low-dimensional dynamics in jet and mixing layer flows is

promising (Broze & Hussain 1994, Narayanan & Hussain 1996).

### 1.4 Fundamental Issues and Potential Benefits in Nonlinear Flow Control

Generally speaking, two control approaches are prevalent: feedback-based and open-loop. The merit of feedback-based methods lies in their use of simple flow models and their success in the presence of multiple (stable and unstable) solutions. In contrast, open-loop control techniques need accurate flow models, may not achieve the desired goal state/dynamics when multiple solutions exist, and are ineffective in nonstationary flow conditions. However, they do not involve cumbersome sensing/actuation and real-time processing, which are essential for feedback control. Furthermore, feedback-based control may not be feasible in spatially developing flows such as jets, mixing layers and boundary layers. Since real-time sensing of a local flow variable is used to modify the future input of control perturbations, sensing must accompany nearly instantaneous actuation. For this, at the least, high-speed control algorithms (for real-time data acquisition and modeling/control computations) and sophisticated sensor/actuator response are required. Even so, the additional time delays associated with the spatial development of flow disturbances are unavoidable. The total delay in providing control makes a (convectively unstable) flow susceptible to undesirable ambient disturbances, which can cause the flow to deviate from a goal state (to be targeted by control). Potential solutions to these issues are presented for the nonlinear control of a circular jet in Chapter 4 and Appendix A.

In the following, the newly developed control approach developed here is contrasted with conventional free shear flow control methods. As discussed earlier, periodic forcing

has been used extensively to control CS dynamics in free shear flows. These methods use single/multiple frequency excitation to induce a periodic response without considering the underlying low-dimensional dynamics in the flow. In the nonlinear control method presented here, intrinsic flow states are targeted. Control perturbations are provided to maintain an inherent (unstable) periodic flow state when the dynamics approach the selected goal flow state. Consequently, the forcing levels to obtain a desirable flow state are expected to be less than those for brute-force control methods. Note, however, that selected goal states may not always be achievable using an open-loop approach (see Chapter 4), and closed-loop (feedback-driven approaches) may be needed.

The control approach presented here also differs from prior jet forcing studies in the method to deduce the control perturbations. To obtain a desirable flow response, conventional methods probe the parameter space of several forcing frequencies, their amplitudes and relative phase differences among them (e.g., see Paschereit et al. 1995). The excitation or control signal needed to generate the periodic response is therefore determined via a separate test for each target flow state (e.g., see Arbey & Ffowcs-Williams 1984). The control approach presented here is more objective and systematic in the development of the "controller." Low-dimensional chaotic dynamics in a relatively small parameter space of the frequency of the primary instability and its forcing amplitude are first identified; this parameter space is chosen for the convenience in imposing external forcing, necessary to reveal low-dimensional dynamics in the flow. Controllable states and the perturbations for their control – the controller – are then determined without further testing.

The objectives of this dissertation are: (i) to present a new *nonlinear* jet control

method; (ii) to experimentally demonstrate the control method as proof-of-principle in the near field of a circular jet; and (iii) to quantitatively demonstrate potential benefits from the jet control via measurements of the turbulence characteristics in the flow field.

### 1.5 Dissertation Outline

The dissertation is organized as follows. Chapter 2 briefly describes the anechoic jet facility, and the data acquisition and instrumentation used for the experiments. In Chapter 3, following a discussion of the critical issues in identifying controllable low-dimensional dynamics in open flows, a brief account of the chaotic dynamics found in the forced circular jet flow is provided. The inherently periodic (but unstable) flow states in the jet are described in terms of their vortex dynamics, involving roll up and pairings of vortex rings in the transitional region. Following this, two methods to determine the spatial development of the periodic flow states from two-point measurements (needed for control) – *direct analysis* and *inverse modeling* – are described.

A new open-loop nonlinear control approach and experimental results from its implementation in the circular jet are presented in Chapter 4. A feedback-based control method is then presented and its effectiveness is experimentally evaluated. Preliminary experimental results, involving qualitative and quantitative measurements in the near and far fields of the jet, demonstrating turbulence enhancement and suppression using the open-loop control method are presented in Chapter 5. Conclusions and discussions of potential future work are presented in Chapter 6. Chapter 7 provides an expanded review of some research developments in chaos control and flow control conducted concurrently to

the present research and following the completion of the research reported here.

Appendix A describes the low-dimensional chaotic dynamics found in the jet using the dynamical systems approach. This includes the description of the chaotic attractor underlying the low-dimensional dynamics analyzed and controlled in Chapter 3. Empirical analysis of the attractor reveals unstable periodic orbits which display striking features, such as bundling of orbits, using which simple empirical representations of the periodic orbits are obtained. Following this, the conceptual approach to chaos control of the jet flow is described and the jet control results (described in Chapter 3) are analyzed in more detail using a dynamical systems perspective. The feedback-based chaos control method and the experimental results are then discussed. Some dynamical systems tools used for the chaotic attractor analysis are also described.

In Appendix B, a newly derived spatial coupling measure – *total coherence* – is used to justify our use of single-/two-point measurements to describe the jet near field. The analytical formulation of coherence as a spatial coupling and "predictability" measure in nonlinear (up to quadratic order) dynamical systems is presented. Computational issues related to coherence estimation and analytical causes for coherence decay (indicative of spatiotemporal dynamics) are also discussed. The low-dimensional chaotic dynamics and the experimental results from using the nonlinear control method in a different free shear flow facility– a plane mixing layer – are described in Appendix C. Appendix D summarizes the least-means-square algorithm to calculate the adaptive filter for "inverse modeling" used in Chapter 3 and Appendix A and related computational issues.

# CHAPTER 2

# EXPERIMENTAL FACILITY AND INSTRUMENTATION

## 2.1 Anechoic Circular Jet Facility

The experiments reported were performed in the Aerodynamics and Turbulence Laboratory (ATL) in the Mechanical Engineering Department of the University of Houston. The majority of the experiments were conducted in a circular jet facility within a large anechoic chamber (AC) at ATL. Brief description of the key attributes of the anechoic facility and modifications made to it are presented below, and details can be found in Bridges (1990). Some additional experiments were performed in a plane mixing layer facility in the ATL air room described in Appendix B.

*Anechoic chamber*. The AC is a well-ventilated, air-conditioned concrete box with 0.3 m thick walls set on air bearings with its inner walls covered with 1 m long fiberglass wedges. The inside dimensions of the chamber from wedgetip to wedgetip are 7.6 m x 5 m x 5 m. The ambient sound level of the chamber is 35 dB above 100 Hz. Vertical pipes attached to the bottom of the chamber provide support for the traverse (described later). Care was needed to provide structural rigidity to the pipes supporting the traverse and to ensure minimal relative motion between the traverse and the circular jet nozzle.

*Flow facility*. The circular jet facility shown schematically in Figure 2.1a is enclosed in the low-noise anechoic chamber. A seven-stage blower, driven by a 40 hp DC motor, is located outside the main building, and provides air supply. The DC blower motor is controlled by a Polyspede HP-3 adjustable speed drive system, with adjustments for speed

regulation, torque limits and acceleration/deceleration. Despite the use of control to minimize fluctuations, the controller was found to "hunt" for a set point thereby introducing low-frequency oscillations of the blower (≈ 0.3 Hz); fortunately, this oscillation frequency is far below that to which the flow instabilities are receptive. A 15.25 cm diameter, 77 m long iron pipe connects the blower to the circular pipe (P) entering the AC. Several flow conditioners, including large-radius elbows, a honeycomb and seven mesh screens (noted on the facility schematic), are inserted in the flow path to provide uniform and low-noise level flow into the chamber. An electrostatic filter was inserted to remove dust and dirt that might adversely affect hot-wire measurements, and a cooling coil was used to regulate the temperature of the flow during high-speed operation thereby minimizing errors in hot-wire measurements (Bridges 1990).

*Bulk excitation*. A bulk acoustic excitation system is located upstream of the settling chamber and outside the AC, to provide a longitudinal component of perturbation to the mean flow. Four acoustic speakers angled downstream (shown just outside the AC in Figure 2.1a) are used to provide a uniform excitation of the flow. Bridges (1990) describes the transfer function of the facility, with resonances revealing discrete frequencies at which effective excitation is possible. This has adverse implications for the control study to be performed here, since a broad range of frequencies are desired to be available for the jet control. Furthermore, the large distance between the excitation system and the nozzle exit plane introduces significant delays between the control signal and the flow response. A new shear layer excitation system installed at the jet nozzle exit was built to overcome these shortcomings and is described further below.

(a)

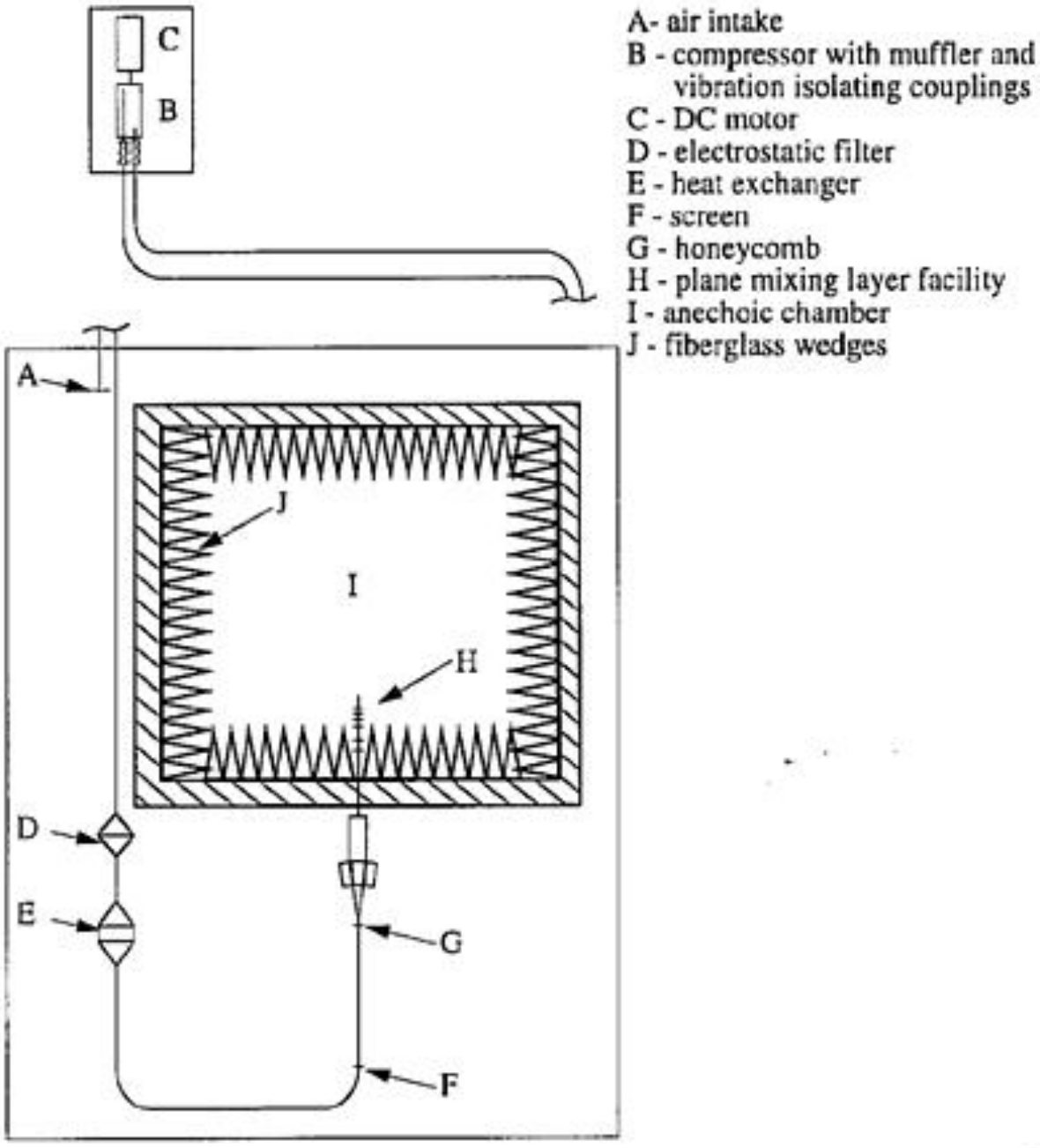


Figure 2.1 (a) Schematic of experimental jet flow facility and the anechoic chamber.

(b)

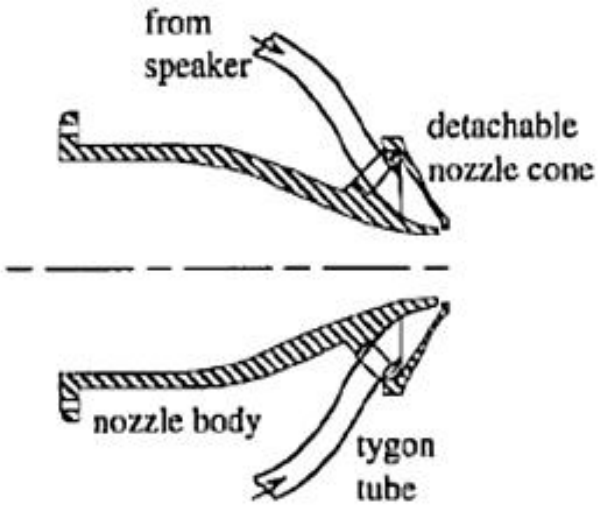


Figure 2 (b) Schematic of shear layer excitation facility for jet nozzle exit control.

*Shear-layer excitation*. Discrete wind tunnel modes result in a highly non-uniform settling chamber transfer function with the use of the bulk acoustic exictation system described above. The frequency response at the nozzle exit centerline varies widely (up to 40 dB), having discrete peaks, for frequencies below 500 Hz. Such a frequency response causes undesirable attenuation of certain frequency components present in the control perturbations provided to the speaker (in addition to inherent delays). To maintain appropriate amplitude ratios of various frequency components in the control signal at the nozzle exit, a new shear layer excitation facility is installed. A 0.38 m acoustic speaker is enclosed in a box (packed with fiberglass wool) and connected through 12 Tygon tubes of equal length ($\cong$ 0.91 m) to twelve 19 mm diameter holes in a casing surrounding the nozzle (see the cross-section in Figure 2.1b), terminating in a uniform 0.6 mm wide slit all around the nozzle lip; the axisymmetry of the excitation was ensured by flow-visualization. As expected, the transfer function of the (shear layer) excitation facility is

far more uniform over the frequencies of interest; less than 10 dB variation and no discrete peaks are observed over the entire frequency range [10–500 Hz].

*Circular jet nozzle*. The circular nozzle in the AC has an inlet diameter of 15.25 cm and an exit diameter of 4 cm, providing a contraction area ratio of 14.5. The contraction shape was designed as a cubic profile with a 1 cm straight section at the nozzle exit to minimize the vena contracta effect.

*Jet exit flow conditions*. Although the jet exit speeds achievable are up to 235 m/s (M = 0.68), the present study is limited to speeds up to 20m/s. Some experiments were performed at higher speeds of up to 35 m/s to demonstrate the robustness of the flow states achieved and the control. The boundary layer characteristics (including mean velocity and turbulence intensity profiles) of the nozzle exit plane flow are discussed and described in Broze (1992). Briefly, nominally laminar boundary layers are found over the range of jet speeds considered, with mean velocity profiles matching the Blasius profile, peak turbulence intensities of up to 0.5% in the boundary layer and even lower ($\approx$ 0.1%) in the free stream, and no abnormal spectral peaks measured inside the boundary layer.

### 2.2 Computer and Data Acquisition System

*Computer and instrumentation*. Data analyses were performed on a SPARCstation 20 with four 50 MHz superSPARC processors. We use an ICS110A 16-bit A/D converter for data acquisition, with which up to 64 channels can be simultaneously sampled at up to a 200 kHz sampling frequency. Data acquired from the hot-wire were transmitted to the digital acquisition system via coaxial cables and were low-pass filtered at 5 kHz (using

Krohn-Hite 3341 analog filters) before sampling in differential mode. Krohn-Hite 331 analog filters and Stanford SR650 digital filters with 115 dB/octave attenuation are used to filter the data and the control signals. Perturbations used for the control experiments are provided to the acoustic speaker via a 12-bit D/A converter in a Masscomp MC6650 computer. Fluctuation amplitudes of individual components, spectra and time-series for documentation of different flow states were recorded on a two-channel Ono Sokki 920 spectrum analyzer (after high-pass filtering at 10 Hz) owing to its increased resolution (16 bit A/D converter). The data acquisition and traverse control software for the Masscomp-bases system were created and documented by a group of research at the Mechanical Engineering Department (including Drs. Kleis, Jenkinson and Brides). The data acquisition software for the ICS110A-bases system was created, tested and documented by ATL researchers recently (Stoesz, Narayanan).

*Probes, traverse and excitation system*. Constant temperature hot-wire anemometers built by AA Labs (Israel) were used for the experiments reported here. Offset and gain adjustments and low-pass filters were included in these anemometers to provide improved signal-to-noise ratio by taking advantage of the entire range of the A/D converter. Calibrations were repeated whenever significant changes in the temperature, humidity and pressure conditions in the flow and chamber were noted. King's law ($E^2 = A + B\ U^c$) was used to convert the voltages to velocities on the computer, following digitization; E denotes the mean voltage and U denotes the mean velocity, with A, B and c as the calibration constants. The fluctuation amplitudes u' from spectral amplitudes of individual frequency components (e.g., for excitation amplitude) were computed as: $u'/U = 2\ E\ U^{-c}\ e`^2$

/ B c. A 4 μm diameter and 2 mm long tungsten-rhodium hot wire (single-wire boundary layer probe (TSI-1218)), and two single-wires with 25 mm (TSI-1210 CS) and 5 mm long prongs, with a 1.4 overheat ratio, were employed for all measurements reported.

An x-y traverse system with stepper motor controls (Slo-Syn SS-150-1021 & SS-400-1010 with 0.025 mm resolution) was used to move the probe. To provide lateral stabilization to the traverse support system, the traverse was anchored to the nozzle. A 50 MHz function generator (Wavetek model 80), a Hafler model P500 stereo power amplifier and an Onkyo model M-501 stereo power amplifier were used for excitation. Phase locking was achieved (for control experiments) using the Wavetek model 186 5 MHz phase lock generator. MKS Baratron (0-1 Torr range) and 223-B (0-10 Torr range) digital pressure transducers, with MKS 270-B signal conditioners, were employed in hot-wire calibrations.

# CHAPTER 3

# LOW-DIMENSIONAL DYNAMICS IN THE AXISYMMETRIC JET NEAR FIELD

## 3.1 The "Open Flow" Problem

In a detailed review of instabilities in spatially developing flows, Huerre & Monkewitz (1990) classified local instabilities in such flows as *absolute* and *convective*. Disturbances in an absolutely unstable flow dominate the dynamics at their origin and eventually everywhere in the domain, while in convectively unstable flows, disturbances are swept away from the origin, leaving the point-of-receptivity susceptible to new disturbances. It was proposed that, in the absence of pressure feedback (e.g., in edge-tone, cavity flows), a sufficiently large region of an absolute instability will excite self-sustained oscillations in a large flow region, viz., a global mode appears; i.e., a single/few active modes dominate the essential flow dynamics. However, convectively unstable flows, in general, were considered to be incapable of sustaining global dynamics; the possibility of a "slightly damped jet-column mode" in convectively unstable jets was only speculated.

The description of low-dimensional dynamics and their modeling has been successful in closed flows, e.g., Rayleigh-Benard convection (Dubois 1982), Taylor-Couette flow (Brandstäter et al. 1983). Being absolutely unstable, these flows are relatively insensitive to "noise" and can sustain global modes, enabling reduced-order modeling using a few active modes in the flow. (In a laboratory flow, noise includes perturbations originat-

ing external to the flow domain of interest, e.g., wind tunnel and room acoustics, blower-originated pulsations.) However, some physically open flows can display intrinsic low-dimensional dynamics. In particular, distinction between "physically open" flows and "dynamically open" flows is needed. "Dynamically open" (convectively unstable) flows might not be amenable to simplified low-dimensional modeling (hence model-based control) due to their noise sensitivity. In particular, spatially amplified "random" noise may not be distinguishable from intrinsic low-dimensional chaotic dynamics (Huerre 1987).

Thus, "the open flow problem is the inability to predict the dynamics of open flows" (Broze & Hussain 1994). In general, since a large variety of technologically significant (free/wall-bounded) shear flows fall in the class of "dynamically open flows," the aforementioned problem poses a, perhaps insurmountable, challenge for the prediction and model-based control of these flows.

Our exploration of the low-dimensional dynamics of the circular jet flow is motivated by the fact that this convectively unstable open flow can also display "intrinsic" dynamics. The mechanism for self-sustained dynamics in these flows could be feedback from flow interaction with solid boundaries (Brown 1937, Hussain & Zaman 1978) or near field flow events such as vortex formation and pairings (Dimotakis & Brown 1976, Grinstein et al. 1991). Broze & Hussain (1994) described the near field of a forced circular jet as a low-dimensional system incorporating feedback due to vortex pairings as a mechanism for "dynamical closure."

In the following sections, some key results are presented showing that the jet near field dynamics are low dimensional and can therefore be described in simpler terms that

are amenable to nonlinear control. This is particularly true in the presence of "spatial coupling" in the flow. Coupling is the mutual dependence of the dynamics at spatially separated locations.

In the presence of spatial coupling, single-point (temporal) measurements suffice to capture the essential flow dynamics. Significantly large flow regions of the circular jet are shown to be "spatially coupled" even for seemingly complex dynamics (see results in Appendix C). This substantially simplifies the analysis of low-dimensional dynamics in the flow using single-/two-point velocity measurements and its use for control. Methods to describe spatiotemporal dynamics in the absence of coupling are yet unavailable; analyses of spatiotemporal data have only been attempted recently (Narayanan et al. 1997, Roy et al. 1997). The dynamical systems approach-based description of the low-dimensional jet dynamics is discussed in Appendix A [see also Broze & Hussain (1994, 1996)].

### 3.2 Low-dimensional Dynamics of the Forced Axisymmetric Jet

Figure 1.1 displayed the spatiotemporal jet dynamics in a top-hat profile jet with vortex rollup and pairings, which feedback perturbations to the nozzle lip. The transition region extends from the nozzle exit (the point-of-receptivity for instabilities) to 4–6D, where the jet develops significant three-dimensionality, leading to the generation of fine-scale random vorticity, hence turbulence. The transition region is subject to several instabilities: (i) a primary Kelvin-Helmholtz instability leading to the formation of axisymmetric vortex rings ("vortex rollup"), (ii) subsequent two-dimensional subharmonic instabilities leading to the merger of neighboring vortices (vortex "pairings"), and (iii)

three-dimensional instabilities leading to vortex fragmentation and transition to turbulence. The unforced jet displays high-dimensional dynamics with broadband modulations centered around the "preferred mode" frequency (see the velocity power spectrum in Figure 3.1 recorded in the jet transition region); the term "preferred mode" refers to the average passage frequency of vortical structures (centered around $St_D \cong 0.4$) in an unforced jet flow (Hussain & Zaman 1981). Due to the lack of evidence of low-dimensional dynamics in the unforced jet, we chose the simplest parameter space, for which low-dimensional flow states were found. The anechoic jet flow was therefore acoustically excited at a single frequency f. Thus, the dimensionless control parameters are: the forcing amplitude $a_f \equiv u'_f/U_e$ and the forcing frequency $St_D \equiv f\ D/U_e$; $u'_f$ is the centerline rms-velocity fluctuation at f, $U_e$ is the centerline exit velocity, and D is the jet diameter. Among a wide variety of dynamical states, two periodic and two low-dimensional chaotic flow states were found over large regions in the parameter space.

Of particular importance (to technological processes such as mixing and aerodynamic noise generation) are the formation and pairings of vortices. While the fundamental frequency f (associated with vortex roll up) is externally forced, the vortical interactions (and hence the associated subharmonic and quarterharmonic frequencies f/2 and f/4) are driven by feedback from vortex pairings (Hussain et al. 1986), i.e., are self-excited. The spatially growing waves associated with these frequencies have linear regions in which they grow exponentially at different rates (evolving at different phase speeds), followed by nonlinear regions where they saturate at different amplitudes and grow or decay due to self- and cross-interactions. The saturation of the fundamental is physically realized by

vortex rollup; pairings result from the (nonlinear) subharmonic resonance phenomenon, where a fundamental and its subharmonic interact to reinforce the subharmonic (i.e., f + (-f/2) = f/2) (Monkewitz 1988, Husain & Hussain 1995). Thus, the relevant and dominant frequencies are the fundamental, the subharmonics, and the sidebands generated by detuned feedback (i.e., when feedback is not exactly at f/2 and f/4) (Broze & Hussain 1996). Although the dynamics of this flow can be relatively simple (nominally two-dimensional and limited to as few as three, or even two, instability modes), this prototypical open flow embodies several important and common features of spatiotemporal flows: spatially evolving, inhomogeneous, and dispersive, with linear and nonlinear instabilities.

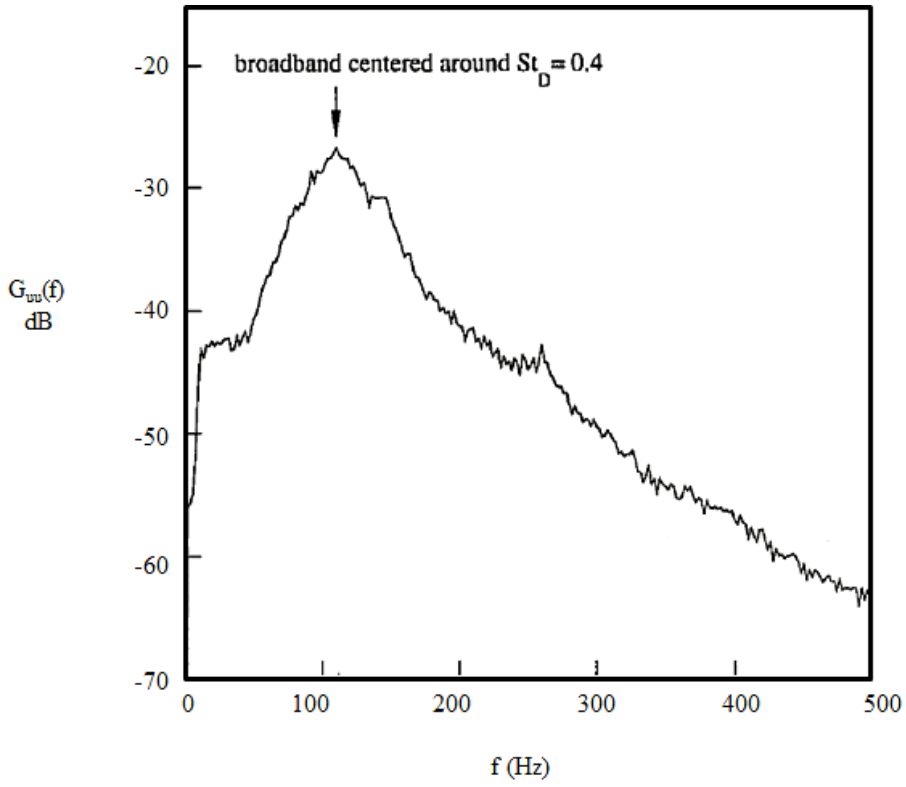


Figure 3.1 Power spectrum of centerline velocity time trace at x/D=2 in an unforced jet flow.

In the following, the salient features of a chaotic state chosen for the present study

are briefly described. A chaotic flow state (the "quarterharmonic chaotic attractor" QCA) is found in the range $0.008 \leq a_f \leq 0.02$ and $1.1 \leq St_D \leq 1.25$. The dynamical systems-based description of the chaotic attractor associated with this flow state is provided in Appendix A. The longitudinal velocity time trace u(t) and its power spectrum $G_{uu}(f)$ in Figure 3.2(a,b) are from a hot-wire sensor located at $x/D \cong 2$ (on the jet centerline) for $a_f \cong 1\%$ and $St_D \cong 1.2$. Here, the Reynolds number $Re_D \cong 23,\ 000$, but such chaotic flow dynamics were found for higher $Re_D$ ($\cong 76,\ 000$) as well. (Analog-to-digital converter (ADC) units are used as units for u(t).)

The power spectrum recorded near the first vortex pairing location ($x/D \cong 2$) shows peaks (due to induced velocities from passing vortices) at f and two sidebands around the subharmonic ($f_l = f/2 - \Delta f$, $f_h = f/2 + \Delta f$), indicating (almost) periodic subharmonic modulations, i.e., a first pairing whose location changes (nearly) periodically in space (see visualization in Broze & Hussain 1996). The broadband centered at f/4 is due to chaotic second pairing occurring farther downstream. The nearly periodic subharmonic modulations and the broadband f/4 indicate vortex pairings whose locations shift in x due to detuned feedback, as opposed to the strong subharmonic and quarterharmonic peaks for the (stable) periodic flow states (found for higher $a_f$) having *phase-locked feedback*.

The above associations between centerline velocity signals/spectra and the axisymmetric vortex dynamics are supported by flow visualization and measurements of the spatial vorticity distribution (Zaman & Hussain 1980). The waves corresponding to the modulated subharmonic and the broadband quarterharmonic have longer spatial evolution

times (than for phase-locked periodic states) and are results of detuned pairing feedback. Correspondingly, the first pairing location for the chaotic flow is delayed to $x/D \cong 2$, and the second pairing may occur as far as $x/D \cong 4$; these events were verified by smoke visualization to be nominally axisymmetric (see results in Chapter 5 and Broze & Hussain 1996). Henceforth, our discussion of "downstream dynamics" will be based on data acquired on the centerline at $x/D \cong 2$ (see Figure 1.1), where the effects (i.e., the induced velocities) of rollup and both pairings are comparable.

Several harmonics appear in the power spectrum in Figure 3.2b, indicating highly nonlinear dynamics in the downstream flow region. The nonlinearities giving rise to the harmonics in the power spectrum result from saturation of the fundamental, subharmonic and quaterharmonic frequencies following their linear instability evolution, and their nonlinear interactions, namely subharmonic resonance and interactions of the sideband frequencies (for example surrounding the subharmonic frequency f/2) with other frequency components in the power spectrum. The quasiperiodic nature of the dynamics results in well-defined harmonics and spectral peaks in the power spectrum, in contrast with the unforced jet spectrum at a similar location (see Fig. 3.1) for which a broadband spectrum is seen. The velocity signals were sampled at sufficiently high frequencies to minimize the effects of spectral aliasing. Sufficiently large numbers of records (more than 1000) were used for computing the discrete Fourier transforms from which smooth power spectra were obtained, and smooth windowing in time domain was employed to minimize effects of spectral leakage that otherwise would result in spurious spectral peaks.

To justify the use of single-point velocity measurements to describe the jet dynamics

a new measure of "spatial coupling" – *total coherence* $\gamma^2_T(f)$ – was evaluated. High values of $\gamma^2_T$ found over a large region (at least 4-6 jet diameters) indicate that the jet displays *temporal*, rather than spatiotemporal, dynamics (see results in Appendix C). Since spatial coupling implies the predictability of dynamics at one location from observables at another, single-point measurements suffice to describe the low-dimensional dynamics in the jet near field. In the jet, the physical mechanism for coupling was verified to be "feedback" from characteristic events such as vortex pairings, caused by upstream propagating pressure perturbations. The rapid drop of $\gamma^2_T$ downstream (past the end of the time-averaged jet potential core end) is evidence of spatiotemporal dynamics. Detailed measurements of the extent of spatial correlation in the jet are presented in Appendix C.

Since vortex ring formation (rollup) and subsequent pairings dominate the essential near-field dynamics, which are of considerable technological interest (e.g., mixing and turbulence/noise generation) (Hussain 1983), we focus on these axisymmetric CS dynamics (see Figure 1.1). In addition to vortex formation (sustained by external forcing), the chaotic flow reveals at least two self-sustained quasiperiodic/chaotic vortex pairings. To enable the control of multiple vortex pairings, we select the chaotic flow state – quarter-harmonic chaotic attractor (QCA) – for further analysis and control, since it has low-dimensional dynamics of both the first and the second pairings. The ensuing analysis was also done for another chaotic flow state found in the jet and the results and conclusions were similar. The significance of these results will be evident in the development and implementation of a novel control approach presented in Chapter 4.

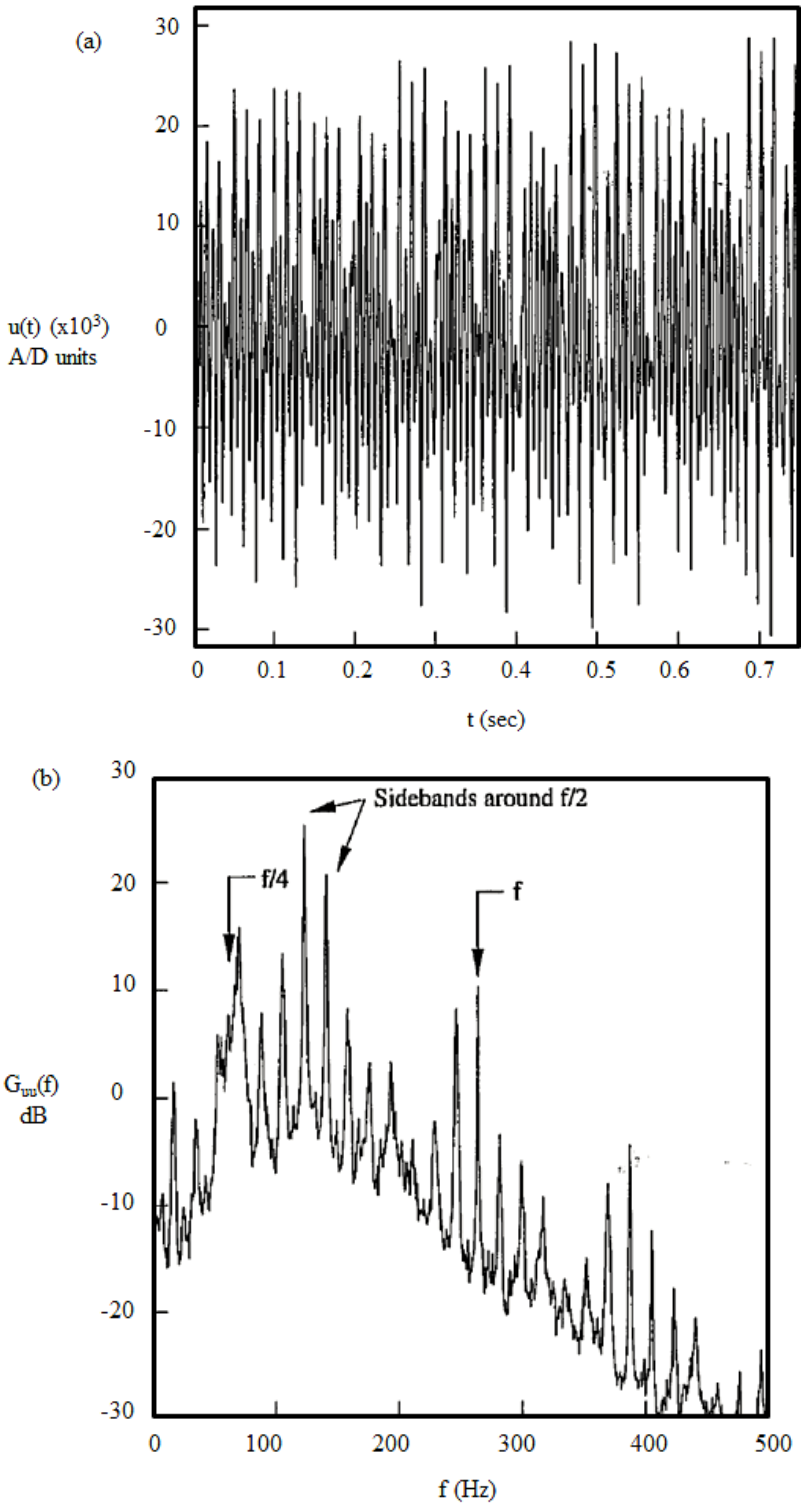


Figure 3.2 (a) A longitudinal velocity time trace for QCA at x/D=2; (b) The power spectrum for QCA (at x/D=2) shows the dynamically significant frequency components: f, f/2 sidebands and broadband f/4.

### 3.3 Unstable Periodic Flow States in the Forced Axisymmetric Jet

It is well known that chaotic dynamics are comprised of an infinity of unstable periodic states; these are otherwise termed unstable periodic orbits of a chaotic attractor and are discussed in detail in Appendix A. Thus, a chaotic flow can be alternatively described as being the result of a combination of infinity of periodic states. Since the periodic states are all unstable, the flow constantly switches between them to produce a chaotic (but deterministic) response. In the following, such unstable periodic states are analyzed using hot-wire velocity signals obtained in the transitional jet region.

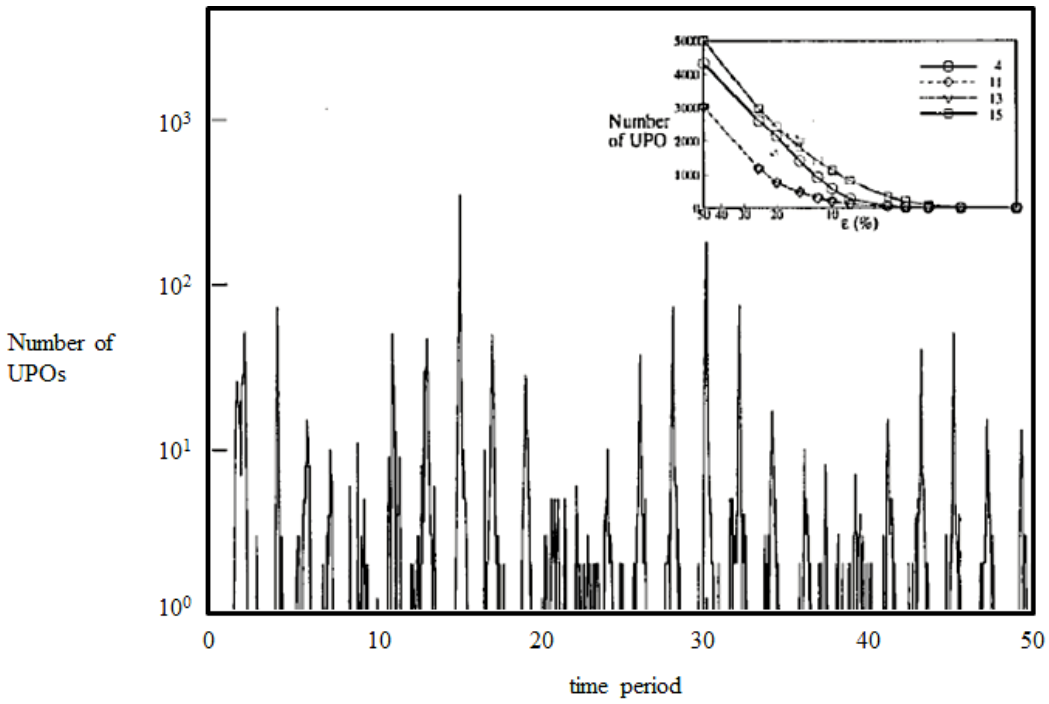


Figure 3.3 The histogram displays the dominant UPO's in QCA; the inset shows the number of UPO's found by varying $\varepsilon_1$, for period-4, 11, 13 and 15 orbits.

The detailed procedures for extracting the unstable periodic dynamics from phase-space reconstructions of a chaotic attractor are described in Appendix A. In summary, segments of a sampled velocity signal are extracted which tend to repeat themselves (at

seemingly random times). The order of the periodicity of these segments (i.e., the number of oscillations) determines the flow state. The recurrence time is normalized by the fundamental period, the smallest significant time scale in the transition region; the fundamental period is the inverse of the fundamental frequency component (which is forced in the jet). Thus, for instance, a period-2 flow state corresponds to oscillations in the velocity trace which last two fundamental periods, which in turn is associated with the passage of two, rolled up ring-type vortices. Such a sequence occurs at several later times but is repeated in a chaotic manner. In the meantime, the flow switches to other periodic states.

For a periodic flow state of period-n the time segments are found to be strikingly similar, indicating the dominance of certain periodic states and hence particular sequences of coherent structure (CS) dynamics. The method for analyzing such dynamics and their statistical significance are discussed in Appendix A. Figure 3.3 displays a histogram revealing the frequency of occurrence of various (unstable) periodic states (also termed, unstable periodic orbits) in a chaotic velocity trace sampled over a long period.

*Physical significance of the (unstable) periodic states*. We interpret the transitional jet CS dynamics in terms of the periodic states using centerline velocity signals, assuming nominally axisymmetric vortex dynamics. The spatial sequence of the vortex dynamics can be inferred from the velocity trace along the time axis in the reverse direction, i.e., by $t \rightarrow -x$ transformation, in the spirit of Taylor's hypothesis. This correspondence is qualitative since the relative orientation, spacing and strengths of vortices change during the structure passage over a stationary sensor. Figure 3.4 displays two snapshots (obtained using smoke visualization) from the chaotic jet flow, revealing vortex roll up and one/two vor-

tex pairings; the two flow states shown correspond to a period-2 UPO and a period-4 flow state (discussed further later).

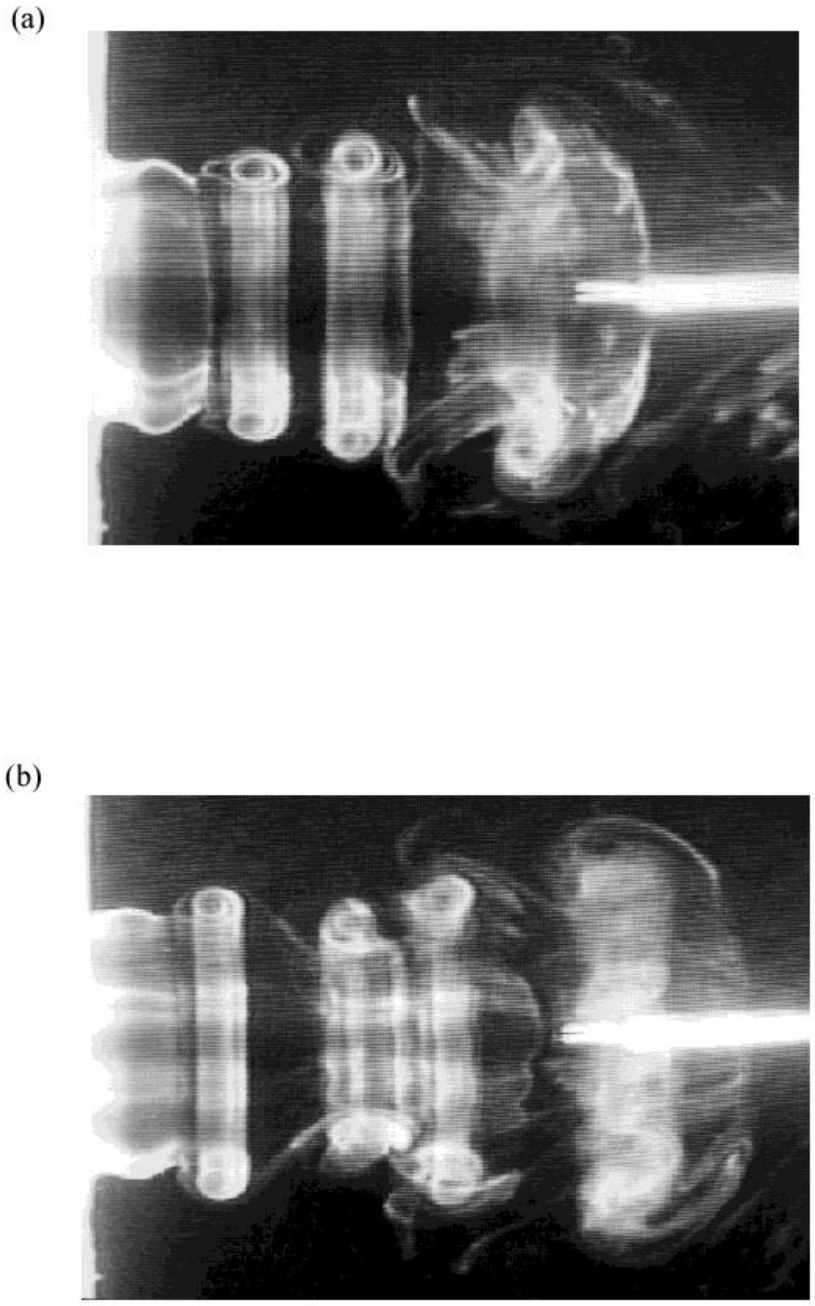


Figure 3.4 Smoke visualization of chaotic jet flow cross-section displaying (a) period-2, and (b) period-4 states, corresponding to transitional axisymmetric jet vortex formation and interaction dynamics.

The realization corresponding to a period-9 flow state shown in Figure 3.5(a) has dominant subharmonic and quarterharmonic frequency components in the induced velocity from advecting once-paired vortices and vortices undergoing a second pairing. This flow state corresponds to a sequence of four once-paired vortices, undergoing two second pairings, and an unpaired vortex (numbered 4). The second pairing process is inferred from the alternating peak-to-peak amplitudes of adjacent subharmonic period segments in the centerline signal; the amplitude variation arises from the different radial locations of the vortex ring cores during pairing (see inset in Figure 3.5a). After 9 periods, the unstable nature of this state causes the deviation of the flow dynamics to other periodic states (with the same or different periods); i.e., the flow undergoes a different sequence of CS interactions.

The signal corresponding to a period-11 state in Figure 3.5(b) reflects a sequence of five first pairings followed by a single unpaired vortex. The period-11 signals in Figure 3.5(c) also reflect a similar sequence of CS dynamics, but the relatively stronger quarterharmonic component implies advanced stages of second pairing (similar to the inset of Figure 3.5a). Thus, more than one kind of periodic state can arise for a given periodicity. Snapshots associated with period-15 flow states (Figure 3.5d) indicate seven first pairings, six of which undergo second pairings, and an unpaired vortex. Similar period-15 realizations containing much lower levels of the quarterharmonic component, i.e., involving no second pairing, are also found (not shown here). The significance of the multiple realizations and the symbols shown in Figures 3.5(c, d) are discussed below.

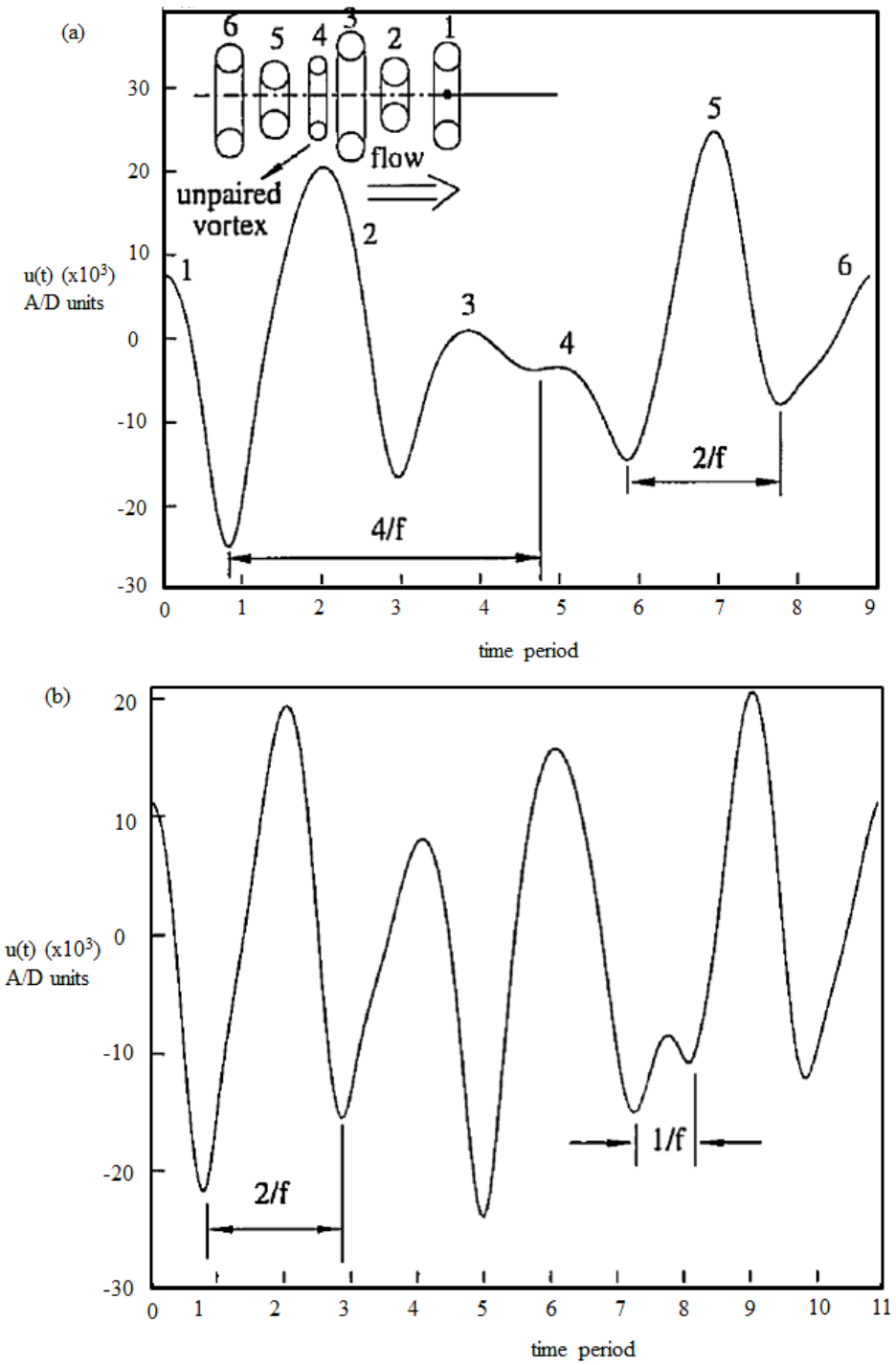


Figure 3.5 (a) A realization of a period-9 UPO obtained from a cluster in Fig. 3.5a; the inset is a schematic of the jet flow vortex dynamics; (b) An instantaneous realization of a period-11 UPO (identified within a phase space cluster, described later).

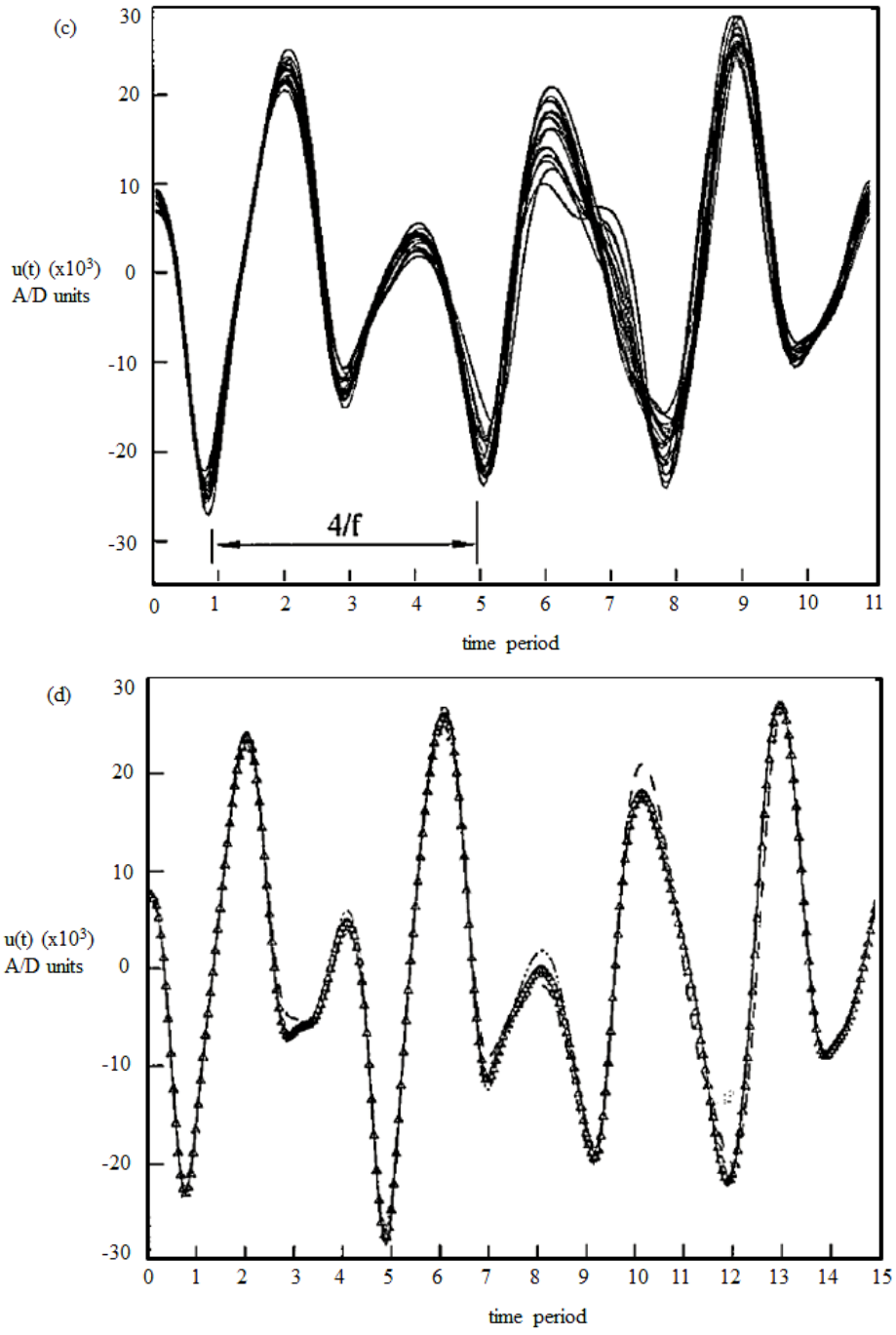


Figure 3.5 (c) Several realizations of period-11 UPO's (identified within a different phase space cluster, discussed later); (d) The solid and dashed lines are snapshots of period-15 UPO's; symbols denote the resulting "average."

In summary, the chaotic flow dynamics sweep through several unstable, nearly peri-

odic states. These states appear as stable periodic flow states, but require high $a_f$ and changes to $St_D$ (Broze & Hussain 1994). It will be shown later that it is possible to stabilize, through control, these unstable states (embedded within the chaotic flow) for lower $a_f$ and fixed $St_D$.

*"Phase-averaged" periodic flow states.* A key feature of the unstable periodic states is that they are found to be nearly identical, with only slight variations in amplitude/phase [see Figures 3.5(c, d)]. Figure 3.5(c) displays realizations corresponding to all period-11 events (sampled from a long velocity trace), revealing striking similarities. Each realization corresponds to the occurrence of a flow state lasting eleven fundamental periods (at different times). The differences between the time traces are most pronounced just after 6 fundamental time periods, when a relatively distinct isolated fundamental period is seen. This represents an unpaired vortex between two stronger, once-paired vortices, which is an unstable configuration that is extremely sensitive to ambient perturbations. This may explain why it is impossible to repeat the same sequence of vortex dynamics each time. Only a few period-15 realizations are shown in Figure 3.5(d) to better illustrate the similarity. The realizations are then averaged, removing slight variations in amplitude/phase, to represent the underlying flow state. Figure 3.5(d) also displays the averaged period-15 realization, which is virtually identical to the individual realizations. Similar results are obtained for other periodic flow states (with same as well as different periods). It is worth noting that the spirit of averaging UPOs described here resembles phase-averaging of multipoint vorticity signals during CS eduction (Hussain 1983), but differs in that the current procedure does not require explicit phase-alignment and thresholding of the signals,

which are necessary subjective features of the CS eduction procedure.

The above results also reveal the flow states which can be targeted for control, due to their intrinsically periodic (albeit unstable) nature. Notably, low forcing levels will suffice to maintain these periodic states via control (see Chapter 4).

Thus far, the dynamics of the jet have been described using single-point measurements made in the downstream region of the jet, where the nonlinearities are significant. In the following section, two-point measurement approaches are presented to determine the spatial evolution of the periodic flow states from the jet nozzle exit plane. This is needed to determine perturbations required at the nozzle lip to stabilize and control periodic flow states observed in downstream velocity signals.

### 3.4 Spatial Development of Unstable Periodic Flow States

The obvious choice for obtaining a unique relationship between the upstream and downstream signals is a "nonlinear transfer function" (Ritz & Powers 1986), which unfortunately involves computationally intensive, error-prone procedures (even for quadratic nonlinearity). The feedback from downstream pairing dynamics, i.e., spatial coupling, guarantees that an upstream velocity signal (at the jet exit) contains footprints of all the periodic states underlying the chaotic flow dynamics. Thus, analyses of periodic segments in the upstream signal, sampled simultaneously with the downstream signal, should reveal (unstable) periodic states as well. For the two-point velocity measurements discussed here, a long-prong hot-wire probe is positioned at an angle at the nozzle exit (near $r/D \cong 0.25$), minimizing probe interference effects, and a second probe is stationed,

aligned with the flow, on the centerline at x/D = 2.

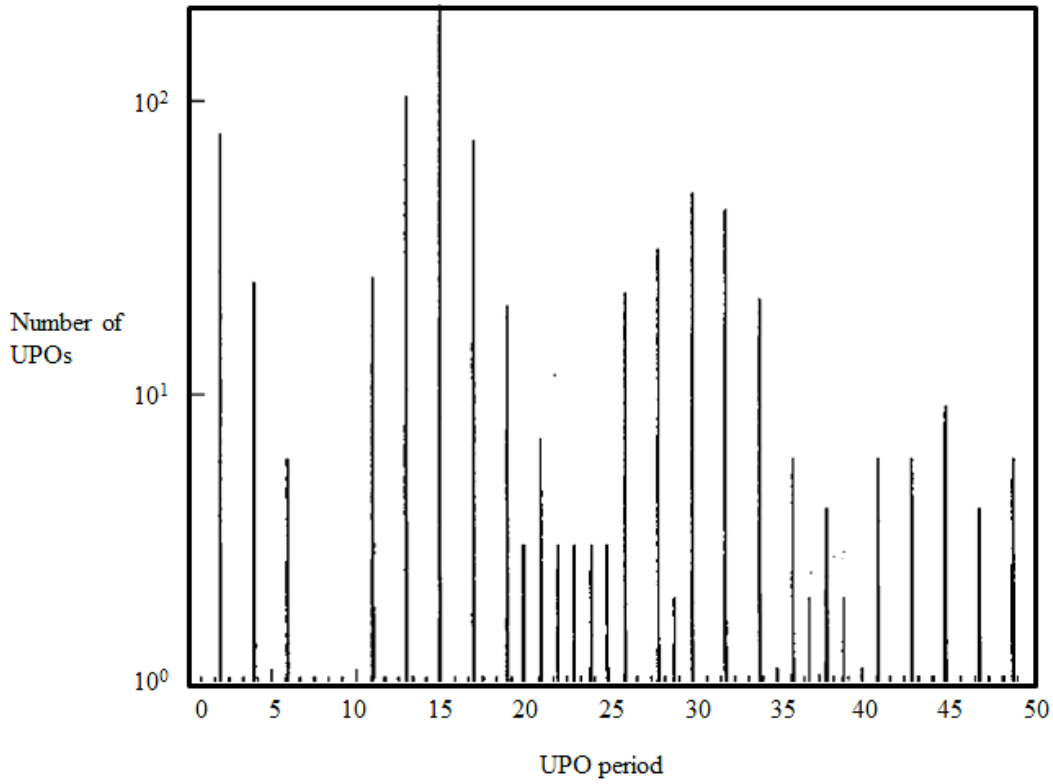


Figure 3.6 The histogram distribution of 'close returns' in upstream velocity signal sampled from chaotic jet flow.

*Direct analyses of upstream signals*. The histogram of the frequency of periodic realizations at the nozzle exit plane shown in Figure 3.6 resembles that in Figure 3.3 (for the downstream signal). The dominance of some frequency components at this upstream location, causes the number of periodic states detected for a certain period to be different in Figure 3.6 (compared to Figure 3.3). The absence of some periodic states in Figure 3.6, which appeared in Figure 3.3, is possibly due to the inability of upstream measurements to resolve some frequency components which are weak in comparison to the dominant fundamental frequency component. Figures 3.7(a, b) display realizations associated with

two different types of period-11 flow states. The small relative variations in the peak-to-peak amplitudes of the dominant fundamental periods are footprints of a periodic downstream CS dynamics sequence; the fundamental has at least an order of magnitude larger spectral energy than the next most significant frequency. Notice that, although the two realizations in Figures 3.7(a, b) are similar, these initial conditions result in entirely different downstream dynamics [see Figures 3.5(b, c)].

To identify the upstream signal segment corresponding to a periodic state found downstream, signals sampled simultaneously at two points are analyzed. It is assumed that feedback is instantaneous and that feedback is dominant compared to background disturbances (evidenced by strong spatial coupling). The downstream vortex pairing feedback signal generated between x/D = 2-4 for the subsonic jet flow is estimated to take 0.3-0.6 msec to propagate upstream to the nozzle exit plane, which is considerably smaller than the dominant time scale of the pairing dynamics which is close to 10 msec (estimated for the subharmonic frequency). This justifies the claim that minimal phase lag is introduced in the feedback recorded in the upstream velocity signal, i.e. feedback is nearly instantaneous. These realizations from the upstream signal are then averaged to determine a perturbation that will guide the downstream flow dynamics to the vicinity of a selected periodic state within the chaotic flow.

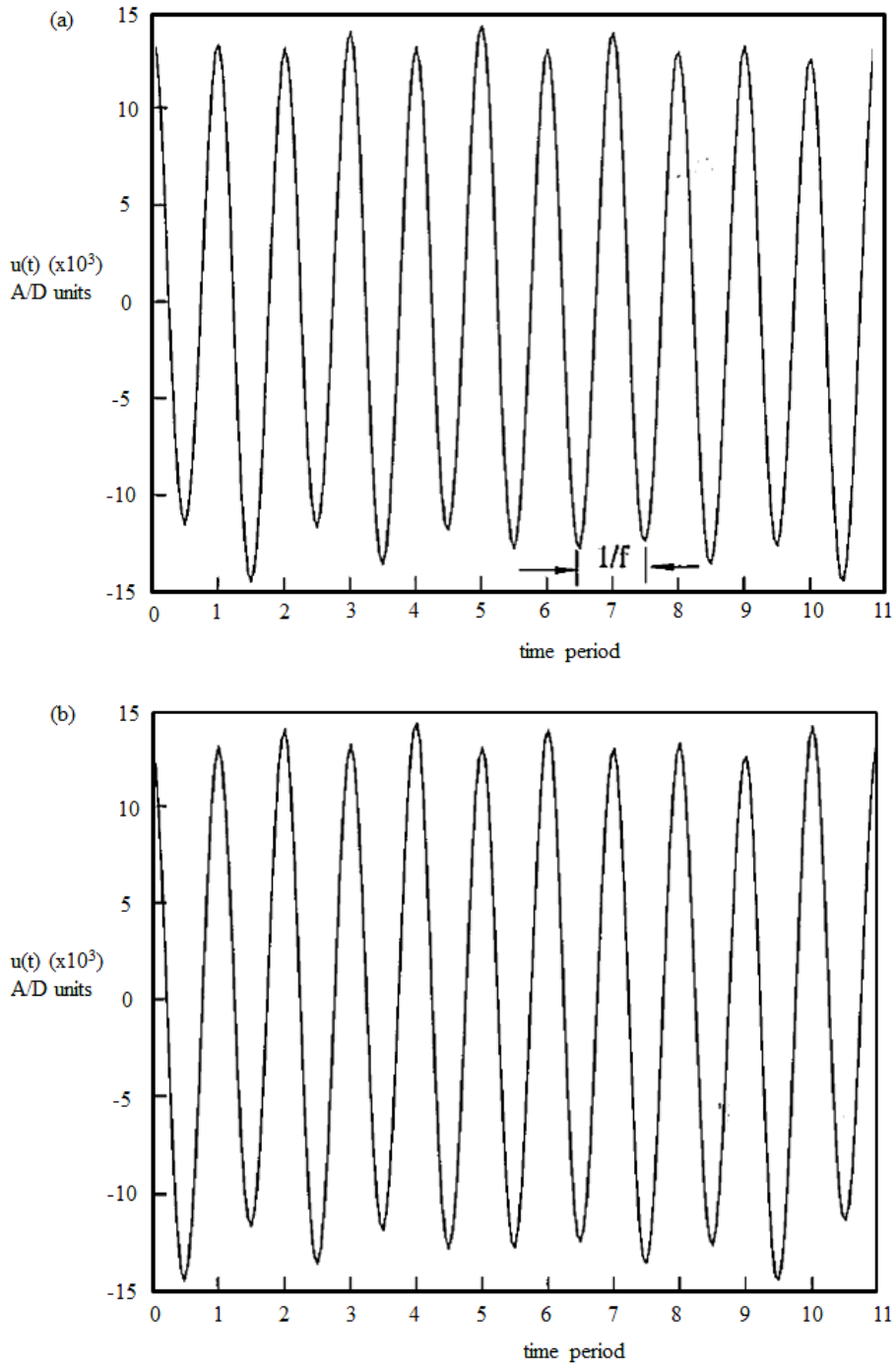


Figure 3.7 (a) An upstream signal realization corresponding to a period-11 UPO extracted from a phase space cluster; (b) An upstream signal snapshot corresponding to a period-11 UPO crossing a second phase space cluster.

Spatial coupling mechanisms for several common open flows (e.g., channel flows,

far wakes, and boundary layers) may not exist or are unknown. However, the well-recognized, dominant role of CS in these flows suggests low-dimensional behavior that can be manipulated for control. For these flows, selective amplification of certain perturbations from a broadband of local disturbances result in nonlinear (perhaps, low dimensional) dynamics downstream. We explore an alternative means to obtain the upstream perturbation needed to produce the desired downstream dynamics – "adaptive filtering" – and test it in the jet experiments. Since this technique does not rely on feedback, it can be used for chaos control in open flows besides jets and mixing layers (where spatial coupling is dominant).

*Adaptive filtering*. This technique has applications in signal-processing areas of modeling, control systems and filter design (Widrow & Stearns 1985). We have used it for "inverse system modeling" by approximating the relationship between a pair of simultaneously sampled signals [x(t), y(t)] using a set of weights. Figure 3.8(a) shows this schematically without displaying the filter weights explicitly. The least-mean-square algorithm to determine the weights is described in Appendix D. Using the estimated adaptive filter and the known averaged downstream realization (corresponding to a particular periodic state) to be controlled $x_{UPO}(t)$, the corresponding upstream perturbation $x_{origin}(t)$ is evaluated (see Figure 3.8b).

Since the periodic states can all be found within the chaotic flow, we use chaotic signals (of at least 300, 000 data points) for evaluating the filter weights, taking simultaneously sampled data at the nozzle exit plane and at x/D = 2. The stepping size $\mu$ (= $10^{-6}$) and the number of weights $N_w$ (= 10, 000) are chosen to yield early error convergence

(within 5000 fundamental periods); these parameters are discussed in Appendix D. The error ε(t) remains converged even after further samples of x(t) and y(t) are provided. The upstream perturbation evaluated is then averaged over the period of the selected periodic state (ignoring initial transients during convergence). This removes effects of slight variations in the filter weights, which continue even after ε(t) appears to converge.

The averaged upstream realization in Figure 3.9 is determined using adaptive filtering on a realization corresponding to a downstream period-11 flow state. Its close resemblance to the averaged perturbation obtained directly from an upstream signal (see Figure 3.7b) demonstrates successful "adaptation". Two means to determine upstream perturbations corresponding to periodic (but unstable) downstream jet dynamics have been presented: the direct analysis of a jet exit signal (which depends on feedback) and adaptive filtering.

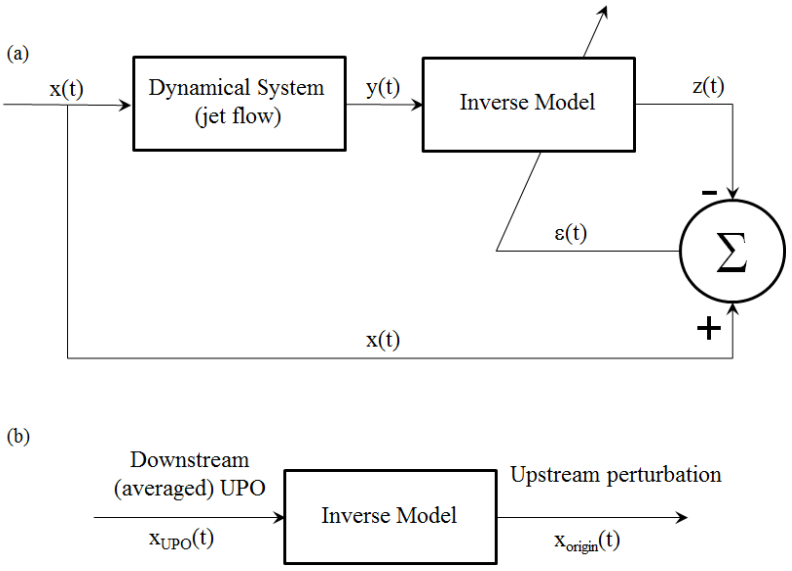


Figure 3.8 Schematic of (a) empirical modeling of spatiotemporal dynamics using adaptive filtering; z(t) is the 'prediction' and ε(t) is the prediction error; and (b) inverse model to determine initial disturbances.

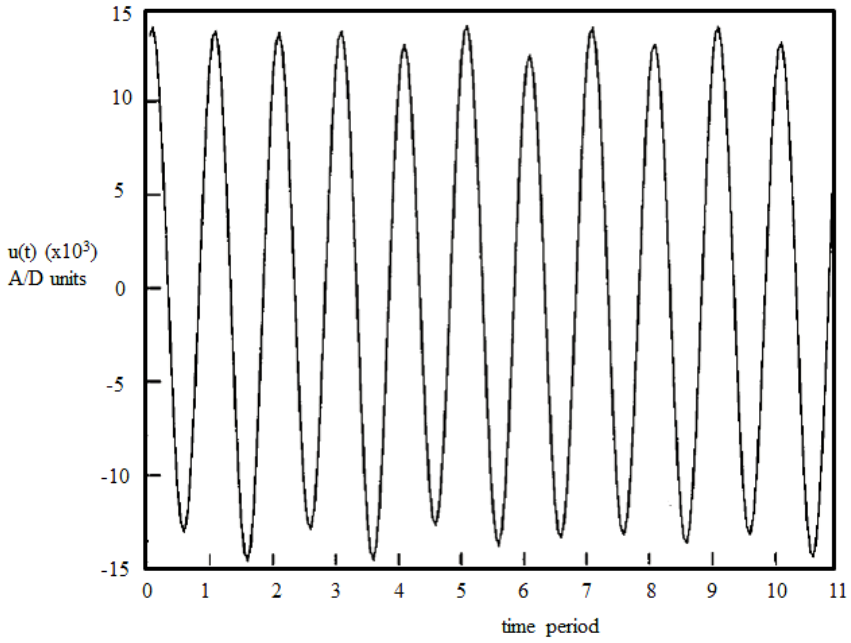


Figure 3.9 The adaptive filter prediction of upstream perturbations for a downstream period-11 UPO from a particular phase space cluster.

# CHAPTER 4

# CONTROL METHOD DEMONSTRATION IN THE AXISYMMETRIC JET

A novel approach to the control of the near-field jet dynamics is presented and demonstrated in this chapter. The problems arising during the control implementation and means to overcome them using a *real-time feedback control* approach are also presented.

## 4.1 Control Approach

Convective instabilities are generally undesirable since their sensitivity to noise makes the description and modeling of open flows difficult. However, they can be taken advantage of for controlling spatially developing flows. By providing appropriate localized perturbations at the point-of-receptivity with sufficient amplitude to dominate over ambient disturbances, one can effect significant changes downstream; conventional methods exploit this for free shear flow control but were restricted to the control of a limited range of (stable) periodic states (Ho & Huerre 1984).

Control requires for a "goal" state to be chosen, which in the present study is desired to be among a large number of periodic flow states. Having chosen the desired periodic state, control can be achieved by providing the appropriate perturbations at the flow origin to maintain the downstream jet dynamics near the selected periodic state. Note that since the chaotic flow switches sweeps through several periodic states, in a long enough time interval the flow dynamics will any selected each periodic state. Evolutions of periodic states (of a selected period) being similar (see Chapter 3), in the absence of "noise"

(i.e., background disturbances within the instability bandwidth), the desired dynamics are expected to be self-sustained for a short duration of at least one oscillation period. Low-level control perturbations must then be provided to prevent the dynamics from wandering away due to the inherently unstable nature of the selected state. For a convectively unstable flow, continuous control is necessary to overpower ambient perturbations, since the growth and advection of disturbances (away from the receptivity point) leaves the flow origin susceptible to new perturbations such as "noise." As noted earlier, pairing feedback induces spatial coupling in this otherwise dynamically open flow; i.e., feedback perturbations generally dominate over broadband ambient disturbances. We expect that, for a chaotic state, although perturbations (primarily from pairings) are fed back to the origin, none of them are strong enough to sustain phase locking. The control provides additional energy at the appropriate frequency components to enhance preexisting feedback and enable phase-locking to a specified flow state, i.e., stabilize the desired periodic flow state. To control the downstream dynamics (i.e., a periodic state), appropriate perturbations needed at the receptivity point are determined as described in Chapter 3. The chaos control concept underlying this nonlinear control method is described in Appendix A.

### 4.2 Open-loop Control Experiments and Results

We now demonstrate the open-loop control approach described above experimentally in the jet. The control effectiveness is evaluated by comparing centerline, longitudinal velocity signals u(t) from the controlled and the desired flows. The periodic flow states chosen to be controlled here were selected to demonstrate the control method and to illustrate the challenges and issues that arise in the implementation of nonlinear control in the

jet flow. Some of these flow states with practically relevant applications have been achieved using prior linear flow control methods (also addressed in Chapter 5), which can successfully target stable periodic states but with significant changes to the control parameters (e.g., high forcing amplitudes). While the practical significance attached to several periodic flow states controlled in the following experiments is yet unclear, their control demonstrates the promise for controlling (potentially useful) unstable flow states.

Following the selection of a (periodic) flow state to be controlled, a periodic signal is generated from the averaged upstream perturbation from the jet exit (see Chapter 3). After filtering out the fundamental frequency component, this signal is provided through a D/A converter and an adjustable external gain to an acoustic speaker, connected through several tubes to a thin slit around the nozzle lip (see Chapter 2).

A period-11 flow state (also see Figure 3.4b) was first chosen to be controlled. This was motivated by the following two reasons: (i) controlling a period-11 state demonstrates the ability to stabilize periodic flow events of relatively large periods, overcoming a common shortcoming in prior nonlinear control methods (e.g., see Ott et al. 1990); and (ii) controlling this flow state having minimal quarterharmonic frequency content will suppress the second vortex pairing. Such suppression has significant implications for the control of practically relevant phenomena such as jet noise, via suppression of quantities such as turbulence intensities or Reynolds stresses; experimental evidence exists which shows far-field jet noise amplification/reduction due to near-field turbulence amplification or suppression (Hussain & Hasan 1985).

The control signal is synthesized from realizations similar to that shown Figure

3.6(b), and low-pass filtered to minimize the otherwise dominant fundamental component, reduced here by more than 2 orders of magnitude. The bulk excitation signal and that provided at the exit are phase-locked at the fundamental frequency, which is not completely eliminated from the exit control signal. Single-frequency bulk forcing is first employed (at $a_f \cong 1\%$ and $St_D \cong 1.2$) to obtain the chaotic flow. The control signal is then continuously applied at the nozzle lip with an external gain which is increased until the desired flow state is sustained, observed by a downstream centerline probe (as in Figure 1.1); the flow is seen to lock on to the selected state after a transient.

For much larger control signal amplitude, we observe a period-11 flow state which does not resemble the desired flow state; i.e., an undesired goal state is obtained. As expected, ceasing control causes the flow to revert back to the (uncontrolled) chaotic dynamics, showing that the low-level control perturbations merely direct the dynamics near the selected flow state.

Figure 4.1(a) displays the close match between a velocity time trace from the controlled flow at x/D = 2 and repeated realizations of the desired period-11 flow state (denoted by symbols) from a downstream chaotic flow signal. (All signals have been time-shifted to best align the desired and the controlled states without amplitude re-scaling.) Note that, the desired period-11 realization is observed only for one orbital period in the chaotic flow, while it is sustained indefinitely (with weak modulations) in the controlled flow. The discrepancies between the controlled and desired flow states are discussed later in this section.

Surprisingly, the nozzle exit signal (near the centerline) and the control perturbation, denoted by symbols, also match very closely (see Figure 4.1b). Thus, the amplitude of the perturbations to achieve the period-11 dynamics is not much larger than that, available via feedback, in the uncontrolled flow; this is because forcing is needed only to preserve the period-11 flow state, not to excite it. The low-level control energy provided is also seen in the power spectrum of an upstream velocity signal from the controlled flow (see solid line in Figure 4.1c).

The power spectrum of the downstream signal in the controlled flow is shown in Figure 4.1(d). In comparison to the velocity spectrum from the chaotic flow (see Figure 3.2b), the sidebands around the subharmonic frequency are sharper, the modulation frequency, now at 24 Hz, is stronger (30 dB above background), and the broadband quarterharmonic is uniformly suppressed by at least an order of magnitude (except for weak modulation frequencies at 48 Hz and 72 Hz). The absence of the quarterharmonic frequency component is also evident in the time trace (Figure 4.1a). Moreover, the broadband spectral background is uniformly suppressed by at least 10 dB. The broadband pedestal below the sidebands around the subharmonic frequency is due partly to slight aperiodic modulations in the controlled flow (also evident in Figure 4.1a) and partly to spectral leakage while resolving nearby frequencies of discrete power spectra. Further interpretation of these control results with a dynamical systems perspective is provided in Appendix A. Similar results (of the control of a period-11 state) were also obtained by using the upstream control perturbation estimated by an adaptive filter approximation described in Chapter 3.

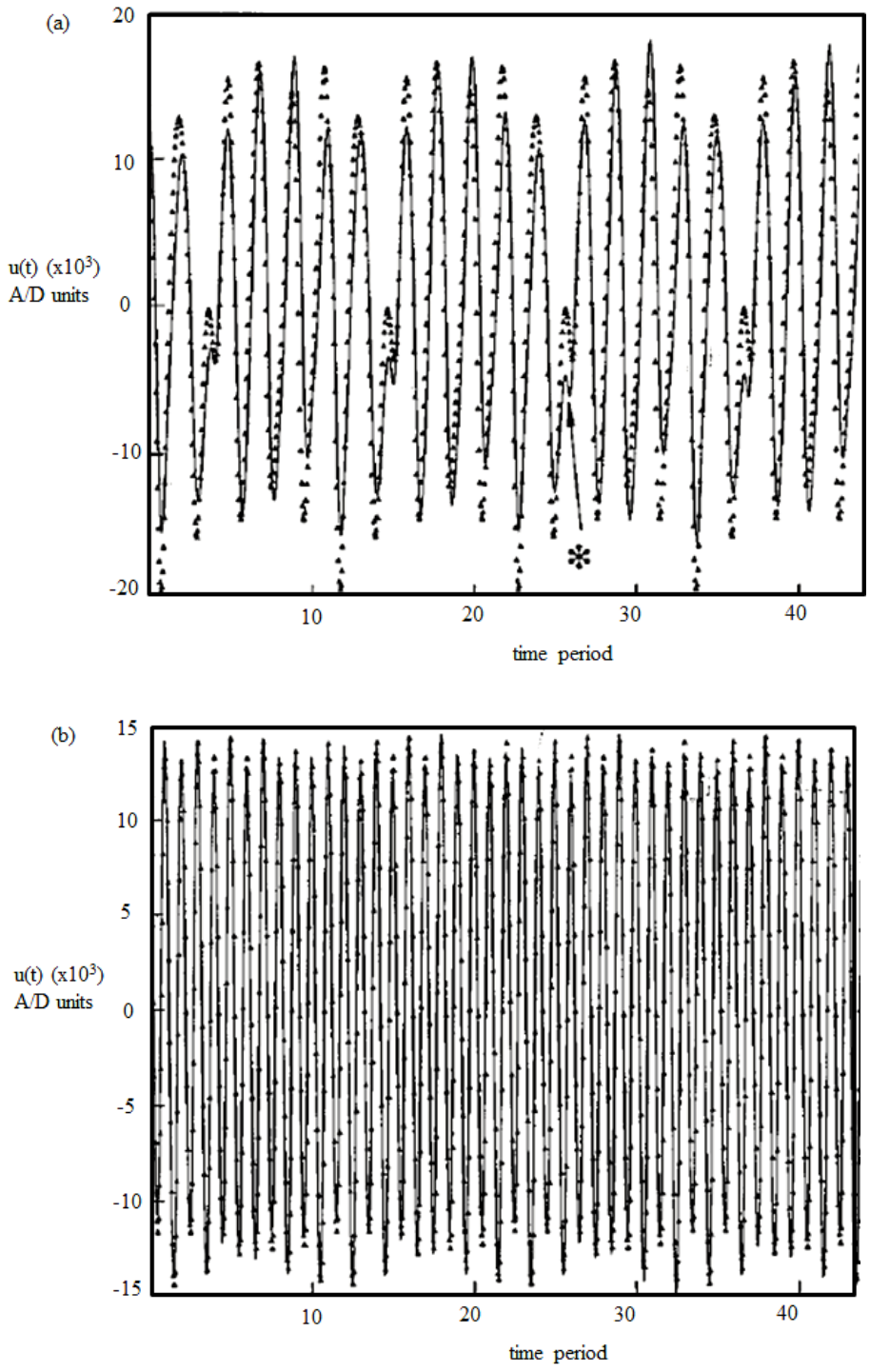


Figure 4.1 (a) The velocity signal from the controlled flow matches that of period-11 UPO in chaotic flow (denoted by symbols); '*' denotes the fundamental period; (b) The similarity of the nozzle exit signal in the controlled and uncontrolled flow (see symbols) show minimal control needed.

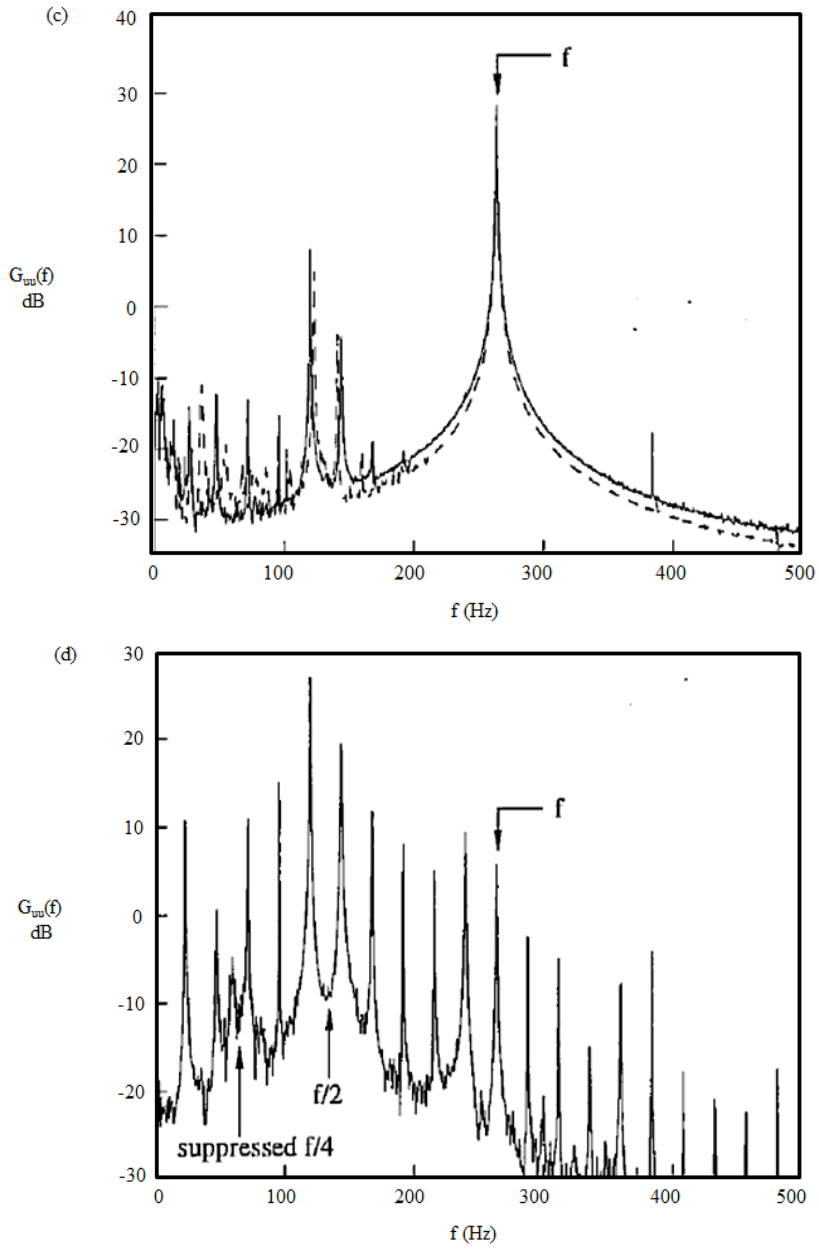


Figure 4.1 (c) Power spectra from controlled (solid line) and uncontrolled (dashed line) flows; (d) Downstream power spectrum of controlled flow (at x/D=2) showing f/4 suppression.

To test the controllability when multiple periodic states of the same period exist, a different period-11 realization like that shown in Figure 3.5(c) was chosen for control. Using an upstream control perturbation resembling that in Figure 3.7(c), the selected period-11 flow state is stabilized. The close match between the controlled flow and the desired period-11 realization in Figure 4.2 demonstrates that the control method can be effective even in the presence of more than one type of periodic state with the same period.

The control of period-13 and period-9 flow states is seen in Figures 4.3 and 4.4, which show signals from the controlled flow and the corresponding averaged realizations from the uncontrolled (chaotic) flow. Absence of the quarterharmonic frequency component in Figure 4.3 indicates nearly complete suppression of the second pairing. Due to the shorter fundamental instability wavelengths at these large $St_D$ (> 1), the second pairing is usually unavoidable in the uncontrolled jet. The periodicity of these controlled states is maintained for about 4 jet diameters, whereupon the jet transitions to turbulence. On the other hand, a different period-13 flow state (with dominant quarterharmonic) could not be controlled; the flow was seen to frequently wandered away from the selected state to the one shown in Figure 4.3. Potential reasons for this loss of control are discussed in Appendix A. "Adaptive" control may be needed to resolve such a problem.

The discrepancies between the controlled flow state and that desired [see signals in Figures 4.1(a), 4.2, 4.3 and 4.4, and spread in the spectral peaks (Figure 4.1b)] – indicating the occasional drift of the dynamics away from the desired periodic flow state – seem to result from: (i) the uncertainty in determining the control perturbations, and (ii) ambi-

ent disturbances (e.g., blower oscillations, wind tunnel acoustics) within the band of frequencies present in the exit control perturbations. Errors in computing appropriate upstream perturbations can make it difficult to achieve "perfect" control of a periodic state, since small changes in initial conditions for this chaotic flow will cause noticeable differences farther downstream. These errors can arise from the averaging of realizations in upstream signals or as random errors in the adaptive filtering method. Occasional drifts in the controlled flow may also arise since the control disturbances at the receptivity point (i.e., the nozzle exit) co-exist with ambient disturbances in the same frequency band, but with randomly varying phases and perhaps comparable amplitudes.

The sensitivity of convectively unstable flows to external noise is well known. A mere increase in the amplitude of the control signal does not solve the problem, since this could force the flow to undesirable dynamics that does not even exist in the uncontrolled flow. The uncontrolled chaotic flow has been verified to be nominally axisymmetric for at least the first two pairings (see flow visualizations in Chapter 5), but the downstream vortex dynamics in the controlled flow is not yet studied. Vortex pairings are known to delay/suppress three-dimensionality, hence transition, in free shear flows. Thus, the controlled flows with suppressed second pairing may develop three-dimensionality at relatively farther upstream locations. Such behavior will also cause aperiodic modulations in a single-point time series measurement.

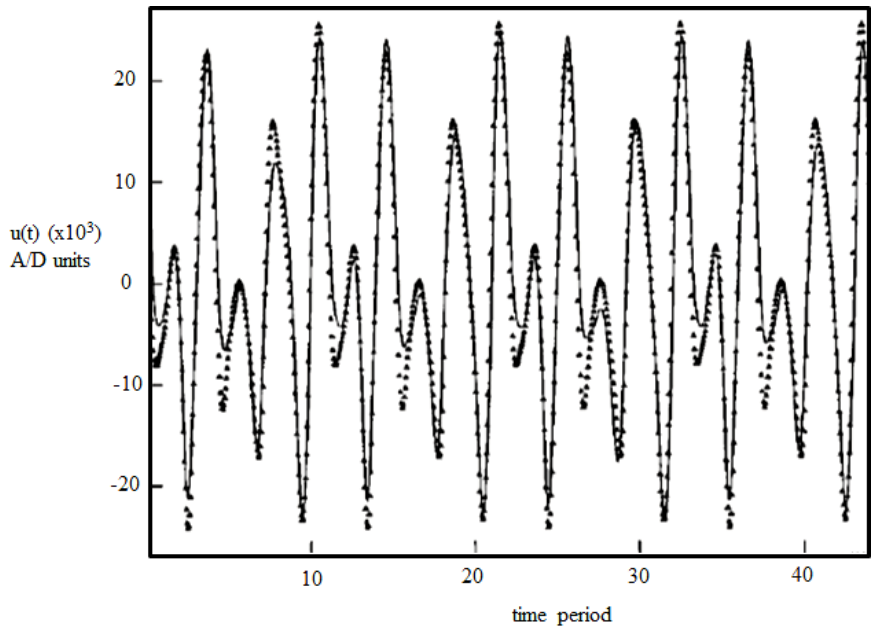


Figure 4.2 The controlled period-11 signal (from cluster-II in Fig. A.3b) compared with repeated realizations of the uncontrolled period-11 UPO (see symbols).

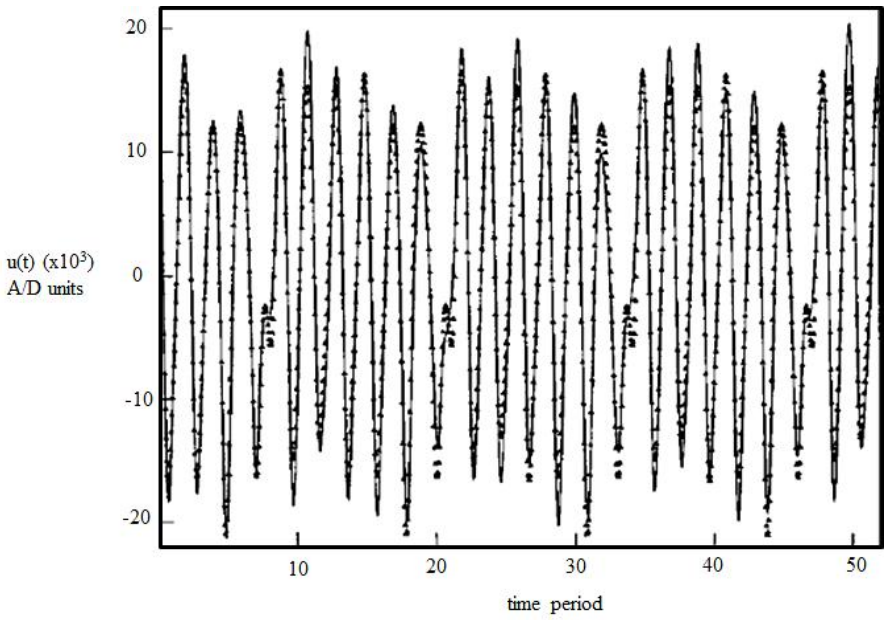


Figure 4.3 The controlled period-13 signal compared with repeated realizations of the uncontrolled period-13 UPO (see symbols).

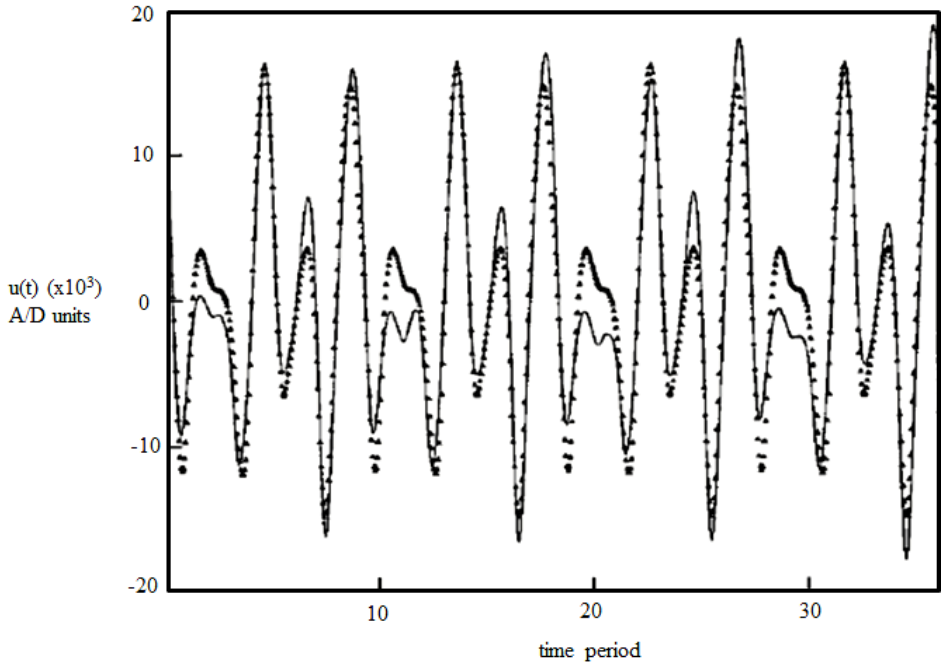


Figure 4.4 The controlled period-4 signal compared with repeated realizations of the uncontrolled period-4 UPO (see symbols).

In summary, the dominant (yet unstable) periodic dynamics in a low dimensional, chaotic jet flow are used to control desirable flow states. Successful control was shown experimentally by verifying the close match between the controlled flow and that selected from the uncontrolled chaotic flow. The use of such an open-loop control approach to sustain otherwise unachievable states (e.g., using linear control methods) is evident from the pairing suppression demonstrated here for $St_D > 1$, wherein second vortex pairing is unavoidable.

### 4.3 Feedback-based Control Approach and Results

The open loop method presented above is sensitive to ambient flow disturbances and empirical modeling errors. A feedback or an adaptive control strategy, having real-time

input about the flow conditions during control, is expected to be more "robust." In particular, the control of flow states with large periods (e.g., greater than period-15) using the open-loop method was ineffective in that frequent excursions from the selected flow state were noticed. It is expected that control using feedback will prevent such deviations from the selected (periodic) goal state; appropriate changes for maintaining the chosen goal state can be made to the controller (which provides the perturbations) in real time, by sensing the departure of the controlled dynamics away from the desired flow state. However, as discussed in Chapter 1, feedback control of spatially developing flows is particularly challenging due to time delays in control computations and that between sensing and actuation.

The presence of feedback in the jet implies that measurements anywhere within the spatially coupled domain will reflect the "global" dynamics of this flow. It may therefore be possible to use a centerline feedback sensor at the jet nozzle exit to sense the controlled flow conditions in real time and feedback changes to the control location (also at the nozzle exit). Note that, due to spatial coupling, there exists a nominally unique relationship between periodic states inferred via the downstream velocity traces and those acquired at the nozzle exit plane. The flow response to the changes in the control signal will be slightly delayed; however, these delays (e.g., for propagation of acoustic perturbations within the excitation system) will be much smaller than the period of the flow state we wish to control.

The simplest form of (linear) feedback control would be to feed a signal proportional to the difference between the controlled flow state and the desired flow state. The control

perturbation, to be provided at the nozzle lip, will have the form: $u_{control}(t) = \alpha*[u_{UPO}(t) - u(t)]$, where $u_{control}(t)$ is provided as excitation at the nozzle lip, $\alpha$ is some adjustable gain, $u_{UPO}(t)$ is the upstream footprint of a selected periodic (but unstable) flow state (obtained *a priori* from a downstream velocity signal) and u(t) is the real-time velocity signal from a probe placed on the jet centerline in the nozzle exit plane. This is analogous to feeding back a "tracking error" (between the controlled flow and the desired flow). Prior analysis of the downstream dynamics is essential for goal state identification (in particular, when multiple types of periodic flow states are present in the uncontrolled flow).

In the following, the experimental results from controlling two periodic flow states with relatively large periods (viz., period-15, 17) are presented, which the open-loop control method failed to stabilize. The control experiment was performed as a proof-of-concept demonstration and the practical significance of controlling these states is not yet evident. The method for determining the control perturbations (using direct analysis of upstream signals) was described in §3.3. A control signal of the form described above (i.e., $\alpha*[u_{UPO}(t) - u(t)]$) was provided at the nozzle lip; u(t) was provided from a probe located on the centerline in the nozzle exit plane.

Figures 4.5(a,b) display the upstream and downstream centerline velocity signals from the controlled period-15 flow. The low forcing levels used (Figure 4.5a) and the periodicity of the controlled flow (Figure 4.5b) are evident. Figures 4.6(a,b) show the upstream and downstream velocity signals from the controlled period-17 flow, revealing successful control using low-level control perturbations.

After being maintained for large times (more than 100 fundamental periods), these controlled flow states deviated from the selected goal state for a short period (typically several fundamental periods) before returning to the desired flow state. When the controlled flow matches with the selected periodic flow state, very low levels of forcing are present at the exit, i.e., $u_{UPO}(t) - u(t) \approx 0$, leaving the flow susceptible to background disturbances. Thus, control may become ineffective and the flow tends to revert to the uncontrolled dynamics. However, as soon as this change in the flow response is detected by the upstream probe, the "tracking error" increases, becoming large enough to maintain the selected flow state. Note that, these episodes of "loss of control" appear only when the controlled flow and the selected flow are very closely matched. This exposes a weakness of the simple feedback-based control of a noise-sensitive flow.

A promising approach is to generate control perturbations using an adaptive filter, wherein the control adapts automatically to changing flow conditions in a "noisy" ambiance. The control computations obviously become more cumbersome, but "tracking accuracy" is greatly improved. Further discussions of prospective methods for "adaptive control" are presented in Chapter 6.

The preliminary results shown above are promising for the development of a "robust" control method for jet flows. Further comparisons of the controlled flows using open-loop control and feedback control including quantitative measurements (of turbulence characteristics) are needed before pursuing the refinements suggested above and in Chapter 6.

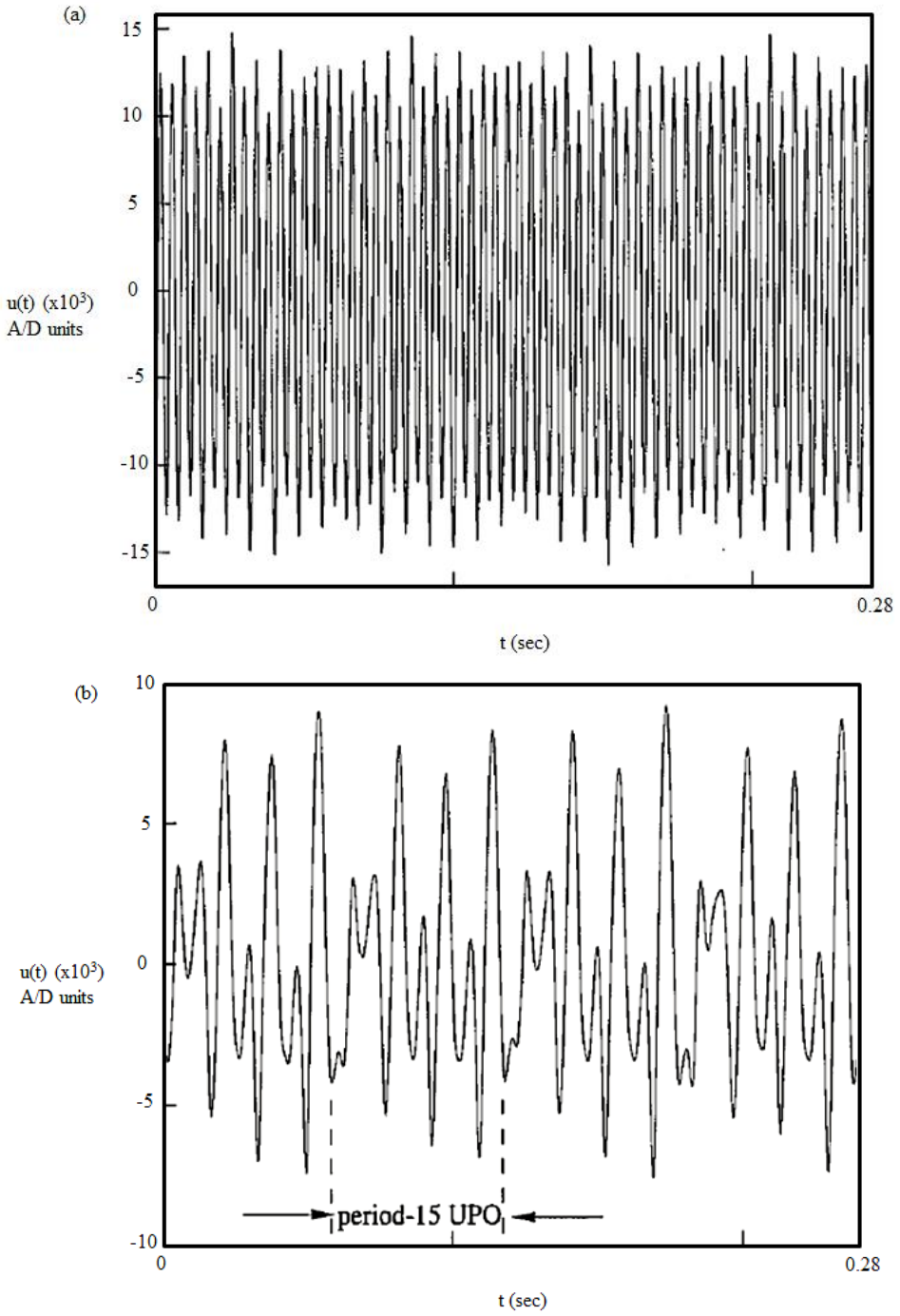


Figure 4.5 (a) Upstream signal from feedback-controlled period-15 flow state, showing a dominant fundamental component; (b) Centerline velocity signal ((at x/D=2) for feedback-controlled period-15 flow state.

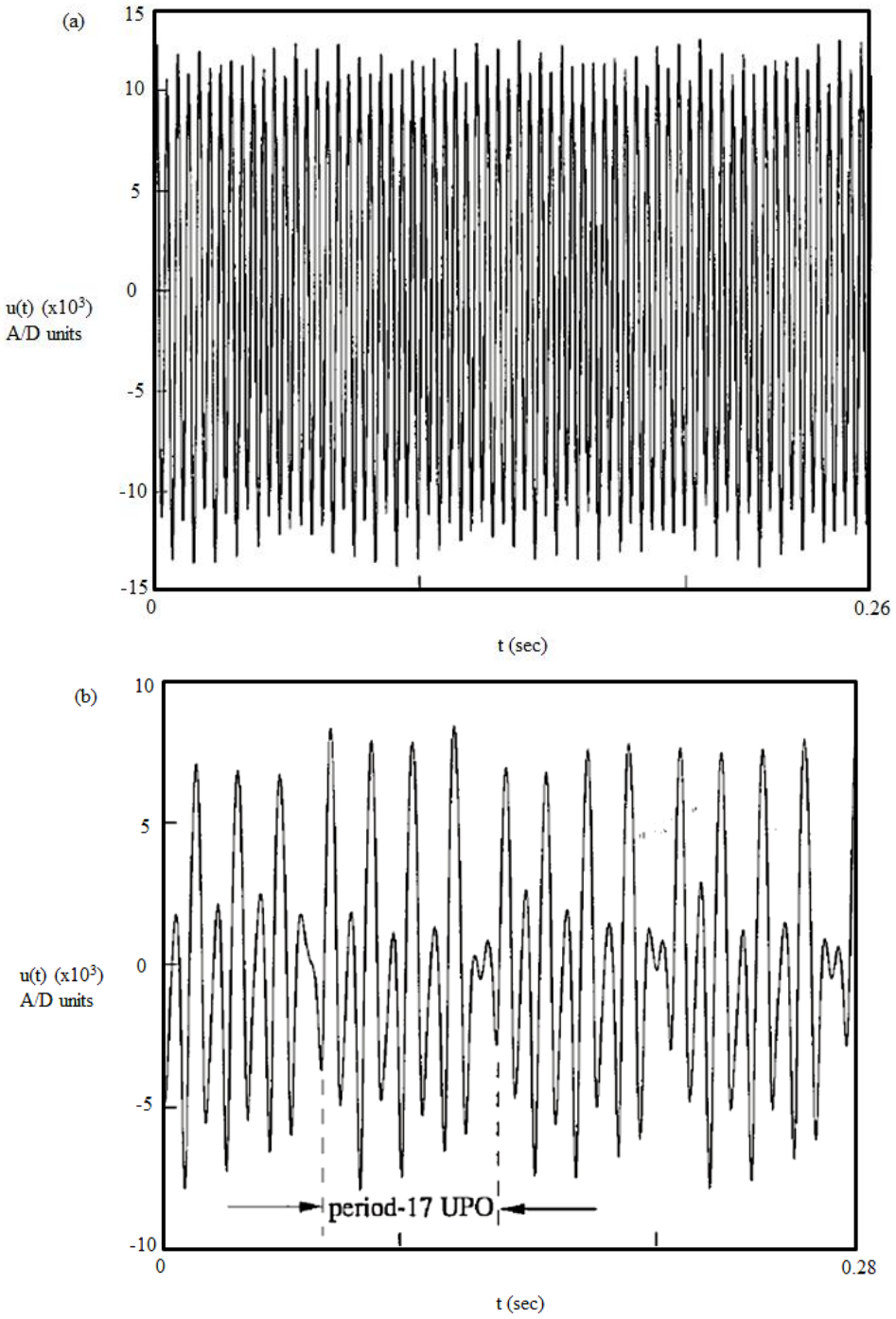


Figure 4.6 (a) Upstream signal from feedback-controlled period-17 flow state, showing a dominant fundamental component; (b) Centerline velocity signal ((at x/D=2) for feedback-controlled period-17 flow state.

# CHAPTER 5

# JET TURBULENCE CONTROL

## 5.1 Turbulence Suppression

The turbulence characteristics in the near field of the jet are dominated by the CS dynamics involving the formation and interactions of ring-like vortical structures. To achieve turbulence suppression, we propose to suppress the energy containing CS in the jet near field, in particular, the vortex pairings. The primary (Kelvin Helmholtz) instability, being forced here to obtain chaotic dynamics, is unavoidable. It is expected that, pairing suppression will result in the formation of relatively weaker (compared to the uncontrolled flow) vortices, creating lower turbulence levels and perhaps breaking down earlier.

Since our chaos control strategy targets goal states in phase space, while control effectiveness is evaluated in physical space, we must associate the UPOs (in the chaotic attractor) with desirable flow states. The most obvious choice of UPOs to be controlled for pairing suppression are the ones that have minimal (in spectral energy) subharmonic/quarterhamonic frequency content. Since UPOs with minimal subharmonic frequency content are not found in the chaotic attractor studied here, we chose a period-2 UPO, which is associated with vortex ring formation followed by a single vortex pairing; i.e., the second pairing is suppressed.

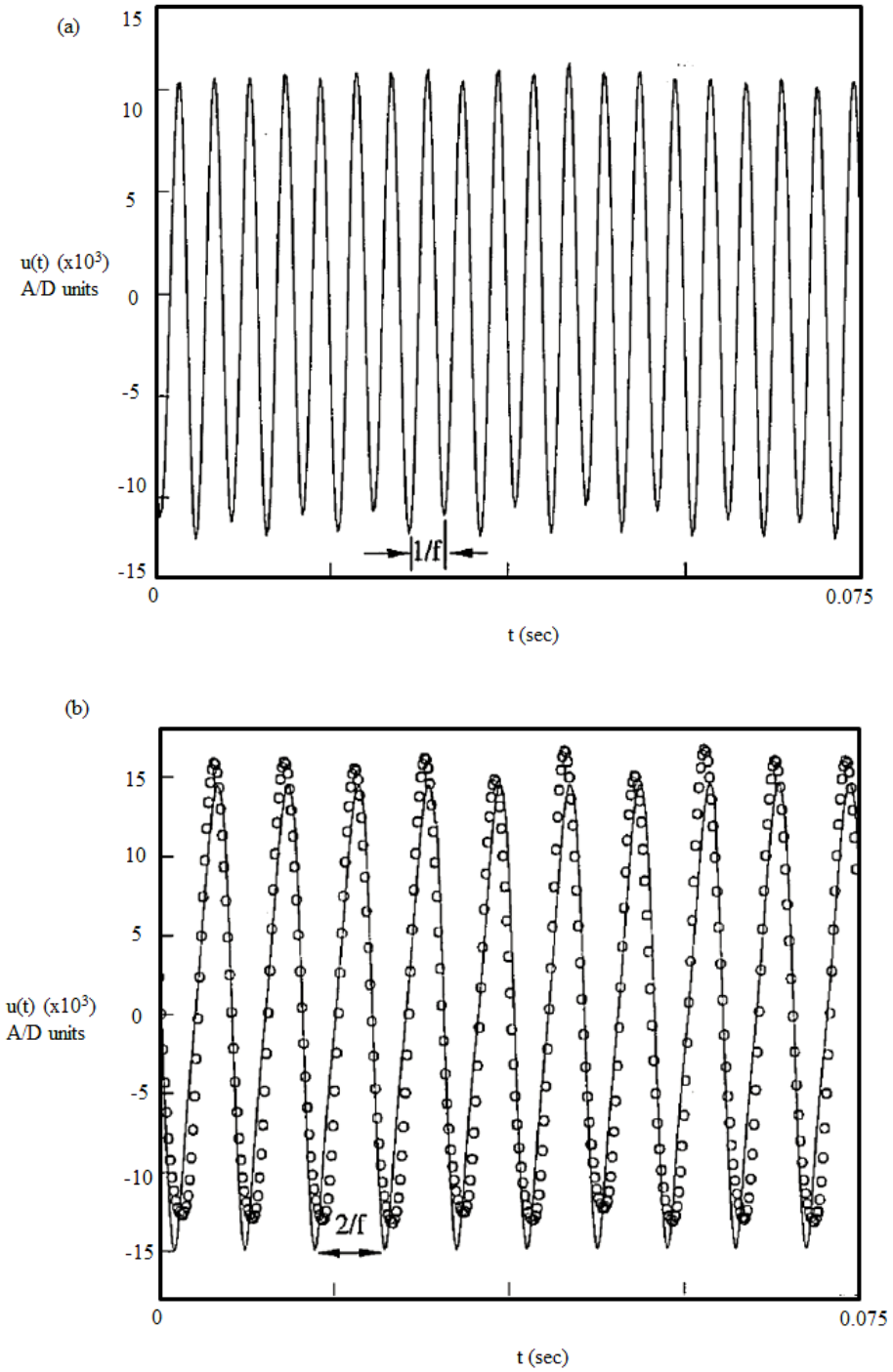


Figure 5.1 (a) Upstream longitudinal velocity signal from controlled period-2 flow state, showing low-level forcing levels (excluding the fundamental frequency f) used; (b) Centerline velocity signals (at x/D=2) for controlled period-2 flow (see symbols) and desired flow state (see solid line).

(c)

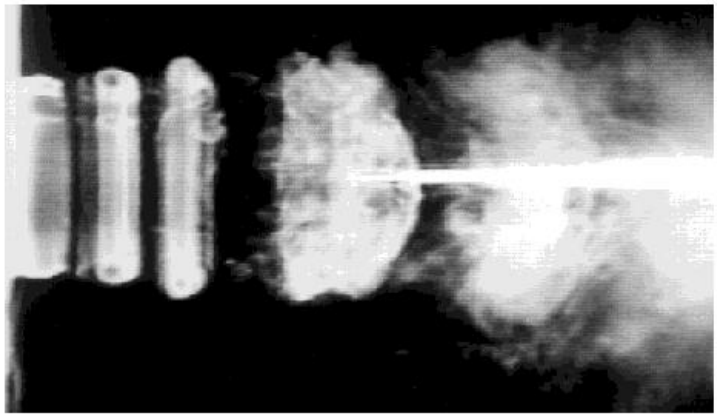

(d)

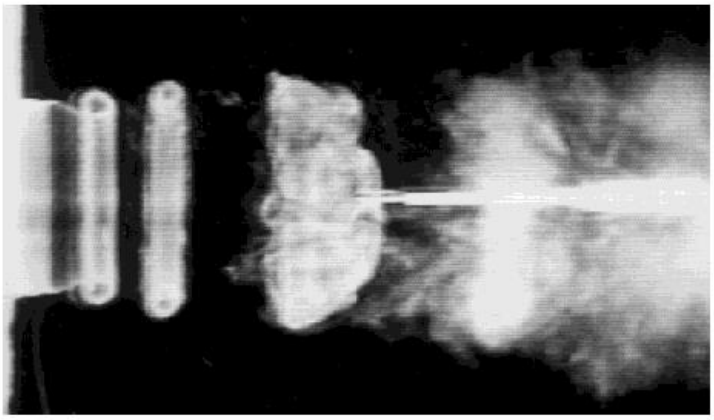

Figure 5 (c) and (d) Smoke visualization snapshots for controlled period-2 jet flow state.

The control signal used to stabilize a period-2 UPO is shown in Fig. 5.1a, displaying a centerline velocity signal at the nozzle exit plane. The control perturbations were determined by the method described in Sec. 3.2. The low forcing levels for the subharmonic frequency component $u'_{f/2}/U_e$ ($\cong$ 0.2%) are evident. The centerline velocity signal (at x/D = 2) from the controlled flow, shown in Fig. 5.1b (see symbols), matches well with the desired period-2 UPO (found in the *uncontrolled* chaotic flow). Smoke flow visualization photographs of the jet near field after applying control are shown in Figs. 5.1(c,d). The snapshot looks very similar to that shown in Fig. 3.6(b), with a single vortex pairing completed near x/D = 2. However, in contrast to the chaotic state, this controlled flow state is maintained indefinitely in time. Identifiable vortices in the controlled flow seem to be present for x/D < 4, after which the jet breaks down to turbulence. The paired vortex rings (with diffuse cores) also appear to develop some three dimensionality around x/D = 3, suggesting earlier (in x) transition compared to the chaotic flow, where the frequent second vortex pairings (on the average) occur.

Figures 5.2(a-e) display the centerline velocity time traces recorded at various streamwise locations (viz., x/D = 1, 2, 3, 4, 5) from the jet nozzle exit. The periodic nature of the controlled flow (with dominant fundamental and subharmonic periods) is evident in these signals up to x/D $\cong$ 4. The lack of discernible periodic features in velocity signals recorded for x/D $\geq$ 4, suggests the breakdown of the jet to turbulence in the range 3 < x/D < 5. The spatial extent of control in this flow is better quantified via coherence measurements, which was shown by us to be a reliable measure of spatial coupling in

spatiotemporal DS (Broze et al. 1997); see Appendix B for coherence computation details. High coherence ($\geq 0.8$) indicates strong spatial coupling, while low coherence is indicative of spatiotemporal behavior arising from phase incoherence; such incoherence can appear due to three-dimensional (or turbulent) CS dynamics. High coherence for the subharmonic f/2 frequency component is indicative of strong spatial coupling in the flow up to $x/D \leq 3$ (see Fig. 6.3); for $x/D > 3$, the rapid drop in coherence, indicating spatiotemporal dynamics, appears to be due to the breakdown of the jet to turbulence (consistent with the above results). As expected, coherence for the fundamental frequency f remains high for similar streamwise distances, but is not shown because it was periodically forced prior to the application of control.

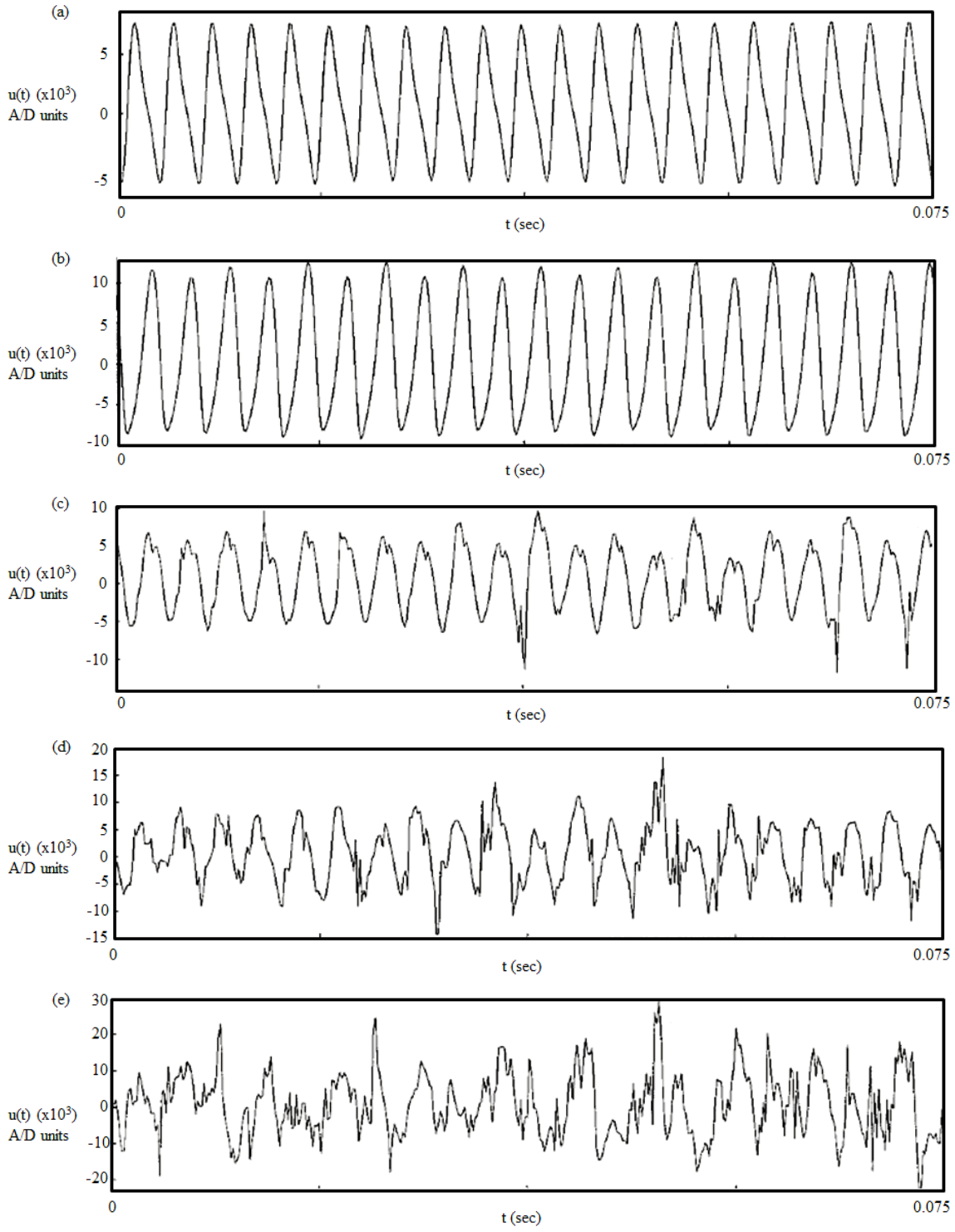


Figure 5.2 Centerline longitudinal velocity signals for controlled period-2 flow state at x/D = 1 (a), 2 (b), 3 (c), 4 (d), 5 (e).

We evaluate the degree of turbulence suppression by comparing the following near-field turbulence characteristics in the controlled flow and the *unforced* flow: the spatial evolution of the (linear and nonlinear) instabilities, the longitudinal turbulence intensity levels and the mean jet spread. Since the CS dynamics being controlled are nominally axisymmetric, we expect the measurements of the longitudinal turbulence intensity levels to be representative of the near-field turbulence characteristics. Note that, comparisons are made with the unforced flow where no external forcing (even of the primary instability) is employed. The single hot-wire probe used for the following measurements was aligned with the flow direction and could be traversed along (in x) and across (in y) the jet in steps of 1/1000in. See Appendix A for further details.

Figure 5.4 displays the streamwise evolution (on the centerline) of the spectral amplitudes of the fundamental $u'_f/U_e$ and subharmonic $u'_{f/2}/U_e$ frequency components in the controlled period-2 flow (see open symbols). The exponential growth and saturation of the subharmonic f/2, resulting in a complete first pairing by $x/D \cong 2$, is preceded by vortex formation (as a result of the saturation of the fundamental f). The quarterhamonic amplitude $u'_{f/4}/U_e$ (see open symbols), although displaying linear instability type growth, remains suppressed (below $u'_f/U_e$ and $u'_{f/2}/U_e$) up to $x/D \cong 5$, i.e., does not reveal (nonlinear) subharmonic resonance (Husain & Hussain 1995). Beyond $x/D \cong 5$, the potential core of the jet collapses and the vortices begin to break down, transitioning to turbulence. We expect that this suppression of the second subharmonic resonance (resulting in a second pairing), which is unavoidable in the uncontrolled chaotic flow, will produce turbulence suppression.

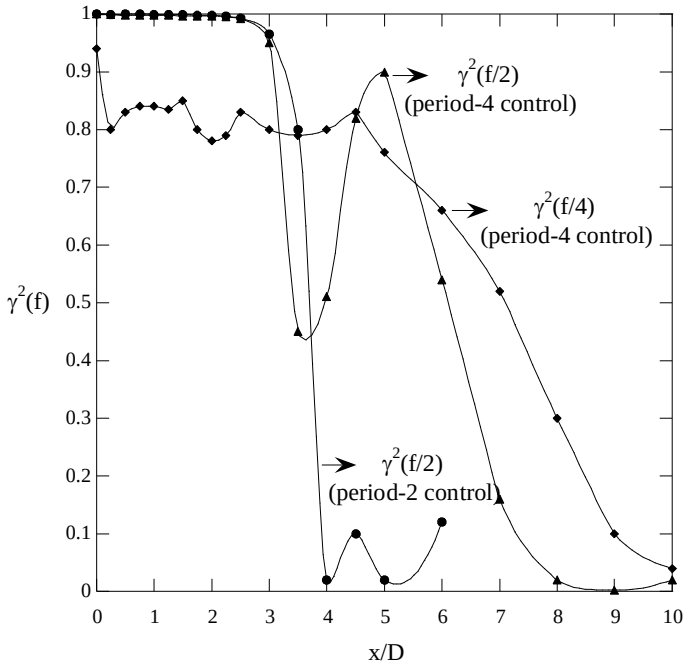


Figure 5.3 Spatial evolution of coherence $\gamma^2(f)$ for dynamically significant frequency components for controlled period-2, period-4 flow states.

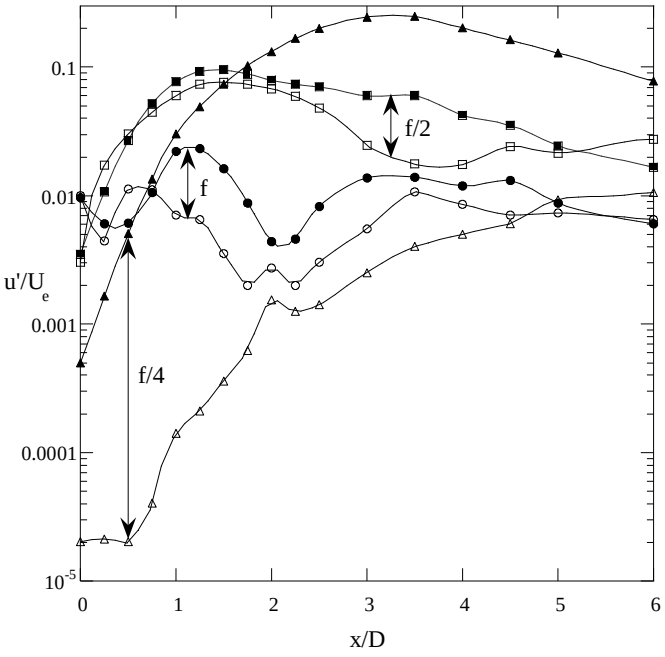


Figure 5.4 Spatial evolution of spectral amplitudes corresponding to instability modes in controlled period-2 (open symbols) and period-4 (solid symbols) flows.

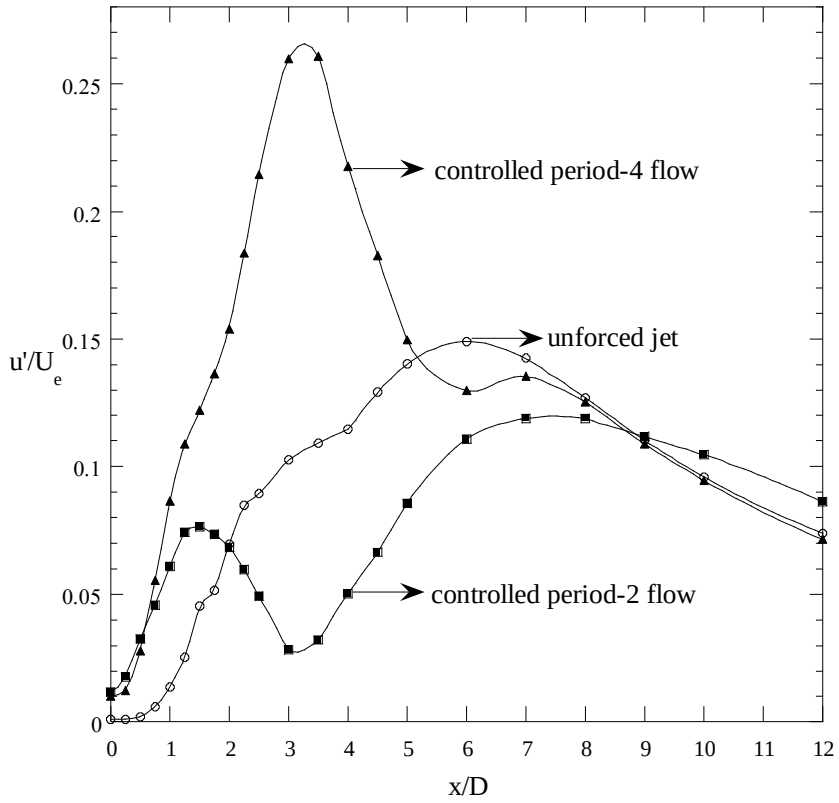


Figure 5.5 Streamwise evolution of longitudinal turbulence intensity levels on jet centerline for unforced and controlled flows.

Figure 5.5 displays the longitudinal turbulence intensity levels $u'(x)/U_e$ for the unforced jet (see circular symbols) and controlled period-2 flow state (see square symbols) on the jet centerline, where $U_e$ is centerline the jet velocity at the nozzle exit plane. The initial increase in $u'(x)/U_e$ for the controlled flow is expected due to the periodic vortex formation (by $x/D \cong 0.5$) and periodic first pairing (by $x/D \cong 2$), as opposed to the unforced jet where these events occur aperiodically in x and time. The extent of suppression ($\leq 70\%$) is evident in the $u'(x)/U_e$ levels for $x/D \geq 2$ and persists up to $x/D \cong 9$, wherein weaker (in circulation) vortices breakdown to lower turbulence levels.

To further evaluate the spatial extent of turbulence suppression, we also present pro-

files of turbulence intensities $u'(x, y)/U_e$ in the unforced and controlled jet flows. Measurements of $u'(y)/U_e$ are reported for streamwise locations $x/D \geq 1$, where suppression effects (due to pairing events) are more evident. Figures 5.6(a-f) display $u'(y)/U_e$ for the controlled period-2 flow (see solid lines and symbols) and the unforced jet (see dotted lines and symbols) for $1 \leq x/D \leq 7$. Significant suppression is evident in the profiles recorded for $1.5 \leq x/D \leq 5$. The tails for the controlled flow are larger than for the unforced flow; this appears to be due to the diffuse vortex ring cores and early (in x) transition noted in the flow visualizations. The peaks and valleys appearing in the controlled flow are expected due to the periodically occurring vortex rollups and pairings; in contrast, the aperiodic nature of the uncontrolled flow results in "smoother" profiles. This integrated suppression effect across the jet is evident in Fig. 5.7, which displays the reduction in $u'_t(x)$ (the integrated $u'(y)$ for each x-location) for the controlled period-2 flow (see solid square symbols); the integration procedure is explained in Appendix A. Suppression in excess of 38% (compared to the unforced jet) is seen in the range $2.5 \leq x/D \leq 4$ and persists well beyond the end of the potential core (which appears to end near $x/D \approx 4$).

Since weaker structures are less effective in engulfment of surrounding ambient fluid into the jet core, we expect that the controlled jet (involving pairing suppression) would (on the average) spread less compared to the unforced jet. We use the jet half width $y_b/D$ (such that $U(y_b) = U_{centerline}/2$) as an indicator of the extent of mean jet spread (see Fig. 5.8). The initial increase in jet spread for the controlled flow (see solid line and square symbols), compared to the unforced flow, is a result of the periodic vortex ring formations and their first pairing. However, the jet spread rate decrease for $x/D \geq 3$ results in

a 10% lower jet spread for $x/D \geq 5$, where stronger vortices in the uncontrolled flow survive and enable larger spread. Our tentative explanation for the observed turbulence suppression is discussed below.

The centerline velocity power spectrum in an unforced jet at a streamwise location close to the end of the potential core (say, $x/D \cong 4$) reveals a broadband surrounding frequencies for which the average $St_D \cong 0.4$; this broadband is evident in the power spectrum recorded at $x/D \cong 2$ in Fig. 3.1. This is representative of the average structure passage frequency in the jet, viz., the preferred mode frequency (Hussain & Zaman 1981). The instability wavelengths corresponding to this frequency can be estimated in terms of the $St_D$ as: $\lambda \sim 1/St_D$, assuming a structure advection velocity proportional to the centerline jet velocity. Since the strength of the vortices formed (i.e., their circulation) is directly proportional to the instability wavelength associated with their formation, low $St_D$ reflects relatively stronger structures.

The suppression of the quarterharmonic frequency component ($St_D \cong 0.28$) implies that the lowest dynamically significant frequency in the controlled jet (viz., the subharmonic frequency) is $St_D \cong 0.56$. Thus, prior to the breakdown to turbulence, vortices formed in the controlled jet will be weaker than that in the unforced flow. This may explain the significantly lower turbulence intensity levels observed in the controlled period-2 flow, the persistence of the suppression in x and the decreased mean jet spread. In conclusion, using a new chaos control strategy, we have achieved effective turbulence level suppression in the jet, while utilizing intrinsic flow states and only low forcing levels.

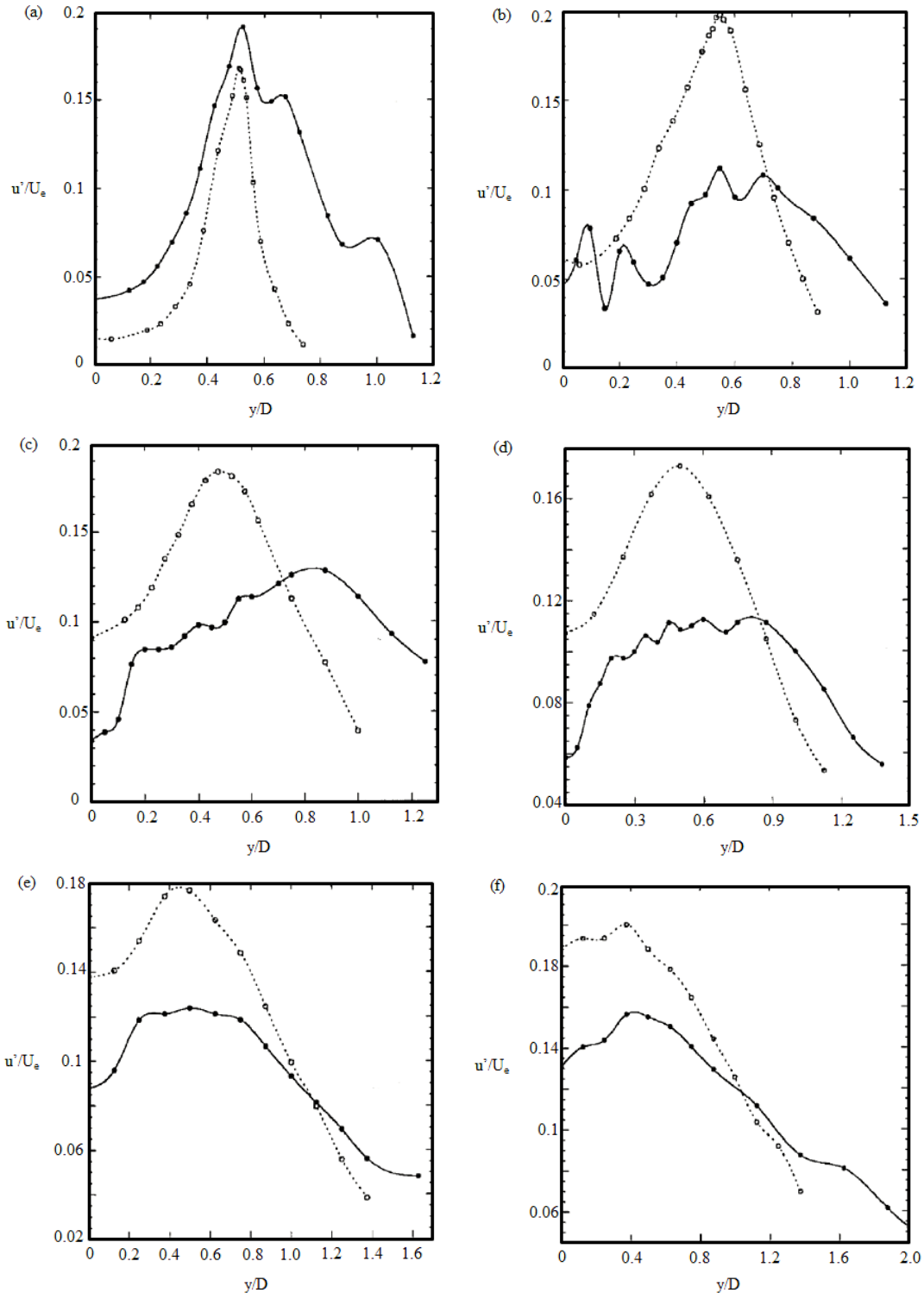


Figure 5.6 Profiles of longitudinal turbulence intensities for controlled period-2 (see solid line) and uncontrolled (see dotted line) flows at x/D = 1 (a), 2 (b), 3 (c), 4 (d), 5 (e), 7 (f).

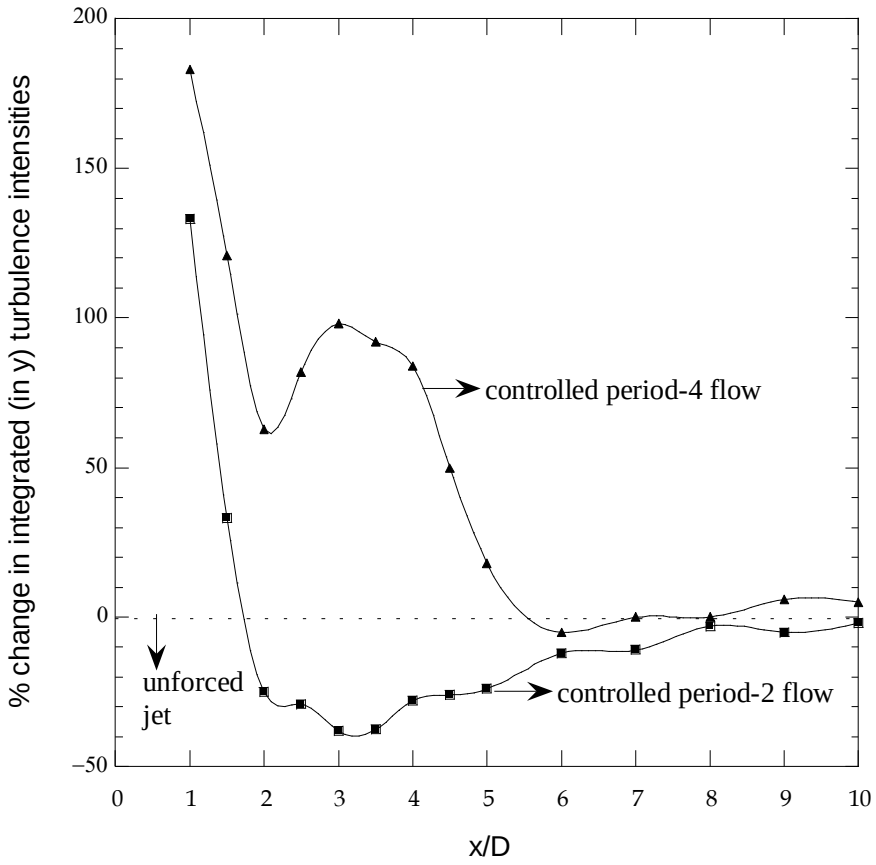


Figure 5.7 Streamwise variation of integrated turbulence suppression and enhancement.

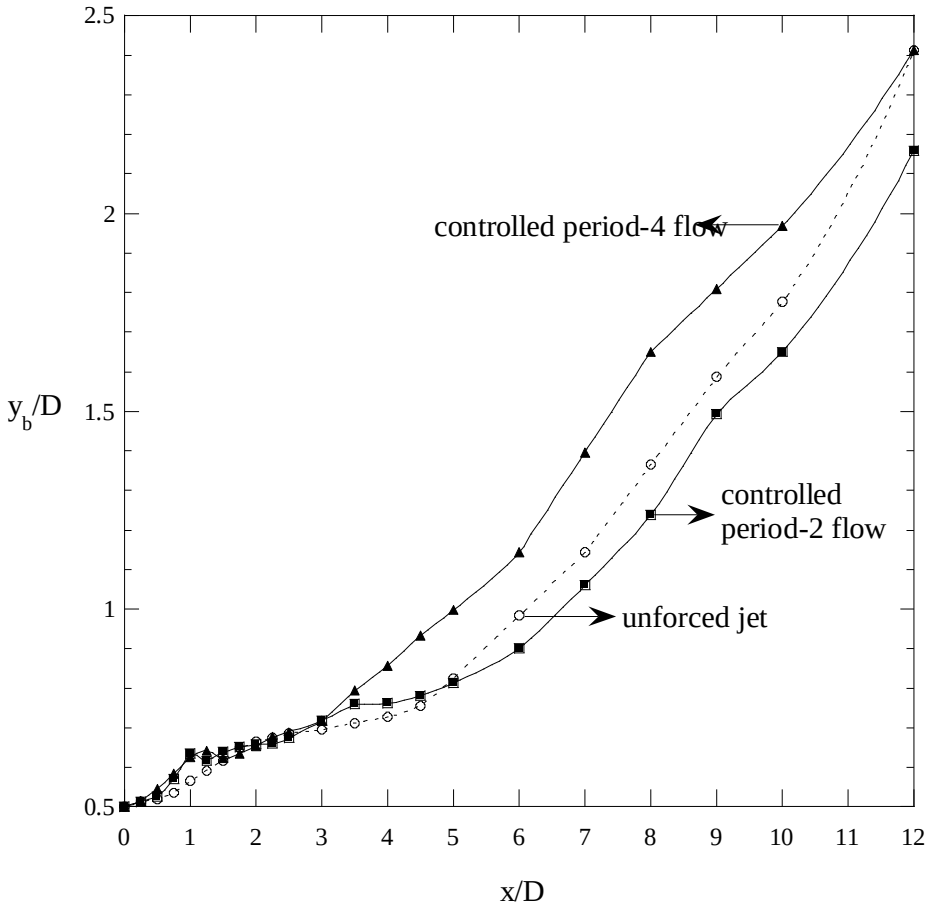


Figure 5.8 Streamwise evolution of jet half width for controlled and uncontrolled flows.

## 5.2 Turbulence Enhancement

To achieve turbulence enhancement, the formation of energy containing CS in the jet should be enhanced. Multiple vortex pairings will result in the formation of stronger (compared to the uncontrolled flow) vortices, creating larger turbulence levels and enhancing mass entrainment in the jet, and surviving farther in x. The most obvious choice of UPOs to be controlled for pairing enhancement are the ones that contain large spectral energy in the subharmonic/quarterhamonic frequencies. We chose a period-4 UPO, which is associated with vortex ring formation followed two vortex pairings.

The nozzle exit plane control signal used to stabilize a period-4 UPO is shown in Fig. 5.9a. The subharmonic and quarterharmonic ferquency forcing levels, $u'_{f/2}/U_e$ ($\cong$ 0.2%) and $u'_{f/4}/U_e$ ($\cong$ 0.05%), are quite low; see Fig. 5.4 for spectral amplitudes close to the exit in the controlled flow. The centerline velocity signal (at x/D = 2) from the controlled flow, shown in Fig. 5.9b (see symbols), matches well with the desired period-4 UPO (found in the uncontrolled chaotic flow). Smoke flow visualizations of the jet near field after applying control are shown in Figs. 5.9(c,d). The snapshots look very similar to that shown in Fig. 3.6(a), with the first vortex pairing completed near x/D $\cong$ 2 and the second pairing completed by x/D $\cong$ 3. In contrast to the chaotic state, this controlled flow state is maintained indefinitely in time. Nominally axisymmetric vortices in the controlled flow seem to be maintained for x/D < 6, after which the jet breaks down to turbulence. The development of three dimensionality is clearly delayed (in x) compared to the period-2 flow state studied earlier.

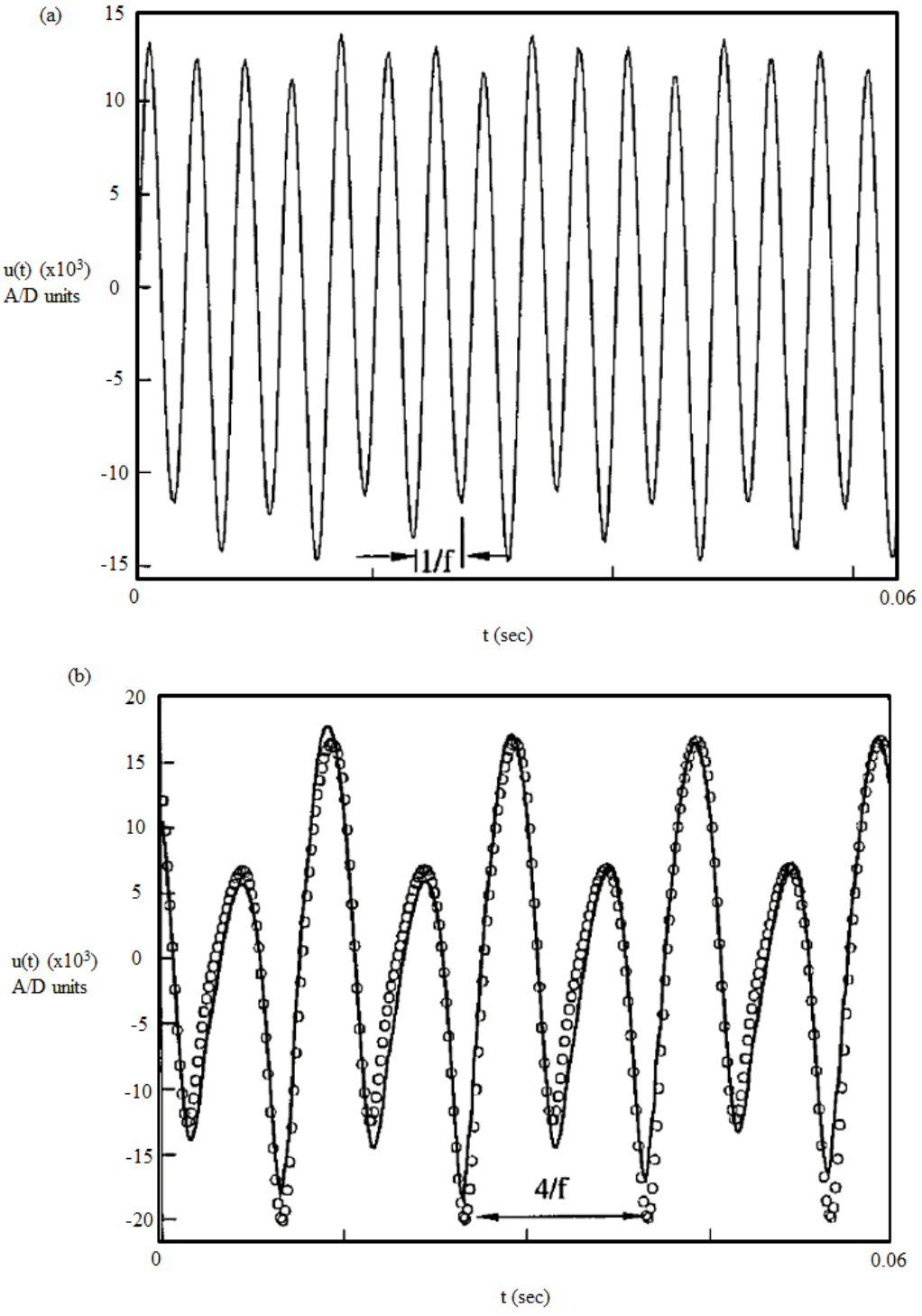


Figure 5.9 (a) Upstream velocity signal from controlled period-4 flow state, with low-level forcing at additional frequencies (other than the fundamental frequency); (b) Centerline velocity signals from controlled period-4 (see symbols) and uncontrolled flows.

(c)

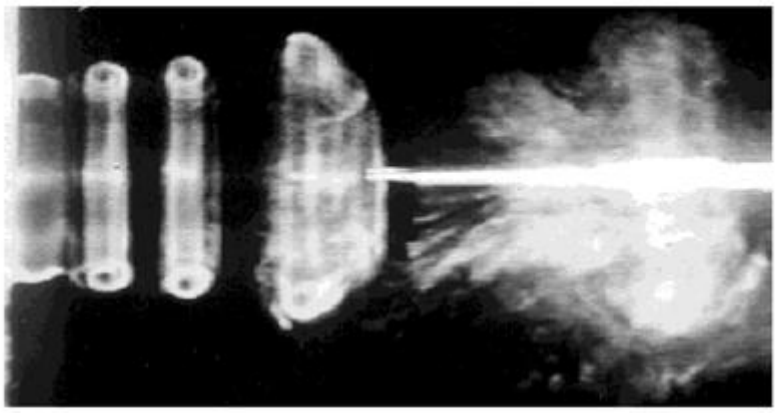

(d)

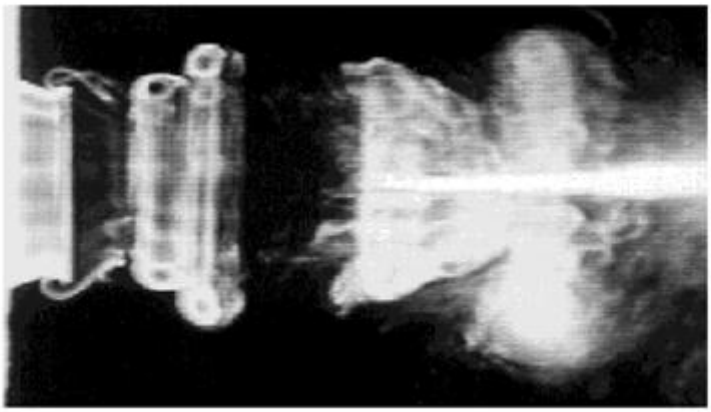

Figure 5. (c) and (d) Smoke visualization snapshots for controlled period-4 flow state.

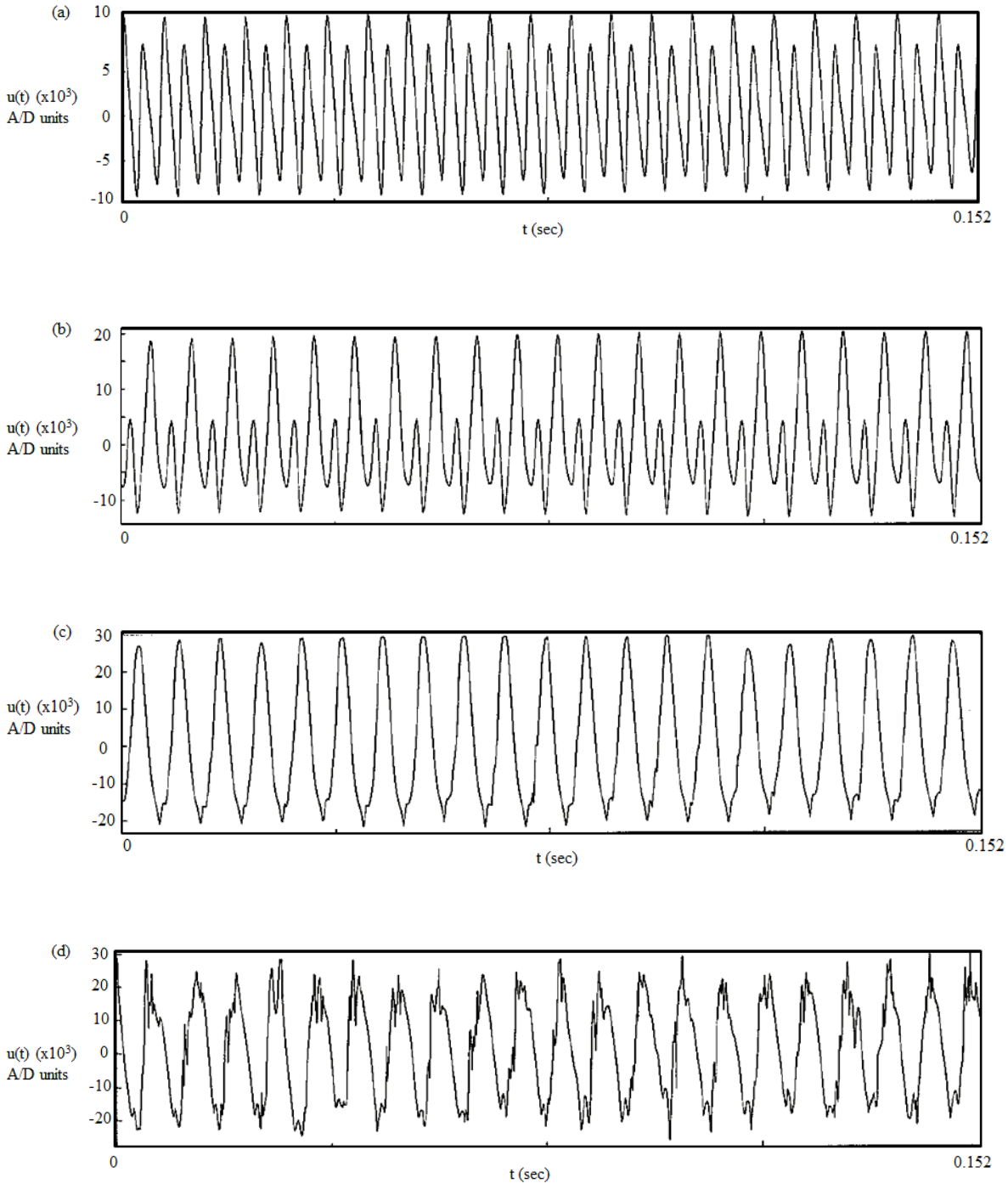


Figure 5.10 Centerline velocity signals for controlled period-4 flow state at x/D = 1 (a), 2 (b), 3 (c), 4 (d).

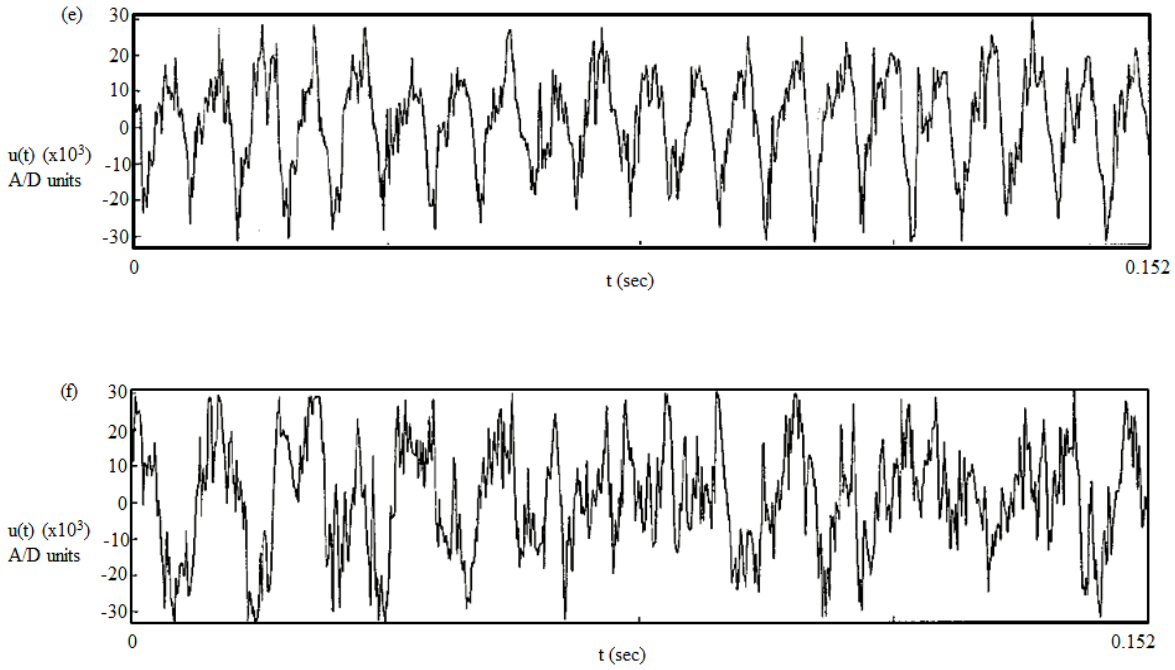


Figure 5.10 Centerline velocity signals for controlled period-4 flow state at x/D = 5 (e), 7 (f).

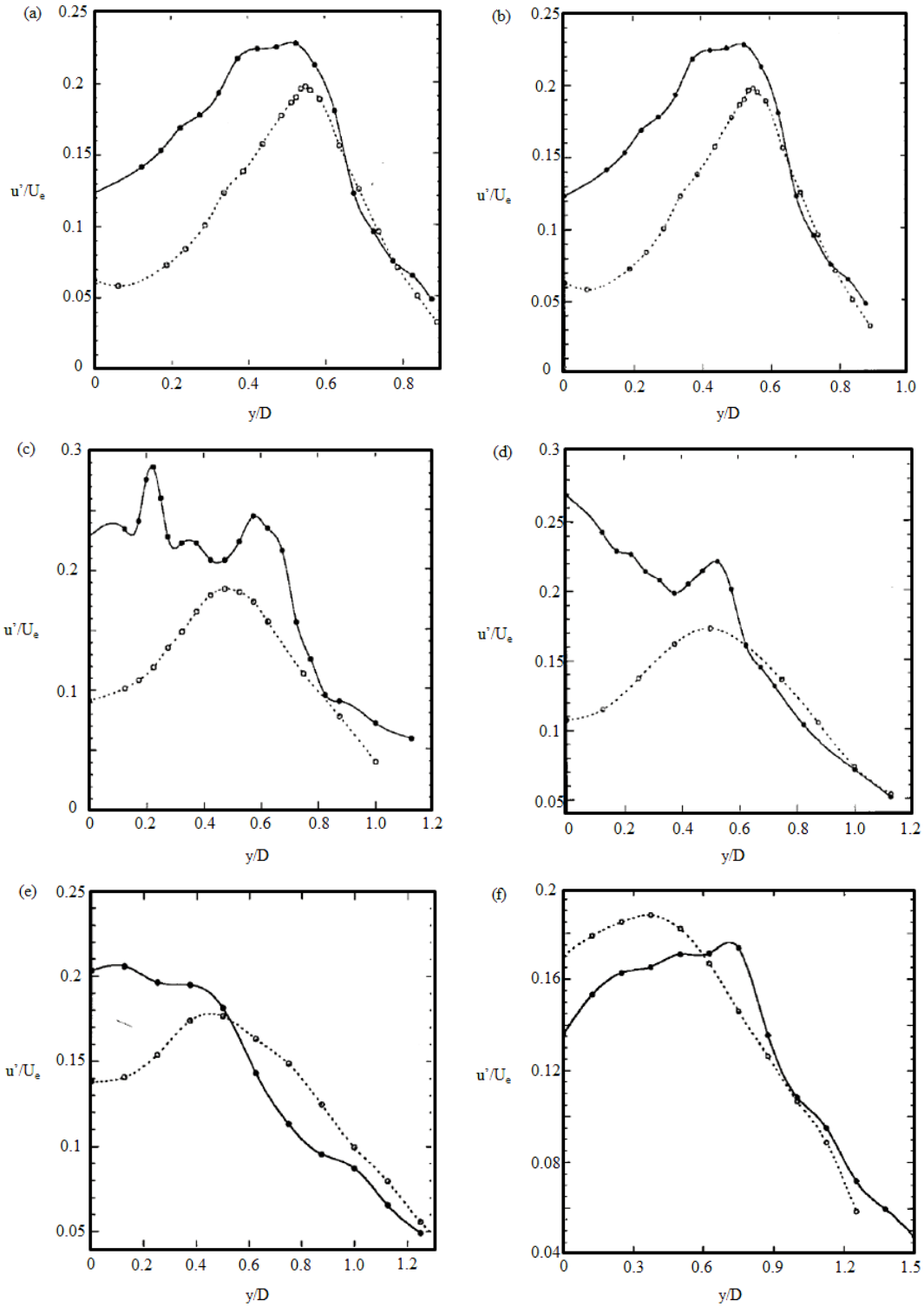


Figure 5.11 Profiles of longitudinal turbulence intensities for controlled period-4 (see solid line) and uncontrolled (see dotted liens) flow states at x/D = 1 (a), 2 (b), 3 (c), 4 (d), 5 (e), 6 (f).

Figures 5.10(a-f) display the centerline velocity time traces recorded at various streamwise locations (viz., x/D = 1, 2, 3, 4, 5, 7) from the jet nozzle exit. The periodic nature of the controlled flow (with dominant fundamental, subharmonic and quarterharmonic periods) is evident in these signals up to $x/D \cong 5$. The lack of discernible periodic features in velocity signals recorded for $x/D \geq 6$, suggests the breakdown of the jet to turbulence in the range $5 < x/D < 7$. The spatial extent of control in this flow is quantified via coherence measurements. High coherence for the subharmonic f/2 and the quarterharmonic f/4 frequency components is indicative of strong spatial coupling in the flow up to $x/D \cong 6$ (see Fig. 5.3); for $x/D > 6$, the rapid drop in coherence, indicating spatiotemporal dynamics, appears to be due to the breakdown of the jet to turbulence (as speculated for the period-2 flow state).

We evaluate the degree of turbulence enhancement, similar to that for turbulence suppression, by comparing the near field turbulence characteristics in the controlled flow and the *unforced* flow. Again, since the CS dynamics being controlled are nominally axisymmetric, we expect the measurements of the longitudinal turbulence intensity levels to be representative of the near-field turbulence characteristics.

Figure 5.4 displays the streamwise evolution (on the centerline) of the spectral amplitudes of the fundamental $u'_f/U_e$, subharmonic $u'_{f/2}/U_e$ and quarterhamornic $u'_{f/4}/U_e$ frequency components in the controlled period-4 flow (see solid symbols). After saturation of the fundamental f (resulting in vortex roll up), the nonlinear instability and saturation of the subharmonic f/2 results in a complete first pairing by $x/D \cong 2$. This is followed by

the nonlinear instability of the quarterharmonic f/4 due to a second subharmonic resonance (with f/2), resulting in a second vortex pairing near x/D ≅ 3. The enhancement of the quarterhamonic amplitude $u'_{f/4}/U_e$ (see solid symbols), compared to that for the period-2 flow, is evident. We expect this second subharmonic resonance to produce turbulence enhancement in the jet.

Figure 5.5 displays the longitudinal turbulence intensity levels $u'(x)/U_e$ for the unforced jet (see circular symbols) and controlled period-4 flow state (see solid triangular symbols) on the jet centerline. The increase in $u'(x)/U_e$ for the controlled flow, due to the periodic vortex formation (by x/D ≅ 0.5), periodic first pairing (by x/D ≅ 2) and periodic second pairing (by x/D ≅ 3.5), is evident from the nozzle exit plane. The significant enhancement (≤ 170%) is evident in the $u'(x)/U_e$ levels for x/D ≤ 5, beyond which the vortices seem to breakdown to fine-scale turbulence.

To further evaluate the spatial extent of turbulence enhancement, we also present profiles of turbulence intensities $u'(x, y)/U_e$ in the unforced and controlled jet flows. Figures 5.11(a-f) display u'(y)/Ue for the controlled period-4 flow (see solid lines and symbols) and the unforced jet (see dotted lines and symbols) for 1 ≤ x/D ≤ 6. Significant increases are evident in the profiles recorded for 1 ≤ x/D ≤ 5; unlike the period-2 flow, the tails extend to cross-stream locations similar to that for the unforced flow due to the vortices still undergoing interactions and perhaps, transitioning farther in x (e.g., see Fig. 5.11f). The peaks and valleys appearing in the profiles are expected due to the periodically occurring vortex rollups and pairings, as in the period-2 flow case. The integrated en-

hancement effect across the jet is evident in Fig. 5.7 (see solid triangular symbols), displaying the increase in $u'_t(x)$ for the controlled period-4 flow. Two-fold enhancement (compared to the unforced jet) is seen in the range $2.5 \leq x/D \leq 4$, where a second vortex pairing occurs periodically; the initial enhancement (for $1 \leq x/D \leq 1.5$) is also attributed to the dominant fundamental frequency component which is being periodically forced. The turbulence enhancement effect disappears beyond the end of the potential core, which appears to end near $x/D \approx 5$.

Since stronger (in circulation) CS are more effective in engulfing surrounding ambient fluid into the jet core, we expect that the controlled jet (involving two vortex pairings) would spread more compared to the unforced jet. The initial increase (for $x/D \leq 2$) in jet spread (indicated by the $y_b/D$ evolution in Fig. 5.8) for the controlled flow (see solid line and triangular symbols), compared to the unforced flow, is a result of the periodic vortex ring formations and a single pairing. The jet spread rate increase for $x/D \geq 3$, caused by the periodic second pairing (whose circulation is nearly four times that of the primary structure), results in a 20-30% higher jet spread for $x/D \leq 10$. The observed turbulence enhancement is further discussed below.

In contrast to the controlled period-2 flow state discussed earlier, the largest structures in the controlled period-4 flow (resulting from two vortex pairings) are found to have $St_D \cong 0.28$. Since the instability wavelength corresponding to these structures are larger than that expected for an unforced flow, we expect the CS in the controlled flow (near $x/D \cong 4$) to be stronger than the CS in the unforced jet. Such stronger, periodically

occurring structures are responsible for the increased turbulence intensity levels observed in the near field and the increased mean jet spread. Farther downstream ($x/D > 6$), the turbulence intensity levels in the controlled flow fall off to the levels observed in the unforced flow.

In summary, we have demonstrated significant turbulence enhancement using chaos control by stabilizing an intrinsic periodic flow state appearing within a chaotic attractor in the jet. Similar to the control of the period-2 flow state, low forcing levels were required.

# CHAPTER 6

# CONCLUDING REMARKS

A novel method for active control of an axisymmetric jet (an *open flow*) has been demonstrated. The essence of the control technique is to stabilize a desirable periodic flow state, among infinity of periodic states embedded within the chaotic dynamics of the transitional jet. Specifically, the jet dynamics in the transitional region involving sequences of axisymmetric vortex roll up and vortex pairings are controlled to be nearly periodic using small-amplitude control perturbations provided at the nozzle lip. The control method was also successfully demonstrated in a transitional planar mixing layer (a prototypical open shear flow), where quasi-two dimensional (alternatively, rectilinear) vortex dynamics of vortex formation and their interactions or pairings were controlled (described in Appendix B). The control method termed *chaos control* is based on the nonlinear dynamical systems approach. Success of this chaos control approach hinges on the crucial finding that the dynamics of vortices in the near field of the jet and mixing layer flows are low dimensional (shown to be the case by previous studies of Broze & Hussain 1994 and Narayanan & Hussain 1996). The overall message of this study: (open) flow control is best achieved, i.e. in the most energy efficient manner (from control input energy use standpoint), by utilizing the underlying (low-dimensional) natural dynamics.

The key contributions of this study are described below in two areas: (i) control of coherent structure dynamics in the near field of an axisymmetric jet, and (ii) nonlinear dynamical systems theory based approach for controlling free shear flows. The findings

and conclusions from the former are described first. The three main results under the first category are: (a) the finding and characterization of low-dimensional, unstable periodic, vortex dynamics in the transitional jet region; (b) a new control method to control the jet vortex dynamics and its experimental demonstration; and (c) demonstration of turbulence reduction and enhancement in the jet flow field using the novel control method.

### 6.1 Periodic States and their Vortex Dynamics in the Jet

Periodic states in jets and other free shear flows are typically recognized as ordered flow states, and commonly realized using periodic excitation of instabilities at pre-determined control amplitudes and phases for one or more forcing frequencies. However, in the present study a different class of periodic states is found, which represent flow states that repeat themselves in a disordered fashion and not time periodically. Such flow states are termed unstable periodic states and were the focus of the present study. Such flow states appear under limited or no flow excitation and are best described as a low-dimensional but chaotic dynamical system.

The vortex dynamics observed in the jet via single-point longitudinal velocity component measurements were determined to be organized and low dimensional in that nearly periodic sequences of vortex ring formation and their pairings were prevalent in seemingly disordered (viz. chaotic) flow dynamics. It has been established that these periodic flow states are intrinsic to the chaotic jet dynamics, and that the vortex dynamics are self-excited by feedback from vortex parings occurring downstream in the jet flow field. The unstable periodic dynamics underlying the vortex ring evolution and interactions present a wide range of controllable flow states. Each flow state comprises a spatially distributed

set of vortical structures at various stages of their evolution and their interactions; this can alternatively be thought of as a snapshot of the transitional jet flow field (extending from the nozzle exit plane to the jet potential core end). Such flow states include vortex ring roll up and their advection until the end of the jet potential core, whereupon the structures breakdown to fine-scale turbulence.

Other flow states involve a sequence of a vortex roll up followed by a single pairing of the vortex rings, which then advect and breakdown past the end of the jet potential core. Vortex ring formation, followed by a single vortex paring, followed by a (second) pairing of the paired vortices, is yet another type of flow state found to be embedded among the chaotic dynamics observed in the jet. To emphasize, given the chaotic nature of the dynamics, none of these states are repeated periodically. In summary, given sufficient observation time, there exists infinity of other number and sequences of vortex ring formation and their pairings in the jet. Some of these flow states have been observed as a result of periodic forcing but at higher levels of control input amplitudes (e.g., see Zaman & Hussain 1980, Paschereit et al. 1995).

The chaotic dynamics in the jet are unique in that such (periodic) flow states are all found naturally in the transitional jet, but are all unstable. Thus, no one flow state is sustained periodically and the flow itself meanders between a multitude of states (observable temporally and spatially) and large-scale vortex dynamics. However, it was found that some of these periodic states are statistically more dominant than others in the context of their dynamical systems characteristics (see Appendix A). Control was therefore targeted at these naturally prevalent (but unstable) flow states.

It should be noted that specific empirical representations for the unstable periodic states obtained for the jet flow here are dependent on the experimental configuration used, namely flow characteristic time and length scales and the ambient environment characteristics (defined by the facility settling chamber resonances and disturbances). Underlying each periodic state (or orbit) is a footprint comprising amplitudes of individual frequency components and relative phase differences among them. The details associated with the sizes and shapes of such orbits in phase space are uniquely related to the integral characteristics of the flow and the dominant large-scale flow structure dynamics. Thus, the targeted periodic states for control will have to be determined for each configuration prior to implementing the control strategy. However, given the presence of a chaotic attractor, the existence of periodic orbits is always guaranteed (since it is a dynamical invariant of the system), and a systematic and automated procedure (as proposed here) can be used to extract unstable periodic orbits of interest. Once the periodic orbits are extracted, physical arguments (such as done for the transitional jet vortex dynamics) are needed to select periodic states to be controlled.

Single-point measurements were used to infer the large-scale structure dynamics of vortex rings and their interactions in the transitional jet region, prior to jet breakdown (as in Broze & Hussain 1994). Following the identification of periodic, but unstable, flow states, their spatial evolution was characterized using two-point velocity measurements. In particular, a model of the streamwise evolution of each periodic flow state was obtained from measured velocity traces in the jet flow field. Two different approaches to model the spatial evolution of the chaotic vortex dynamics in the transitional jet region

were developed: direct analysis (invoking intrinsic hydrodynamic feedback from vortex pairings) and adaptive filtering (applicable also to flow situations where no spatial coupling mechanism is evident). Whereas, infinity of such flow states exist in the flow, a "generalized" empirical representation (but specific to the chaotic state of the jet flow) was developed, which was used for control. The existence of spatial coupling in the jet domain was essential for the description of the complex jet dynamics using at most two simultaneous, spatially separated measurements. As the spatial coupling degrades, the expectation is that multiple measurement stations are going to be needed.

### 6.2 Novel Jet Control Method

The basic principle of conventional free shear flow control approaches is to use single/multiple frequencies to excite the relevant instability modes (e.g., Paschereit et al. 1995, Husain & Hussain 1995). Since these brute-force methods do not fully utilize the low-dimensional dynamics underlying the flow, appropriate forcing forms (or control laws) can be determined only by trial and experimentation; high levels of forcing may be necessary, depending on initial conditions and flow parameters. The new nonlinear control method presented here utilizes the low-dimensional dynamical features underlying the flow, namely the unstable periodic states. Consequently, small amounts of external control to accentuate the intrinsic dynamics suffice to achieve desirable flow response. Indeed, the control method has been demonstrated to require smaller levels of control energy input compared to prior methods. The control perturbations for selected flow states are specified and known *a priori* by analyzing the low-dimensional dynamics from the flow, not requiring exploration and *a posteriori* tuning by experimentation. Specifically,

the enhancement as well as suppression of vortex pairings demonstrated here are for a fixed single frequency forcing amplitude. Only "small" additional forcing at a few frequency components (at a fraction of the forcing amplitude of the primary instability) was used for control. Note that, using single frequency excitation, fundamental forcing levels to obtain chaotic dynamics are 5-10 times lower than that for obtaining periodic flow states; for instance, see results from Zaman & Hussain (1980) and Broze & Hussain (1994) for jet excitation, and Ho & Huerre (1984) and Narayanan & Hussain (1996) for mixing layers forcing. Measurements of the velocity traces on the jet centerline in the uncontrolled (chaotic) and controlled (periodic) jet flow, within the jet potential core, were first made to ascertain the effectiveness of control in stabilizing periodic sequences of vortex formation and pairings specified *a priori*. The controlled flow closely tracks the desired periodic flow state, with minimal deviations.

The jet control method is simple in that it is open loop, avoiding cumbersome and not always practically realizable feedback control, and uses empirical modeling. While empirical modeling is needed for the flow prior to control, there is no need for elaborate, often intractable, analytical modeling of the flow field. The inherent convective instabilities in jet enable control of spatiotemporal dynamics for substantial spatial extents using temporal control at a single spatial location - the point of receptivity, namely the jet nozzle lip. This contrasts with conventional (distributed) control of spatiotemporal flows requiring sensing and actuation at several locations (e.g., see Keefe 1993, Choi et al. 1994, Bewley et al. 2001), which is difficult (maybe infeasible) to implement. Since the flow region where control is desired is spatially separated from the actuation location, model-

ing of the spatial development of the jet was necessary (as described above).

The effects of small changes in upstream jet nozzle exit conditions on the drifting of downstream dynamics and controllability when multiple periodic states exist are issues needing further investigation; trapping of the controlled flow in an undesirable flow state may be the cause for such drifts. To resolve these and provide a "robust" control scheme, an *adaptive* approach (i.e. requiring real-time feedback) may be unavoidable. A simple feedback-based control method was also presented and demonstrated in the jet to control flow states for which the open loop control method failed. Potential modifications to this control method are proposed as future research directions in §8.2.

*Nonlinear control in other open shear flows*. In the following, we discuss the outlook for using the newly developed control method in other open shear flows such as wakes and boundary layers. Evidence for the existence of such low-dimensional dynamics in wakes (Van Atta & Gharib 1987) and (transitional and turbulent) boundary layers (Aubry et al. 1988, Healey 1993) is promising, since the use of the control method developed here hinges on the presence of low-dimensional dynamics in the flow. Thus, a desirable flow response can be achieved by stabilizing or controlling a periodic state (albeit unstable) underlying the natural dynamics. For instance, via simulations, Coller et al. (1994) have demonstrated feedback control of an unstable fixed point in a "reduced model" of boundary layer turbulence, believed to be associated with near-wall longitudinal vortices. For boundary layers, due to the spatiotemporal nature of the flow and the lack of a single and well-defined point of receptivity (as for free shear flows), actuation at several spatial locations may be necessary to ensure control. The spatial extent of correlation in the flow,

which can be quantified using coherence measurements (Broze et al. 1997), will dictate the sensor placement for reconstructing the dynamics and hence the actuator locations. The reconstruction of the CS dynamics from multi-point measurements is a subject for further studies; e.g., see Narayanan et al. (1997) for application to the transitional jet.

### 6.3 Jet Turbulence Manipulation Using Control

Using the new control method, two contrasting forms of turbulence control were demonstrated in the jet: (a) turbulence enhancement, and (b) turbulence suppression, both with significant technological implications. Prior flow control methods to achieve these required elaborate testing of jet exit plane control signals with varying amplitude ratios and phase differences among frequency components associated with the near-field instabilities, as well as significant changes to the flow parameters (Paschereit et al. 1995, Husain & Hussain 1995, Zaman & Hussain 1981).

The present control approach aims to maintain the flow in the vicinity of a periodic state, comprising a sequence of vortex ring interactions, intrinsic to the jet dynamics in the transitional region. A wide array of flow states can be controlled for fixed flow parameters and low levels of control perturbations. For instance, stable pairing and stable double pairing were both obtained at a fixed parameter space location for the jet; conventional methods to achieve these states would require significant changes to the parameters such as a fundamental forcing frequency and its amplitude (e.g., see Broze & Hussain 1994). Near-field turbulence enhancement is achieved by increasing the number of vortex pairings and rendering them periodic. On the other hand, turbulence suppression is

achieved by suppressing or minimizing the pairings, resulting in weaker structures that breakdown to turbulence sooner.

For turbulence enhancement a period-4 flow state discovered in the chaotic dynamical system was stabilized via control. Control of this flow state resulted in the periodic formation of vortex rings, followed by two successive periodic pairings of these vortices; this state was also referred to as stable double pairing by Broze & Hussain (1994) and excited using periodic forcing in prior studies such as those by Zaman & Hussain (1980). Here, the periodic state is shown to be controllable with minor modifications to the flow parameters for an inherently chaotic flow state. Significant increase in the longitudinal turbulence intensity was evidenced across the jet for several jet diameters. Integrated rms-velocity profiles revealed nearly two-fold turbulence intensity enhancement (compared to an unforced jet flow), accompanied by increased jet spread of more than 20% compared to the unforced flow; this is expected to result in significantly increased mass entrainment. The near-field entrainment/mixing characteristics in the jet can be further enhanced by controlling non-axisymmetric coherent structure (CS) dynamics, a subject of further studies discussed later in Chapter 8. The description of three-dimensional vortex dynamics (involving tilted vortex rings and their interactions) as a low-dimensional (spatiotemporal) dynamical system (DS) is also a subject of ongoing research.

The control of a period-2 flow state resulted in turbulence suppression of about 38% in integrated rms-velocity profiles for several jet diameters, well beyond the end of the potential core. Note that, the comparisons are relative to the unforced jet flow characteristics, not the flow excited by a single frequency to establish the chaotic dynamics of the

jet. The controlled flow state is one in which the second vortex pairing of the jet is nearly completely suppressed or substantially delayed. Thus, vortices interact and pair with each other only once prior to breakdown at the end of the jet potential core. This concomitant turbulence intensity suppression has significant implications for the reduction of aerodynamic noise, since experimental evidence suggests far-field jet noise amplification/reduction due to excitation/mitigation of near-field organized motion and turbulence amplification/suppression (Hussain & Hasan 1985). In particular, since the large-scale structures prior to the collapse of jet potential core are known to be a significant contributor to the sound generation in aft angles (Narayanan et al. 2002, Reba et al. 2010), turbulence suppression as a result of delaying the formation of large-scale structures is expected to be beneficial for noise reduction. Note also that *external forcing* has been used to suppress turbulence levels below that in an *unforced* flow, a counter-intuitive result.

The key findings and conclusions from use of the nonlinear dynamical systems theory based approach to control free shear flows is described next. Only the salient findings are pointed out, leaving details of the findings to be described in Appendices A, B and C. The three main results under this category are: (a) a new spatial coupling measure – *total coherence* – for (inhomogeneous) spatiotemporal DS; (b) a novel approach – *phase space eduction* – to reconstruct the organized jet flow structure dynamics; and (c) a *chaos control* strategy for open flows and its experimental demonstration in two open shear flows: a circular jet and a plane mixing layer.

### 6.4 New Spatial Coupling Measure for Spatiotemporal Dynamical Systems (DS)

To justify the use of single-/two-point measurements for analyzing and modeling the

(temporal) chaotic dynamics in the jet and the plane mixing layer (see Appendix B), spatial coupling in the flows must be verified. Correlation-based measures (e.g., correlation length), used to measure coupling in various spatiotemporal DS, are inadequate (even misleading) in inhomogeneous (multimode) systems. Total coherence $\gamma^2_T(f)$ was analytically formulated and proposed as an accurate identifier of coupling in spatiotemporal DS, particularly inhomogeneous ones; this is believed to be applicable to spatiotemporal dynamical systems more broadly. Coherence is applicable to homogeneous systems as well; when dynamics are dominated by a single frequency, coherence and correlation results are identical. With multiple modes, coherence can be used to identify frequencies and interactions responsible for coupling decay. Since coherence can be interpreted as the predictable energy fraction, this appeared to be the first method for measuring predictability in multimode spatiotemporal systems. Consequently, this result is an important step in addressing the problem of modeling and controlling technologically relevant spatiotemporal (*open*) flows. Total coherence measurements in the jet (for chaotic flow states) indicate large spatially coupled regions (extending up to 4 jet diameters), implying high predictability of dynamics (using single-point measurements) in these flow regions.

### 6.5 Reconstructing Jet CS Dynamics from Phase Space Dynamics

A new approach, although qualitative, has been developed to describe the large-scale CS dynamics in the circular jet, termed *phase space eduction*. This is similar to physical space coherent structure eduction (e.g., see Hussain 1983) in that the procedure is aimed at describing the organized aspects of complex flow fields, but is differentiated in that the

procedure does not require commonly used subjective features such as templates and thresholds for feature extraction.

While traditional CS eduction methods have been applied to a variety of distributions such as velocity, vorticity and Reynolds stress fields, the phase space eduction approach developed here has been attempted with a single component of the velocity field only. The CS dynamics are characterized using empirical averages of "nearly periodic" trajectories of the chaotic attractor (viz., the unstable periodic orbits (UPOs)) in narrow phase-space windows. Such averaging is enabled by the finding of a few distinct "trajectory bundles" surrounding the (statistically) dominant periodic orbits in the chaotic attractor, suggesting frequent occurrence of certain sequences of CS dynamics. Each UPO reveals a specific spatiotemporal sequence of vortex ring formation and interactions, whose spatial extent depends on the UPO period; the presence of spatial coupling enables the reconstruction of a spatial sequence from a temporal attractor. The averaging of phase-space trajectories is simplistic in that only large-scale events (viz., vortex roll up, initiation/completion of vortex pairings) are detected and the details of its spatial structure (e.g., vorticity distributions) are not explored. However, it provides sufficient detail to identify desirable goal states for controlling the vortex dynamics, e.g., the choice of period-2 and period-4 UPOs for turbulence suppression and enhancement respectively.

Since UPOs are topological invariants of chaotic attractors, i.e., are generic attractor features, such a simple approach to describe other CS-dominated shear flows such as, coaxial jets, mixing layers, bluff body wakes and boundary layers, is also possible. In fact,

trajectory averaging in phase space to extract CS signatures in a "high dimensional" turbulent channel flow has been attempted (Keefe 1987), but the placement and size of phase-space windows for averaging was arbitrary. The UPO bundles analyzed herein provide an unambiguous feature of the attractor for "structure identification". Identification of low-dimensional attractors is essential for such "eduction".

### 6.6 Chaos Control of Open Flows

A chaos control scheme for a spatially developing flow was developed and demonstrated experimentally in two open flows, viz., a jet and a mixing layer; the latter application is described in greater detail in Appendix B. Since prior chaos control methods were applied only to simple temporal DS and spatially homogeneous DS, the present approach constitutes a significant contribution for the nonlinear control of spatially extended DS. The jet control method is a simple open loop one, avoiding cumbersome feedback, and requires empirical modeling. This is unlike conventional open loop chaos control techniques that require elaborate analytical modeling.

The inherent convective instabilities in open flows enable control of spatiotemporal dynamics for substantial spatial extents using control at a single location (the point of receptivity). This contrasts with conventional (distributed) control of spatiotemporal DS (Keefe 1993) requiring sensing and actuation at several locations, which is difficult to implement. Since the flow region to be controlled is spatially separated from the actuation location the spatial development of the flow needs to be modeled (described earlier). The prospect of using chaos control in other open shear flows such as wakes and bounda-

ry layers was discussed earlier. The finding of low-dimensional chaotic attractors in wakes (Van Atta & Gharib 1987) and boundary layers (Aubry et al. 1988, Healey 1993) is promising. Accordingly, in the dynamical systems context, a desirable flow response can be obtained by tracking an unstable periodic orbit underlying the chaotic attractor embedded in a low-dimensional phase space.

# CHAPTER 7

# RETROSPECTIVE ON DEVELOPMENTS IN CHAOS CONTROL AND FLOW CONTROL

The research reported here was conducted during the period of 1994-2000 when several other applications of chaos control and a variety of nonlinear control techniques for hydrodynamic systems were being pursued and matured. The objective of this chapter is to review some of those concurrent as well as more recent developments in the fields of chaos control, its alternatives, and open flow control. First a summary of advancements in controlling nonlinear spatiotemporal systems using dynamical systems methods is provided. Following this, recent developments in hydrodynamic flow control are reviewed.

## 7.1 Dynamical Systems Methods for Control

During the last decade or more, control of complex irregular dynamics has evolved as one of the central issues in applied nonlinear science (Schöll & Schuster 2008). The notion of chaos control has been extended to a much wider class of problems involving stabilization of unstable periodic or stationary states in nonlinear dynamic systems. More recently major progress has been made with respect to:

- extending chaos control methods to spatiotemporal patterns
- extending control methods for deterministic dynamical systems to stochastic and noisy systems
- development of novel control schemes
- applications to various areas in physics, chemistry, biology, medicine and engineering

Many practically relevant phenomena including turbulence, plasma, combustion instabilities, multi-mode lasers, flow reactors, cardiac arrhythmia and brain epilepsy display chaotic behavior. Such high dimensional systems, due simply to complexity in temporal dynamics or due to presence of spatially extended or spatiotemporal behavior, have remained notoriously difficult to control. Various forms of chaos control have been attempted on such systems and the following presents a treatment of some of the more recent attempts and lessons learned. A modern treatment of the principles of chaos control, its many variants and applications are also described in Schöll & Schuster (2008). Fradkov & Evans (2005) provides a more detailed treatment of methods tailored to engineering applications of chaos control and the rich literature documenting them.

Roy et al. (1992) conducted a study of a multimode, autonomously chaotic laser system. An occasional proportional feedback method was applied to stabilize certain desirable periodic laser output behavior. The principle of feeding back a control signal proportional to the deviation of the system from an unstable fixed point or periodic orbit is akin to the Ott et al. (1990) approach. The system is an example of a globally coupled system of nonlinear oscillators with chaotic behavior. The proportional control signal applied to the pump excitation results in an ordered, periodic state of the originally chaotic ensemble of oscillators. Although there was no external periodic modulation for the chaotic dynamics observed, the relaxation oscillations of the laser intensity provided a natural time scale for perturbative corrections.

The basic technique to achieve dynamical control was as follows. The total laser output intensity (a system variable) is sampled in a selected window. A signal propor-

tional to the deviation of the sampled intensity from the center of the sampling window is generated and applied to perturb a system parameter from its ambient value. The control signal repeatedly attempts to bring the system closer to a periodic unstable orbit that is embedded in the chaotic attractor, resulting in a realization of the periodic orbit essentially limited by the positive Lyapunov exponent characterizing the orbit. For low period orbits, control was achieved with small perturbations near the relaxation oscillation frequency or its sub multiples. For higher period orbits (e.g. period-4, period-9), synchronization frequency had to be adjusted to a simple rational fraction of the relaxation frequency. Clearly the control signal waveforms become more complex with higher order periodic orbits. In most cases, the drive current signals were only a few percent of the ambient-bias current for the laser, so for these cases the original attractor were claimed to be preserved.

While the above study provided an early verification of the feasibility of chaos control, the control signal synchronization frequency selection and tuning was somewhat manual. Given a selected periodic orbit to be controlled, the primary synchronization frequency is automatically inferred, but rational fractions of it are needed to ensure control of higher order periodic orbits. An automated and systematic procedure to do so was not discussed or available, and the tools for this are the focus and key outcomes of the current research. Another aspect of practical applications that this study did not address was the complexity and higher dimensionality that arises when additional degrees of freedom arise from spatial behavior in additional to temporal dynamics.

Petrov and Showalter (1996) studied the stabilization of unstable states in a multi-dimensional, nonlinear single-input, single-output equation system, called the Gray-Scott model that represents autocatalysis in a flow reactor. In contrast to the traditional Ott et al. (1990) approach to control of unstable periodic states, involving linearized models and use of small perturbations in the linear regime, Petrov & Showalter presented an integrated approach for nonlinear feedback control. The approach involved using the response of the system to random perturbations to construct the control law as a multi-dimensional surface in the time-delayed space.

For the Gray-Scott model, the control surface was constructed by observing the transitions from an initial state to a time-delayed final state and the perturbation applied during the elapsed interval. The identification stage involving observation of finite number of points in the above space can be interpolated to construct the entire control surface. This was generalized for m-dimensional systems, and a general expression for the stabilization of unstable states was derived in terms of a system invariant function. Once constructed, from datasets, the system invariant function can be used to target unstable states from anywhere in phase space provided system dynamics do not exceed the limits imposed by the system dynamics and the function is single valued. The control action is generated using *m* delay readings (where *m* is the system dimension) and *m-1* delayed perturbations, constituting the current state. Model-based simulation results confirmed the effectiveness of the approach. Since the control laws are obtained directly from time series, they are robust and convenient to implement experimentally.

Petrov et al. (1994) reported a study of stabilizing periodic states in a premixed flame problem. The tracking of steady and oscillatory flame fronts considered is motivated by practical applications such as extending the regime of stable burning to enhance the efficiency of combustion processes. Premixed flames with thermo-diffusive instabilities can be described by a system of two partial differential equations, one for temperature and the other for the concentration of a stoichiometrically deficient reactant.

The control of two-dimensional premixed flames was investigated with a one-variable reduction of this model given by the Kuramoto-Sivashinsky equation (assuming that reaction takes place in an infinitely narrow zone). They presented an algorithm to stabilize steady flame fronts, suppressing the natural oscillatory behavior, but also to stabilize periodic oscillations of the front that would otherwise be unstable. A map-based scheme was used for this since a linear stability analysis subroutine can be readily incorporated into the tracking procedure for control. The map-based scheme is a reduction of the Ott et al. (1990) algorithm.

In certain mixtures of fuel and oxidizer, propagating flame fronts may exhibit both stable and unstable cellular structures. Such flames represent spatially extended chemical systems, with coupling from diffusion of heat and reactants. A new algorithm was proposed that allows the stabilization and tracking of a steady, two-cell front through a bifurcation sequence that eventually leads to chaotic behavior. Periodic modes of the front can also be stabilized and tracked. The system was stabilized by monitoring one experimentally accessible variable and perturbing one boundary condition. The algorithm au-

tomatically provides information about the locations of the unstable steady states and periodic orbits and the magnitudes of the associated eigenvalues and Floquet multipliers.

Hall et al. (1997) adapted the Ott et al. (1990) method for chaos control to stabilize unstable fixed points in the presence of drifting system parameters in a one-dimensional map representation of cardiac arrhythmia. Fixed-point estimates were computed for each step so that the control algorithm can target the desired unstable fixed point. Such computations and control action generation accommodate drifts in the one-dimensional map. Robust performance of the control technique was demonstrated to successfully suppress cardiac alternans.

In a very recent study on a reacting bluff body wake problem, aimed at flame stabilization in combustors, Hua et al. (2012) conducted analysis of experimental data to describe the underlying low dimensional dynamics of the vortex street shed in the wake. As the equivalence ratio (describing proportion of fuel air mixture) is reduced, a symmetry-breaking transition to Karman vortices is initiated. One of the goals was to validate that unstable periodic orbits exist within the flow, so that they could be used to reduce or eliminate irregular facets of bluff-body stabilized flames. Combining principle component analysis with a symmetry-based filtering, bifurcation diagrams were computed for the onset and growth of Karman vortices. (Unstable) periodic orbits were computed, embedded in the complex flows, prior to and following the bifurcation. For each of the four flame holders, a single cycle prior to and a pair of cycles subsequent to the onset of Karman vortices were found which govern the organized dynamics underlying the flow. Periodic orbits within the flow were identified using a Poincare section, as in current re-

search. It was not possible to find more than one orbit prior to the transition and two subsequent to it, suggesting that the large-scale flow is in fact periodic (and not chaotic), and that the irregular facets of the flow likely result from the small-scales.

### 7.2 Advances in Flow Control

Recent reviews such as by Gad-El-Hak (1996) outline key advances in flow control. The broad area of flow control research remains of great interest for its potential benefits in military and civilian sector applications. Spurred by the recent developments in chaos control, micro-fabrication and neural networks, reactive control of turbulent flows is now within reach of practical applications.

Keefe (1993) compared two nonlinear control strategies for flow control; Ott et al.'s (1990) feedback method and the model-based control strategy originated by Lüscher and Hübler (1989). Both are a generalization of the perturbation cancellation technique; namely apply a prescribed forcing to subtract the undesired dynamics and impose the desired one. The Ott et al. approach exploits the sensitivity of chaotic systems to stabilize existing periodic orbits and steady states. Some feedback is needed to steer the trajectories toward the chosen fixed point, but the required control signal is small. Hübler's scheme does not explicitly exploit the system sensitivity. It produces control response (periodic or aperiodic) and needs little or no feedback, but its control inputs can be large. The Ott et al. approach relies on and exploits the sensitivity of the nonlinear dynamical system to initial conditions. Hübler's scheme works well for both linear and nonlinear systems.

Keefe (1993) first investigated numerically the two schemes for fully-developed and transitional solutions of the Ginzburg-Landau equation that governs the initially weakly nonlinear stages of transition in several flows and that display transitional and chaotic solutions with absolute and convective instabilities found in closed and open flows. The main conclusion was that control is best obtained by exploiting underlying natural dynamics. Keefe (1993) extended the numerical experiment to explore drag reduction in a channel flow with spatially periodic boundary conditions demonstrating 60-80% reduction in skin friction compared to the uncontrolled value. Use of Hübler's scheme failed to achieve any drag reduction when starting from a fully-turbulent initial condition but shows potential for suppressing or slowing the transition from laminar to turbulent flow.

Hu and Bau (1994) used a feedback control strategy to demonstrate that the critical Reynolds number for the loss of stability of planar Poiseuille flow can be significantly increased or decreased. Their feedback control approach employed a variant of the Ott et al. (1990) chaos control technique, by sensing the deviation of critical flow variables from desired values at several locations in the flow and then altering control variables at the to suppress or to enhance the deviations, hence in the gain or loss of stability.

As discussed in Chapter 1, Coller *et al.* (1994) developed a feedback control strategy for strongly nonlinear dynamical systems, representing turbulent channel flow, subject to small random perturbations that intermittently push the system from one saddle point to another along heteroclinic cycles. Using a low-dimensional coupled ODE model that mimics turbulent boundary layer dynamics, the approach used local, weakly nonlinear feedback control to keep a solution near a saddle point as long as possible and to let the

natural nonlinear dynamics govern the flow when *bursting*. While conceptually similar to Ott et al.'s technique, this method did not actually stabilize the state but held the system near the desired point longer than it would otherwise stay. The potential benefits of doing so include skin friction reduction by manipulating the dynamics of streamwise, counter-rotating pairs of vortices lying close to the wall. More recently, using simulations of a low-dimensional temporal dynamical system model representing a shear flow bounded in a channel, chaos control was demonstrated for unstable fixed points, which were believed to be associated with streamwise vortices and wavy streaks (Pausch & Eckhardt 2011).

Shinbrot and Ottino (1993) presented a strategy better suited to control organized motion and coherent structures in area-preserving turbulent flows. They applied the technique to a one-dimensional chaotic map, a two-dimensional chaotic map, and a chaotically advected fluid. Their geometric method exploited the repeated stretching and folding of "horseshoes" that are prevalent in chaotic systems. Their research demonstrated numerically as well as experimentally the ability to create, destroy and manipulate coherent structures in chaotic fluid systems. The key idea was to intentionally place folds of horseshoes near low-order periodic points. In a dissipative dynamical system, such as involved during mixing, volumes contract in state space and the co-location of a fold with a periodic point leads to an isolated region that contracts asymptotically to a point. Done correctly, the folding counteracts stretching.

Alternative low order model-based control schemes that do not explicitly utilize chaos control concepts have also been pursued actively in flow control. A few studies are highlighted and summarized next.

Simplest among the control schemes that have been explored the most is the use of linear control theory. Kim & Bewley (2007) provided a comprehensive review of the essential ingredients of linear systems and control theory for the fluid mechanics community and described the relevance of the theory to open problems in the optimization, control, and forecasting of practical transitional and turbulent flow systems of engineering interest. The focus was primarily on the feedback problem to coordinate actuator inputs with sensor outputs to achieve a desired effect. The review for the most part considered near-wall flows since this configuration facilitates both surface-mounted sensors and actuators to be placed near the flow instabilities of interest, such as the channel flow with skin friction and pressure sensors continuously distributed over the walls to provide the system measurements, and zero-net blowing/suction continuously distributed over the walls to provide the actuation.

It was recognized that various extensions were needed to connect the formalisms to more realistic situations such as for spatially developing boundary layers with discrete locations of sensors and actuators with various types of uncertainties. It was recognized that the applicability of linear control strategies to turbulence is predicated upon the hypothesis that appropriately linearized models (e.g., Orr-Sommerfeld/Squire) faithfully represent the inputs, outputs, and at least some of the important dynamic processes of turbulent flows. The relevance of linearized models to the turbulence problem can only be valid up to a point, as linear models of fluid systems do not capture the nonlinear scattering or cascade of energy over a range of length scales and time scales. So, linear models fail to capture an essential dynamic effect that endows turbulence with its inherent

multi-scale characteristics. In complex flows, a linear system model is often not readily available or is too large to handle. For such problems, a system identification approach can be used to construct an approximate linear model of the input-output relationships of the original system. This approach estimates the system matrices from well-designed input-output data sequences. Once the approximate low-dimensional system matrices are so obtained, control design strategies using iterative adjoint-based optimization and direct Riccati-based feedback may be employed (see Kim & Bewley 2007 for a more complete treatment). Applications of such an approach to control separated flows were presented in Huang et al. (2004) and Huang (2005).

Gillies (1998) demonstrated the feasibility of a low-dimensional control strategy using a simplified cylinder wake flow model. Low Reynolds number flow past a circular cylinder exhibits self-excited flow oscillations, which are sustained by the flow itself and are not caused by amplification of external noise. This flow exhibits self-sustained periodic vortex shedding above a critical Reynolds number. Control of such flows requires stabilization of many globally unstable modes. Using a representation of the flow field by a finite set of coherent structures or modes, obtained from proper orthogonal decomposition, a closed-loop control algorithm was designed. A neural network was used to provide an empirical prediction of the modal response of the wake to external control forcing. However, it was recognized that implementation of the control strategy on a full Navier-Stokes solution of the cylinder flow, in a practically relevant moderate to high Reynolds number regime, would add a significant amount of spatial complexity and more POD modes will be necessary for flow characterization.

Rowley & Williams (2006) reviewed advances in active control of cavity flows, particularly the use of low order, nonlinear, dynamic models for closed loop control and suppression of highly nonlinear oscillations in the system. Self-sustained and self-excited oscillations arising in the shear flow render the system dynamically closed resulting in low-dimensional dynamics that lend themselves to computationally tractable nonlinear modeling. Consequently, the use of POD to obtain control oriented models for the large-scale structure dynamics has received much attention for such problems. The system models obtained for such flows are highly configuration dependent in that closure of the models often require tuning and careful attention to ensure higher order terms in the model are captured well and result in stable and physically meaningful dynamics. The use of dynamic invariants such as unstable periodic orbits for nonlinear control proposed in the present study enables representation of the underlying low dimensional behavior in a form that is inherently more robust and therefore readily usable for control.

More classical advancements in flow control have been made as well, such as the control of co-axial jet dynamics by Burratini & Talamelli (2007). Measurements in the near field of a coaxial jet under unperturbed and controlled conditions for a low Reynolds number jet were reported. The initially laminar unperturbed flow develops shear layer instability in the outer shear layer of the outer jet, followed by vortex pairing. A control perturbation, composed of sinusoidal acoustic waves at the frequency of the instability and its half, is applied actively. Acoustic excitation at two harmonically related frequencies (the natural instability and its subharmonic) was employed. Using the phase difference between the two sinusoidal waves for control attenuation and enhancement of the

mean jet spread characteristics and turbulence intensity were achieved. These are similar to findings of Husain & Hussain (1995) in single stream jets where active forcing of natural instabilities was accomplished for flow control. The flow mixing and turbulence characteristic changes were also consistent with findings in Husain & Hussain (1995) and the present study (where control amplitudes were much smaller and choices of frequencies for control were automatically arrived at through exploitation of the underlying chaotic dynamics).

# CHAPTER 8

# RECOMMENDATIONS FOR FUTURE WORK

There are several key fronts on which the research described here can be expanded, including: (i) robust jet control; (ii) comprehensive flow field measurements to evaluate control effectiveness for jet turbulence manipulation; (iii) hybrid control approach to combine effective passive and active jet control; (iv) control approach for higher dimensional, spatially complex flows; (v) model-based control of the coherent structure dynamics in open flows. These will first have to be investigated in the circular jet flow, where low-dimensional dynamics have been established and a proven method for nonlinear control exists. Extension to other shear flows, e.g., mixing layers, co-axial jets, wall jets, bluff body wakes, boundary layers, channel flows can then follow, particularly with regard to items (iv) and (v). Several challenges exist in realizing these extensions and developments in the context of the nonlinear dynamical systems theory as well, and will be highlighted where appropriate.

## 8.1 Adaptive Control Strategy

The simple (linear) feedback control alternative proposed and tested here was successful in controlling periodic flow states with relatively large periods, for which the open loop method failed. However, the occasional (chaotic) deviations or bursts in the controlled flow reveal a shortcoming of such feedback control. This occurs because the control signal comprised of the difference between a real-time flow state and the desired state vanishes when control is achieved, and this is detrimental for a convectively unsta-

ble flow that is intrinsically susceptible to external disturbances. An approach to overcome this problem of "loss of control" is to generate the control signal using an "adaptive filter." Such control will automatically adapt to changing flow conditions in a "noisy" ambient. The adaptation would require an inversion of the transfer function between the flow signal from an upstream location (close to the actuation) and from a downstream location; prior knowledge of the dynamics is not required. This method is similar to the open loop method presented here in that "inverse system modeling" must be performed. However, in contrast to the open loop method, for "adaptive control," the "inverse model" is altered in real time to account for changing flow conditions (e.g., arising due to "noise"). This is obviously challenging for the control system hardware (namely, required analysis and response time). It may also be possible to use the control strategy proposed by Ott et al. (1990) provided one can overcome the difficulties in applying intermittent, time-delayed (for real-time computations) control in the flow.

### 8.2 Assessment of Jet Flow Field Control Effectiveness

To further quantify and conclusively demonstrate the effects of turbulence enhancement as well as suppression in the jet, measurements of near-field turbulence characteristics, such as mass entrainment, Reynolds stresses, and of far-field characteristics, such as the overall sound pressure levels (OASPL), are necessary.

*Turbulence enhancement*: The substantial increase in turbulence intensity levels and the subsequent jet spread enhancement indicate improved near-field entrainment characteristics (perhaps mixing) for the controlled period-4 flow state. This turbulence enhancement can be further quantified by measuring the near-field spatial distribution of the Reynolds

stresses and the mass entrainment characteristics of the jet, e.g., see Zaman & Hussain (1980) study of a periodically excited jet displaying vortex pairings.

*Turbulence suppression*: The primary motivation for using the newly developed nonlinear control method to suppress near-field jet turbulence is to reduce the far-field noise signature. Hussain & Hasan (1985) showed that broadband (as well as total) far-field jet noise can be reduced by controlled excitation of a jet in the frequency range $0.01 < St_{\theta e} < 0.02$, where $St_{\theta e}$ is the Strouhal number based on the exit momentum thickness $\theta_e$ of the shear layer. They also demonstrated that the noise suppression was a consequence of near field turbulence suppression. Significant suppression of turbulence levels in the jet near field ($x/D \leq 8$) in the present experiments, with suppression effects persisting for larger streamwise extents, suggests potential for corresponding reduction in far field sound radiation. To demonstrate this reduction, measurements of the far-field sound-pressure spectra and integrated levels (OASPL), say along an arc at a radius of about 50-60 D, are needed. Control is expected to impact the far field sound radiation, namely spectra as well as their directivity, owing to the modification of CS dynamics in the jet and hence its turbulence characteristics. Measurements of various components of the Reynolds stress in the near field ($x/D \leq 6$) will also more clearly reveal the suppression effect, which in this study has been inferred from longitudinal turbulence intensity levels alone.

### 8.3 Hybrid Control

The use of controlled three-dimensionality to significantly improve the entrainment and mixing characteristics in jets is well known (e.g., Zaman 1996); passive embodi-

ments include small modifications to the jet nozzle such as the addition of tabs, or larger modifications to the nozzle shape (e.g., to rectangular and elliptic shapes). On the other hand, forced elliptic jets reveal much more mass entrainment compared to forced circular jets or unforced elliptic jets, making them suitable for applications such as passive combustion control (Husain & Hussain 1983). Preliminary studies in the elliptic jet reveal low-dimensional dynamics in the near field (private communication, Broze), even with single-point measurements on the jet centerline. The use of (active) control in conjunction with (passive) geometry modification – *hybrid* control – will likely improve the performance (e.g., mass entrainment) of elliptic jets for practical applications. Analysis of the chaotic dynamics in the elliptic jet (potentially requiring multipoint azimuthal measurements) may be necessary, following which a nonlinear control strategy, similar to that developed for the circular jet, can be devised and assessed for varying aspect ratios.

Another aspect of jet control worth investigating is the prospect of using the nonlinear control method developed here for controlling (actively) the three-dimensional CS dynamics of the jet. The three-dimensional structure dynamics and their interactions are known to be effective for turbulence enhancement, and can therefore provide superior entrainment and mixing characteristics for the jet. While the control of nominally axisymmetric vortex dynamics in this study has permitted the use of two-point measurements to devise the control signals, multi-point measurements will be necessary to control three-dimensional vortex dynamics. This will be discussed in the next sub section.

### 8.4 Control Approach for Complex Spatiotemporal Flows

The CS dynamics of the flows studied here (namely, the transitional regions of the

jet and the mixing layer) were known to have nominally axisymmetric/2D vortex dynamics with primarily temporal complexity (achievable due to spatial coupling). For the jet, three-dimensional dynamics due to tilted vortex rings and their partial pairing (termed aperiodic modulations in Broze & Hussain 1994) are prevalent for much lower forcing levels than that for the chaotic jet state having nominally axisymmetric vortex dynamics studied here. The control of these seemingly high-dimensional flow states (based on single-point measurements) have potential for enhanced jet mixing due to the prevalence of three dimensionality while utilizing reduced input of control energy (compared to that used for the axisymmetric chaotic flow states). There is an obvious inadequacy of analysis techniques to describe such spatially complex dynamics, requiring development of tools to identify low-dimensional dynamics from multi-point data. Such tools using the dynamical systems approach are yet unavailable; some promising preliminary results are summarized below.

Using two-point mutual information MI (Fraser & Swinney 1986), coherence and singular value decomposition SVD (Broomhead & King 1986), spatiotemporal dynamics of three-dimensional vortex dynamics in the jet were reconstructed from simultaneously acquired multi-point data from azimuthally placed hot-wire sensors (Narayanan et al. 1997). Two-point MI and coherence was employed to select the sensor density (i.e., placement and number) and SVD was used to reconstruct the spatiotemporal dynamics. Low-dimensional chaotic dynamics (dimension less than 5) were found for the aperiodically modulated states, which have three-dimensional vortex dynamics. These preliminary results show promise for the identification and analysis of complex spatiotemporal

dynamics. The (unstable) periodic flow states can be extracted and modeled for control in a manner similar to that for the temporal dynamics (from single-point measurements). Control can be applied via azimuthally non-uniform acoustic forcing at the nozzle lip. A natural extension of these ideas would be the control of three-dimensional flow structures in the plane mixing layer. Furthermore, multi-point measurements can also be used to describe the dynamics of spatially evolving flows such as wall jets, far wakes and boundary layers, where spatial coupling mechanisms (such as vortex pairing-driven feedback in the jet and the mixing layer) are not evident. In such flows, multiple measurements can be made with a streamwise distributed sensor array, from which the spatiotemporal dynamics could be reconstructed and used for control (as for the azimuthal sensor array described above). The development of tools to describe and control spatiotemporal phenomena is a research problem in nonlinear dynamical systems theory, with applications across a much wider range of physical systems.

### 8.5 Model-based Control of CS Dynamics

In this study, the essential large-scale CS dynamics in the circular jet were inferred from experimental measurements of the temporal dynamics in the transitional region of the flow. The occurrence of sequences of vortex roll up and pairings were inferred from "nearly periodic" realizations of chaotic signals obtained from the jet. These empirical descriptions of the periodic flow states embedded in the chaotic jet dynamics were then used for control. A prevalent semi-empirical alternative to this form of modeling is proper orthogonal decomposition (POD), which has been used in several flows such as boundary layers (Aubry et al. 1988), mixing layers and jets (Ukeiley et al. 2001). Dynam-

ical models, involving a coupled system of nonlinear ordinary differential equations (ODE), are extracted by projecting the Navier Stokes equations with the appropriate boundary conditions onto a truncated data set obtained from numerical simulations or experiments. However, such models have yet to be used for jet control, and their use for control is a promising avenue to pursue. Interestingly, research has been active in this area recently with promising progress for the use of POD-based models for active control of cavity flows (see Rowley & Williams 2006); these flows have self-sustained and self-excited oscillations making their closed flow behavior low-dimensional and more amenable to robust control.

The phase space eduction approach presented here can also be utilized to provide a dynamical model of the jet dynamics (reconstructed from single-point measurements). A potential approach to do this is outlined below. The empirically averaged unstable periodic flow state realizations could be used to construct a reduced order *predictive* model for the statistically dominant CS dynamics in the flow. For example, local phase-space neighborhoods of the chaotic attractor, reconstructed from single-point measurements of the jet dynamics, can be approximated using an ensemble of unstable periodic orbits (UPO), which in physical space correspond to an ensemble of nearly periodic (but unstable) flow states. A nonlinear ODE system can be used to approximate the time evolution for the periodic states, which correspond to orbits in the chaotic attractor. Thus, one can determine the model evolution to predict the next sequence of CS dynamics in the chaotic flow. This may only be viable for short times since the inherently chaotic behavior deteriorates the predictability. The prediction accuracy will depend on the ensemble size used

and can be evaluated by comparing the originally reconstructed dynamical system (namely, the chaotic attractor) and that obtained by (numerically) solving the empirical coupled ODE model. The successful prediction of chaotic dynamics using UPOs in a low-dimensional coupled ODE system (the Röessler system) by Pawelzik & Schuster (1991) is promising. The finding of low-dimensional chaotic attractors in wakes and boundary layers indicates that this approach to modeling CS dynamics can be attempted in other open shear flows as well.

# REFERENCES


Ahlers, G., Cannell, D.S. & Steinberg, V. 1985 *Phys. Rev. Lett*., **54**, 1373.

Aranson, I., Levine, J. & Tsimring, L. 1994 *Phys. Rev. Lett*., **72**, 2561.

Arbey, H. & Ffowcs-Williams, J.E. 1984 *J. Fluid Mech*., **149**, 445.

Aubry, N., Holmes, P., Lumley, J.L. & Stone, E. 1988 *J. Fluid Mech*., **192**, 115.

Auerbach, D. 1994 *Phys. Rev. Lett*., **72**, 1184.

Bendat, J.S. & Piersol, A.G. 1986 *Random Data Analysis and Measurement procedures 2nd ed. Wiley-Interscience.*

Bewley, T.R., Moin, P. & Temam, R. 2001 *J. Fluid Mech.* **447**, 179.

Bonnetti, M. & Boon, J-P. 1989 *Physical Review A,* **40** 3322.

Brandstäter, A., Swift, J., Swinney, H.L., Wolf, A., Farmer, J.D. & Jen, E. 1983 *Phys. Rev. Lett*., **51**, 1442.

Bridges, J.E. 1990 "Application of coherent structure and vortex sound theories to jet noise," Ph.D. Dissertation, Mechanical Engineering Department, Univ. of Houston.

Broomhead, D.S. & King, G.P. 1986 *Physica D,* **20**, 217.

Browand, F.K. & Laufer, J. 1975 *Turb. Liquids* **5**, 333-344, Univ. of Missouri-Rolla.

Browand, F.K. & Weidman, P.D. 1976 *J. Fluid Mech.*, **76**, 127.

Brown, G.B. 1937 *Proc. Phys. Soc.*, **49** 493.

Brown, G.L. & Roshko, A. 1974 *J. Fluid Mech.*, **64**, 775.

Broze, G. 1992 "Chaos in an "open flow": Experiments in a transitional jet," Ph.D. Dissertation, Mechanical Engineering Department, Univ. of Houston.

Broze, G. & Hussain, F. 1994 *J. Fluid Mech.*, **263**, 93.

Broze, G. & Hussain, F. 1996 *J. Fluid Mech*., **311**, 37.

Broze, G., Narayanan, S. & Hussain, F. 1997 *Phys. Rev. E*, **55**, 4179.

Burattini, P & Talamelli, A. 2007 *J. Turbulence*, **8**(47), 1.

Chen, G. & Dong, X. 1993 *Int. J. Bifurc. Chaos*, **3**, 1363.

Choi, H., Moin, P. & Kim, J. 1994 *J. Fluid Mech*., **262**, 75.

Cohen, J. & Wygnanski, I.J. 1987a *J. Fluid Mech*., **176**, 191.

Cohen, J. & Wygnanski, I.J. 1987b *J. Fluid Mech*., **176**, 221.

Coller, B.D., Holmes, P. & Lumley, J.L. 1994 *Physica D*, **72**, 135.

Coller, B.D., Noack, B.R., Narayanan, S., Banaszuk, A. & Khibnik, A.I. 2000 "Reduced-basis model for active separation control in a planar diffuser flow," in *Proceedings of AIAA FLUIDS 2000 & Exhibit*, June, 2000, Denver, CO, U.S.A., *AIAA paper 2000-2562*.

Corke, T.C., Glauser, M. & Berkooz, G. 1994 *Applied Mech. Rev.*, **47**(6), part 2, S132.

Corke, T.C. & Kusek, S.M. 1993 *J. Fluid Mech*., **249**, 307.

Cortelezzi, L. 1996 *J. Fluid Mech*., **327**, 303.

Cross, M. & Hohenberg, P.C. 1993 *Rev. Mod. Phys.*, **65** 851.

Crow, S.C. & Champagne, F.H. 1971 *J. Fluid Mech*., **48**, 547.

Cvitanovic, P., Gunaratne, G.H. & Procaccia, I. 1988 *Phys. Rev. A*, **38**, 1503.

Deissler, R.J. & Kaneko, K. 1987 *Phys. Lett*., **119**, 397.

Delville, J., Ukeiley, L.S., Cordier, L., Bonnet, J.-P. & Glauser, M.N. 1999 *J. Fluid Mech*., **391**, 91.

Dimotakis, P.E. & Brown, G.L. 1976 *J. Fluid Mech.*, **78**, 535.

Dubois, M. 1982 *Stability of Thermodynamic Systems*. Lecture Notes in Physics, **164**, 117.

Fraser, A. & Swinney, H.L. 1986 *Phys. Rev. A*, **33**, 1134.

Fradkov, A.L. & Evans, R.J. 2005 *Annual Reviews in Control*, **29**, 33.

Freund, J. & Moin, P. 2000 *AIAA J.*, **38**(10), 1863.

Gad-el-Hak, M. 1996 *Appl. Mech. Rev*., **49**(7), 365.

Gad-el-Hak, M. & Bushnell, 1991 *J. Fluids Engr*., **113**, 5.

Gillies, E.A. 1998 *J. Fluid Mech*., **371**, 157.

Gills, Z., Iwata, C., Roy, R., Schwartz, I.B. & Triandaf, I. 1992 *Phys. Rev. Lett*., **69**, 3169.

Glauser, M.N., Zheng, X. & Doering, C.R. 1989 The dynamics of organized structures in the axisymmetric jet mixing layer. In *Turbulence and Coherent Structures* (Ed. O.

Metais & M. Lesieur). Kluwer.

Glauser, M.N., Zheng, X. & George, W.K. 1990 The streamwise evolution of coherent structures in the axisymmetric jet mixing layer. In *Recent Developments in Turbulence* (Ed. T.B. Gatski, S. Sarkar & C.G. Speziale). Springer.

Gollub, J.P. & Ramshankar, R. 1991 *New Perspectives in Turbulence*, L. Sirovich, Ed. (Springer-Verlag, New York), 165.

Grassberger, P. & Procaccia, I. 1983 *Physica D*, **9**, 189.

Grinstein, F.F., Oran, E.S. & Boris, J.P. 1991 *Phys. Fluids A*, **3**, 2401.

Guan, S., Zhou, Y.C., Wei, G.W. & Lai, C.-H. 2003 *Chaos*, **13**(1), 64.

Hall, K. Christini, D., Tremblay, M., Collins, J.J., Glass, L. & Billette, J. *Phys. Rev. Lett.*, 1997, **78**(23), 4518.

Haritonidis, J.H., Fan, X. & Herbert, T. 1993 *Bull. Am. Phys. Soc*., **38**, 2251.

Healey, J.J. 1993 *J. Fluid Mech*., **255**, 667.

Ho, C-M. & Huang, L.S. 1982 *J. Fluid Mech*., **119**, 443.

Ho, C-M. & Huerre, P. 1984 *Ann. Rev. Fluid Mech.* **16**, 365.

Ho, C-M. & Gutmark, E. 1987 *J. Fluid Mech*., 383.

Hu, H.H. & Bau, H.H. 1994 *Proc. Roy. Soc. Lond. A* **447**, 299.

Hua, J-C., Kostka, S., Jiang, N., Gunaratne, G.H., Gord, J.R. & Roy, S. 2012, submitted to Combustion and Flame.

Huang, S.C., Kim. J. & Gibson, J.S. 2004 A*dv. Turb. X, Proc. 10th Eur. Turbulence Conf.*, Trondheim, Norway, ed. HI Andersson, P-A Krogstad.

Huang, S.C. 2005 *Numerical simulation and feedback control of separated flows*. PhD Thesis. Dept. Mech. Aerospace Eng., UCLA.

Huerre, P. 1987 Spatio-temporal instabilities in closed and open flows. In *Instabilities and Nonequilibrium Structures* (ed. E. Tirapegui & D. Villaroel), p.141. Reidel.

Huerre, P. & Monkewitz, P.A. 1990 *Ann. Rev. Fluid Mech.*, **22**, 473.

Husain, H.S. & Hussain, F. 1983 *Phys. Fluids*, **26**, 2763.

Husain, H.S. & Hussain, F., 1995 *J. Fluid Mech*., **304**, 343.

Husain, Z.D. 1982 "An experimental study of effects of initial and boundary conditions on near and far fields of jet flows," Ph.D. Dissertation, Mechanical Engineering Department, Univ. of Houston.

Hussain, F. 1983 *Phys. Fluids* **26**, 2816.

Hussain, F. & Hasan, M.A.Z. 1985 *J. Fluid Mech*., **150**, 159.

Hussain, F., Husain, H.S., Zaman, K.B.M.Q., Tso, J., Hayakawa, M., Takaki, R. & Hasan, M.A.Z. 1986 *AIAA 24th Aerospace Sciences Meeting* AIAA-86-0235.

Hussain, F. & Zaman, K.B.M.Q. 1978 *J. Fluid Mech*., **87**, 349.

Hussain, F. & Zaman, K.B.M.Q. 1981 *J. Fluid Mech*., **110**, 39.

Hussain, F. & Zaman, K.B.M.Q. 1985 *J. Fluid Mech*., **159**, 85.

Jeong, J., Hussain, F., Schoppa, W. & Kim, J. 1997 *J. Fluid Mech*., **332**, 185.

Keefe, L.R. 1987 *Bull. Am. Phys. Soc.*, **32**, 2026.

Keefe, L.R. 1993 *Phys. Fluids A*, **5**, 931.

Kelly, R.E. 1967 *J. Fluid Mech*., **27**, 657.

Kennel, M., Brown, R. & Arbabanel, H. 1992 *Phys. Rev. A*, **45**, 3403.

Kim, J. & Bewley, T.R. 2007 *Ann. Rev. Fluid Mech*., 39**,** 383.

Kim, K.I. & Powers, E.J. 1988 *IEEE Transactions on Acoustics, Speech and Signal Processing*, **36**, 1758.

Koumoutsakos, P., Fruend, J. & Moin, P. 1998 Evolution strategies for parameter optimization in jet flow control. *Proceedings of the Summer Program, Center for Turbulence Research*, 121.

Lasheras, J.C. & Choi, H. 1988 *J. Fluid Mech.*, **189**, 53.

Lee, K. H., Cortelezzi, L., Kim, J. & Speyer, J. L., 2001 *Phys. Fluids*, **13**(5), 1321.

Lee, M. & Reynolds, W.C. 1985 Bifurcating and blooming jets. *Fifth Symposium on Turbulent Shear Flows*, Ithaca, New York, 1.7-1.12.

Liu, J., Paul, J.D., Banilower, E. & Gollub, J.P. 1992 *Proceedings of the First Experimental Chaos Conference*, S. Vohra, M. Spano, M. Schlesinger, L.M. Pecora, W. Ditto, Eds. (World Scientific, Singapore), 225.

Lumley, J. 1967 The structure of inhomogeneous turbulent flows. In *Atmospheric Turbulence and Radio Wave Propagation* (Ed. A.M. Yaglom & V.I. Tatarsky), pp. 166-

178. Nauka, Moscow.

Lumley, J. & Blossey P. 1998 *Ann. Rev. Fluid Mech*., **30**, 311.

Lüscher, E. & Hübler, A.W. 1989 *Helv. Phys. Acta*, **62**, 544.

Mayer-Kress, G. & Kurz, T. 1987 *Complex Systems*, **1**, 821.

Mankbadi, R.R. 1985 *J. Fluid Mech*., **160**, 385.

Mattingly, G.E. & Chang, C.C. 1974 *J. Fluid Mech*., **65**, 541.

Miksad, R.W., Jones, F.L. & Powers, E.J. 1983 *Phys. Fluids*, **26**, 402.

Michalke, A. 1965 *J. Fluid Mech*., **23**, 521.

Michalke, A. 1971 *Z. Flugwiss*., **19**, 319; also NASA TM 75190.

Moin, P. & Bewley, T.R. 1994 *Appl. Mech. Rev*., **47**, S3.

Monkewitz, P.A. 1988 *J. Fluid Mech*., **123**, 91.

Moore, C.J. 1977 *J. Fluid Mech*., **80**, 321.

Morris, P.J. 1976 *J. Fluid Mech*., **77**, 511.

Narasimha, N. 1983 *J. Indian Inst. Sci.*, **64(A)**, 1.

Narayanan, S. & Hussain, F. 1996 *J. Fluid Mech.*, **320**, 71.

Narayanan, S., Roy, S. & Hussain, F. 1997 In *Proceedings of the 7$^{th}$ Asian Congress of Fluid Mechanics*. Dec. 8-12, 1997, 327.

Narayanan, S., Barber, T.J. & Polak, D.R. 2002 *AIAA J*., **40**(3), 430.

Ott, E., Grebogi, C. & Yorke, J. 1990 *Phys. Rev. Lett*., **70**, 3031.

Parekh, D.E., Reynolds, W.C. & Mungal, M.G. 1987 Bifurcation of round air jets by dual-mode acoustic excitation. *AIAA Paper 87-0164*.

Paschereit, C.O., Wygnanski, I. & Fiedler, H.E. 1995 *J. Fluid Mech*., **283**, 365.

Pawelzik, K. & Schuster, H.G. 1991 *Phys. Rev. A*, **43**, 1808.

Pausch, M. & Eckhardt, B. 2011 In *Proceedings of 13$^{th}$ European Turbulence Conference, Journal of Physics: Conference Series* **318**.

Petersen, R.A., Kaplan, R.E. & Laufer, J. 1974 *NASA Contractor Rep*. No. 134733.

Petrov, V., Crowley, M. F. & Showalter, K. 1994 *J. Chem. Phys*., **101**(8), 6606.

Petrov, V. & Showalter, K. 1996 *Phys. Rev. Lett*., **76**(18), 3312.

Plaschko. P. 1979 *J. Fluid Mech*., **92**, 209.

Pyragas, K. 1992 *Phys. Lett. A*, **170**, 421.

Rajaee, M., Karlsson, S.K.F. & Sirovich, L. 1994 *J. Fluid Mech*., **258**, 1.

Rathnasingham, R. & Breuer, K.S. 1997 *Phys. Fluids*, **9**(7), 1867.

Reba, R., Narayanan, S. and Colonius, T. 2010 *Intl. J. of Aeroacoustics*, **9**(4).

Reisenthel, P. 1988 "Hybrid Instability in an Axisymmetric Jet with Enhanced Feedback," Ph.D. Dissertation, Mechanical/Aerospace Engineering Department, Illinois Institute of Technology.

Ritz, Ch.P. & Powers, E.J. 1986 *Physica D*, **20**, 320.

Rowley, C.W & Williams, D.R. 2006 *Ann. Rev. Fluid Mech*., **38**, 251.

Roy, R., Murphy, Jr., T.W., Maier, T.D., Gills, Z. & Hunt, E.R. 1992 *Phys. Rev. Lett*., **68**(9), 1259.

Roy, S., Narayanan, S. & Hussain, F. 1997 *Bull. Am. Phys. Soc*., **42**, 2131.

Sano, M. & Sawada, Y. 1985 *Phys. Rev. Lett*., **55**, 1082.

Schöll, E. & Shuster, H.G. 2008 Handbook of Chaos Control (Second edition), John Wiley & Sons.

Schoppa, W., Hussain, F. & Metcalfe, R.W. 1995 *J. Fluid Mech*., **298**, 23.

Shermer, R., Hübler, A. & Packard, N. 1991 *Phys. Rev. A*, **43**, 5642.

Shinbrot, T. 1995 *Adv. in Phys*., **44**, 73.

Shinbrot, T. & Ottino, J.M. 1993 *Phys. Rev. Lett.* **71**, 843.

Singer, J., Wang, Y-Z. & Bau, H.H. 1991 *Phys. Rev. Lett*., **66**, 1123.

Sreenivasan, K.R. 1985 in *Fundamentals of Fluid Mechanics*, edited by S.H. Davis and J.L. Lumley (Springer), p.41.

Strange, P.J.R 1981 Ph.D. Thesis, University of Leeds, UK.

Strange, P.J.R. & Crigton, D.G. 1981 *J. Fluid Mech*., **134**, 231.

Ukeiley, L., Cordier, L., Manceau, R., Delville, J., Glauser, M. & Bonnet, J.P. 2001 *J. Fluid Mech*., **441**, 67.

Van Atta, C.W. & Gharib, M. 1987 *J. Fluid Mech.*, **63**, 237.

Widrow, B. & Stearns, S.D. 1985 *Adaptive Signal Processing*, (Prentice-Hall, Inc.).

Wiltse, J.M., & Glezer, A. 1993 *Bull. Am. Phys. Soc.*, **38**, 2275.

Wolf, A., Swift, J.B., Swinney, H.L. & Vastano, J.A. 1985 *Physica D*, **16**, 285.

Zaman, K.B.M.Q. 1996 *J. Fluid Mech.*, **316**, 1.

Zaman, K.B.M.Q. & Hussain, F. 1980 *J. Fluid Mech.*, **101**, 449.

Zaman, K.B.M.Q. & Hussain, F. 1981 *J. Fluid Mech.*, **103**, 133.

Zhou, M. & Wygnanski, I. 2001 *J. Fluid Mech.*, **441**, 139.

# APPENDIX A

# CHAOTIC ATTRACTOR IN THE AXISYMMETRIC JET AND THE CHAOS CONTROL CONCEPT

As described in Chapter 3, the anechoic jet was acoustically excited at a single frequency f, providing the following dimensionless control parameters: the forcing amplitude $a_f \equiv u'_f/U_e$ and the forcing frequency $St_D \equiv f\ D/U_e$; $u'_f$ is the centerline rms-velocity fluctuation at f, $U_e$ is the centerline exit velocity, and D is the jet diameter. Among a wide variety of dynamical states (including low- and high-dimensional temporal attractors), two periodic and two low-dimensional chaotic attractors were found over large regions in the parameter space. The phase diagram, the attractors' invariants and transitions between dynamical states are extensively discussed in Broze & Hussain (1994, 1996). In the following, the dynamical systems (DS) approach to describe the near field jet dynamics is presented. In particular, the dynamical systems-based approach to nonlinear control, termed *chaos control*, presented in Chapter 4, is discussed.

## A.1 Chaotic Attractor in the Forced Axisymmetric Jet

As explained earlier, while the fundamental frequency f (associated with vortex roll up) is externally forced, the vortical interactions (and hence the associated subharmonic and quarterharmonic frequencies f/2 and f/4) are driven by feedback from vortex pairings, i.e., are self-excited. Figure A.1 displays the phase diagram for the forced jet (reproduced from Broze & Hussain 1994), displaying the dynamical states found for a forced circular jet. In the following, the salient features of the chaotic attractor from this

phase diagram chosen for the present study are described. The chaotic state (the "quarter-harmonic chaotic attractor" QCA) is found in the range $0.008 \leq a_f \leq 0.02$ and $1.1 \leq St_D \leq 1.25$. The ensuing analysis was also done for another chaotic attractor found in the jet and the results and conclusions were similar.

*QCA*. This attractor reveals a correlation dimension in the range $2.5 \leq \nu \leq 3$ and a positive Lyapunov exponent in an embedding dimension of 4 (Broze & Hussain 1994). The longitudinal velocity time trace u(t) in Figure 3.3a was from a hot-wire sensor located downstream at $x/D \cong 2$ (on the jet centerline) for $a_f \cong 1\%$ and $St_D \cong 1.2$. Further discussion of "downstream dynamics" will be based on analyses of similar data acquired on the centerline at $x/D \cong 2$ (see Figure 3.1), where the effects (i.e., the induced velocities) of rollup and both pairings are comparable.

*Unstable periodic orbits*. It is well known that chaotic attractors comprise an infinity of unstable periodic orbits (UPO). These orbits will return arbitrarily close to their initial conditions in phase space; subsequently, the unstable nature of these orbits exponentially diverts them to other attractor neighborhoods. *UPOs are therefore everywhere dense in chaotic attractors*. Being easily tractable, UPOs have been used to compute attractor invariants such as Lyapunov exponents and topological entropy (Cvitanovic et al. 1988), and for control (Ott et al. 1990). In the following, we analyze the UPOs belonging to a chaotic attractor in the jet, viz., QCA. The unstable periodic flow states described and controlled in Chapters 3 and 4 have a one-to-one correspondence with the unstable periodic orbits described here. For fixed $St_D$, as $a_f$ is increased from low background levels,

QCA appears and persists up to high $a_f$; a periodic attractor (termed SDP in Figure A.1) appears at still higher $a_f$. We use velocity signals from parameter space locations where QCA had just appeared (with increasing $a_f$), since these states have small, yet positive, largest Lyapunov exponents, enabling clearer analyses of UPOs for their control.

### A.2 Analysis and Empirical Modeling of Unstable Periodic Orbits

*UPO identification*. The chaotic attractor QCA is first reconstructed from a single-point velocity signal measurement using the method of time delays. The time delay $\tau$ corresponds to that for the first minimum of the mutual information (Fraser & Swinney 1986). A Poincarè section is then selected to record the UPOs. A false-nearest-neighbor algorithm (Kennel et al. 1992) is used to estimate the attractor's minimum embedding dimension m. To determine close returns on the attractor (i.e., the UPOs) images of the time series u(t) that intersect the Poincarè section in one direction are examined. That is, we seek the smallest recurrence time T such that $\| u(t+T) - u(t) \| < \varepsilon_1$, where u(t) is an m-dimensional vector comprising the time-delays $u(t), u(t+\tau), u(t+2\tau), \ldots, u(t+(m-1)\tau)$. Thus, the first return of a trajectory to the $\varepsilon_1$-neighborhood is recorded.

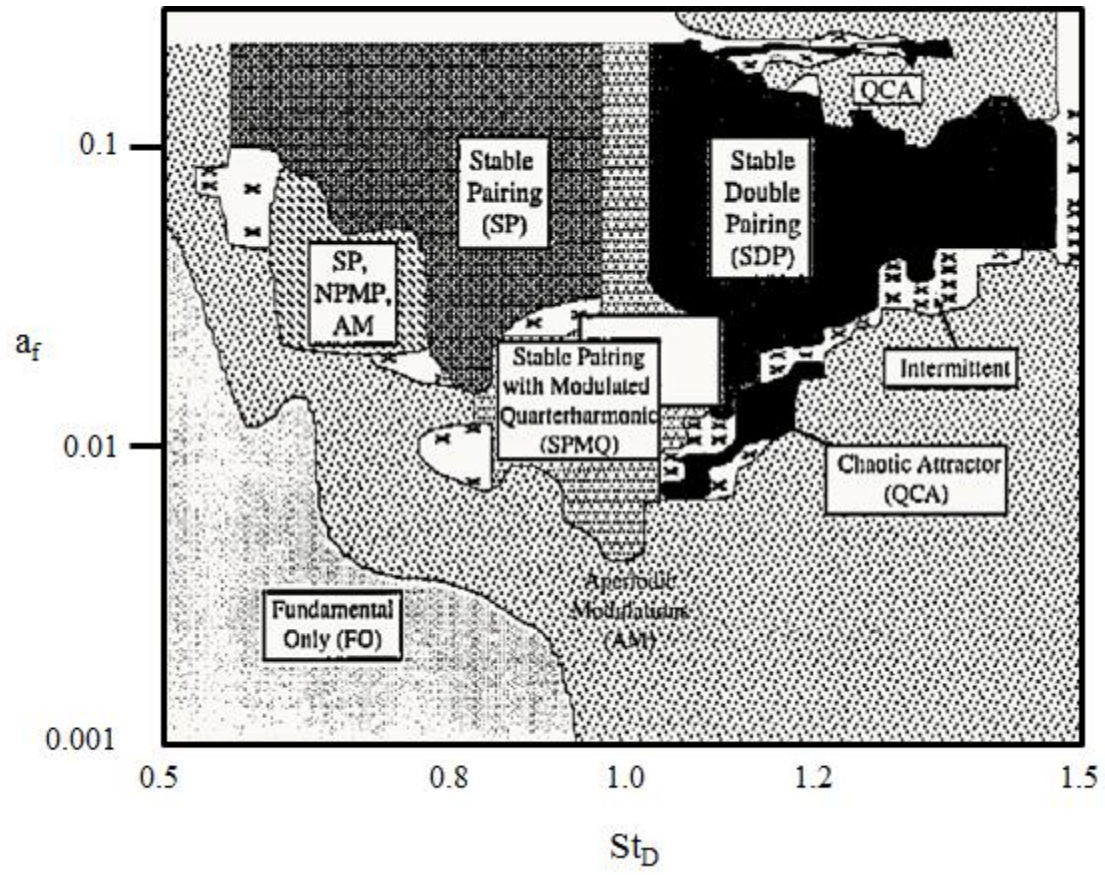


Figure A.1 Phase diagram of forced jet displaying parameter space location for chaotic attractor studied (QCA); figure reproduced from Broze & Hussain (1994).

The large and uneven scatter in the 2D projection of the QCA Poincarè section (Figure A.2) is expected due to the low-dimensional chaotic dynamics; the time series was 300, 000 data points long and, for well-resolved Poincarè sections, was sampled at 20 times the fundamental frequency. The $u(t+2\tau) = u(t) + u(t+\tau)$ plane (i.e., passing through the $u(t+2\tau)$ axis and intersecting the $[u(t), u(t+\tau)]$ plane at $45^o$) was used to obtain the 3D Poincarè section. The histogram of UPOs shown earlier in Figure 3.4 was determined from the above Poincarè section with $\varepsilon_1 \cong 5\%$, the fraction of the Poincarè section coordinates' range; the UPOs shown comprise 53% of all the positive Poincarè section cross-

ings detected. The recurrence times were normalized by the fundamental period. We chose $\varepsilon_1 \cong 5\%$, since the number of UPOs, of a given period, reached a plateau for $\varepsilon_1 \leq 8\%$ (see inset in Figure 3.4).

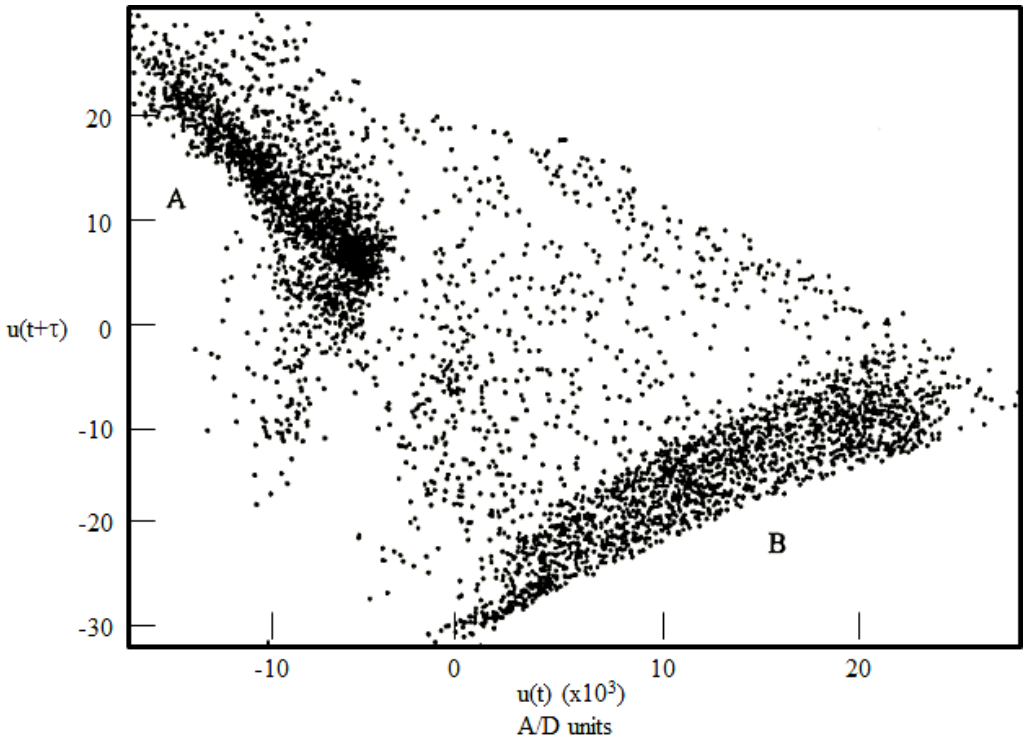


Figure A.2 The positive (A) and negative (B) crossings in a QCA Poincaré section.

For a selected orbit period, say a period-n orbit, Poincarè section crossings were found to cluster, i.e., successive orbit returns belong to the same neighborhood in the Poincarè section. This indicates the dominance of certain types of UPOs. The clusters were identified using a probability density function for the number of UPO crossings in the Poincarè section. Figures A.3(a,b,c) display the peak regions of the pdf for period-9, period-11 and period-15 orbit crossings. The clustering of the crossings is evident from these distributions. The bin size for the pdf was chosen to be 10% of the Poincarè section

range, so that only phase-space clusters were identified without resolving details within a cluster.

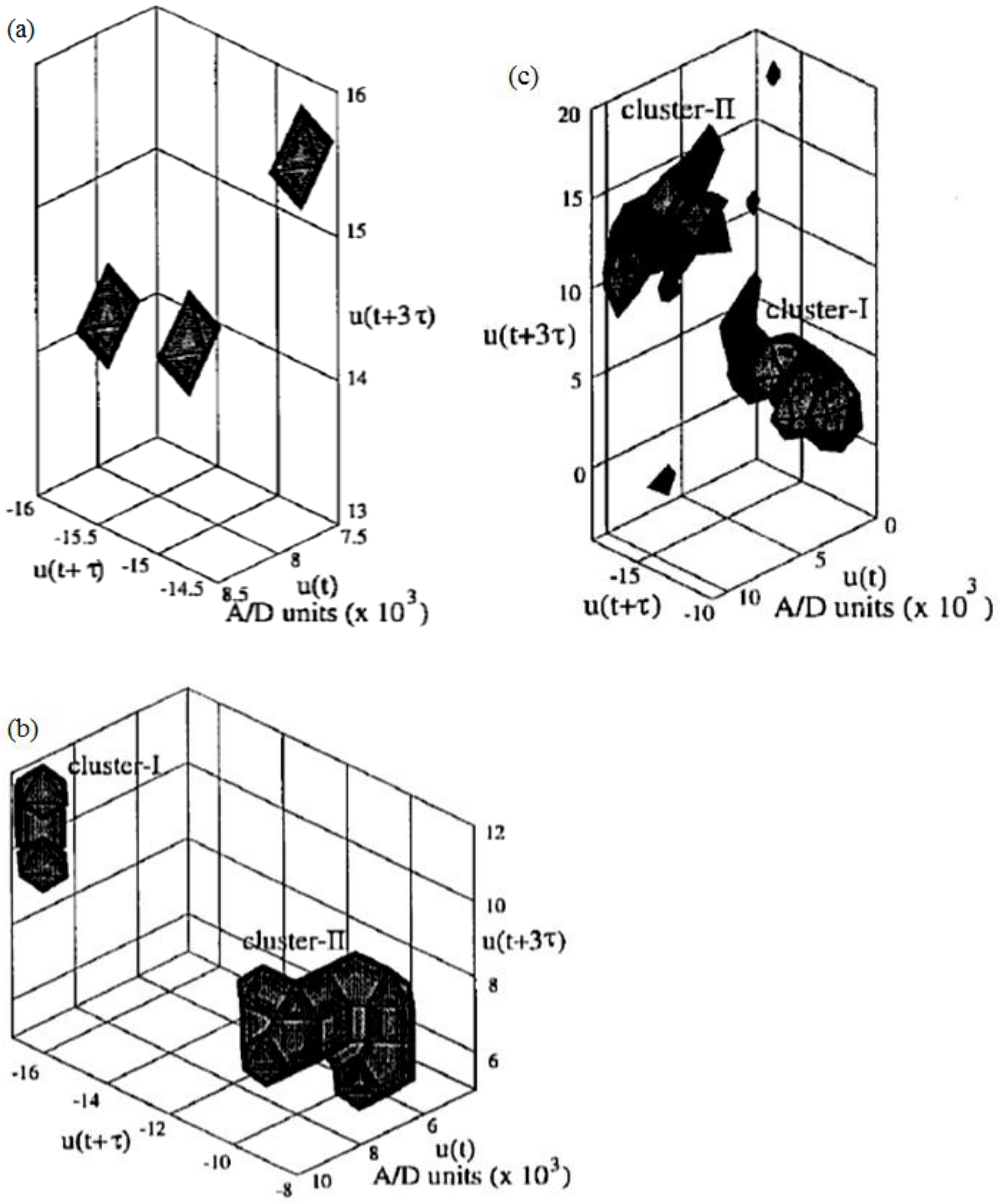


Figure A.3 (a) Shaded contour surfaces of pdf for UPO crossings in a Poincaré section shows: 3 clusters in time delayed embedding of phase space for peiod-9 UPO; (b) Two phase space clusters for period-11 UPO crossings; (c) Two large clusters and some scattered clusters for period-15 crossings. Contour levels in the range [0.4-1] are plotted in intervals of 0.1.

These clusters were also observed in Poincarè sections at other attractor locations. The contour surfaces for the period-9 UPO crossings are poorly resolved due to the few number of UPOs found (around 3 per cluster). The larger number of UPO for period-11 and period-15 orbits result in better resolved contours. These clusters are further analyzed below. There is no obvious structure in the uneven distribution of crossings within a cluster [see Figures A.3(b,c)]. Clusters of UPO crossings with large periods are found to be smeared and scattered, e.g., the period-15 crossings on Figure A.3(c). Smearing occurs when lower contour levels are chosen so that clusters are not distinct. Scattered orbits (i.e., not belonging to distinct, large clusters) are ignored for further analysis. A threshold on the pdf ($\cong 0.4$) is used to distinguish smeared clusters (i.e., clusters without distinct boundaries).

In summary, the chaotic orbits sweep through several unstable, nearly periodic states. These phase-space states are accessible as stable periodic attractors, but require high $a_f$ and changes to $St_D$ (see Figure A.1 and Broze & Hussain 1994). The objective of the present study is to stabilize, through control, these unstable states for lower $a_f$ and fixed $St_D$. The significance of the observed clusters (of UPO crossings) and the associated trajectories are explained below.

*The averaged UPO representation.* As discussed in Chapter 3, a key feature of the UPOs (associated with unstable periodic flow states) is that the orbits crossing a Poincarè section cluster are found to be nearly identical, with only slight variations in amplitude/phase [see Figures 3.6(c,d)]. As the above-mentioned clusters are preserved in several sections around the attractor, orbits crossing these clusters must remain in “bundles” and conse-

quently evolve similarly. The realizations of unstable periodic flow states shown in Chapter 3 correspond to such "bundled" UPOs. For the jet, at most three distinct clusters in the Poincarè section are found surrounding all UPO crossings with periods lower than 15. This is to be expected since, in general, for UPOs with not too large unstable eigenvalues, nearby chaotic orbits must also evolve similarly along the stable and unstable manifolds of the UPOs. Studies have shown that low period UPOs yield the coarsest features of chaotic attractors and successively higher period UPOs (which tend to be scattered) reveal finer details (Cvitanovic et al. 1988). Thus, UPOs with low periods visit only few attractor neighborhoods.

After distinct clusters in a single QCA Poincarè section are identified, UPOs for the time interval between their origin from a cluster and their return are recorded. Figure 3.6(c) displayed all period-11 UPOs crossing cluster-II in Figure A.3(b), revealing striking similarities. Each realization corresponds to an orbit visit (at different times) to the cluster. As pointed out earlier, the differences between the UPOs are most pronounced just after 6 fundamental time periods, when a relatively distinct isolated fundamental period is seen. From the viewpoint of the phase space dynamics, it appears that trajectories that are close in one Poincarè section diverge at another phase; the reason for such behavior is not yet clear although, such behavior may be a result of including "spurious" UPOs. Use of smaller $\varepsilon_1$ reduces the differences but does not eliminate them. Only three period-15 orbits from cluster-II in Figure A.3(c) were shown in Figure 3.6(d) to better display their average. Similar results are obtained for other UPOs (with same as well as different periods). Orbits crossing distinct clusters are averaged, removing slight variations in am-

plitude/phase, to reveal the underlying UPO. Figure 3.6(d) displays the averaged period-15 UPO for QCA (indicated by symbols), which is virtually identical to other orbits from the cluster. Such is obviously the case in Figure 3.6(c) also.

The above results support the expectation that orbits neighboring a UPO evolve similarly. The UPOs analyzed also reveal the periodic dynamical states which can be targeted for control. The clustering of UPO crossings signifies preferential occurrence of certain sequences of CS formation and interactions; thus, low forcing levels will suffice to maintain these UPOs for control. UPOs of smaller periods are also the statistically dominant ones (see Figure 3.4).

*Phase-space eduction*. The averaging of phase-space trajectories was proposed as an alternative eduction approach by Keefe (1987), who pointed out that structure eduction by phase averages implicitly assumes "nearly periodic" evolution and that the phase averages were equivalent to trajectory averaging within "narrow" phase space windows. Since Keefe's averaging procedure was unable to prescribe appropriate phase space window sizes, the disadvantage of subjective window-based averaging and thresholding in conventional CS eduction remained. The present method for averaging trajectories near UPOs can be used as a new objective tool to describe the evolution of dynamically significant CS – a new eduction procedure. Furthermore, using a weighted average of these UPOs (e.g., based on the number of close returns found or the magnitude of the most unstable eigenvalue), it should be possible to construct a predictive model capturing the essential CS dynamics. Pawelzik & Schuster (1991) used a finite set of "dominant" UPOs to predict the evolution of chaotic dynamics in much simpler temporal DS, viz., the

Rössler system. However, it remains unclear how smooth transitions of the attractor dynamics among different UPOs (with different local stability characteristics) can be captured in a dynamical model.

Below, the two approaches (described in Chapter 3) to determine upstream perturbations (required at the nozzle lip) to stabilize/control unstable periodic flow states (i.e., the UPOs) observed in downstream chaotic signals described are investigated using the DS approach.

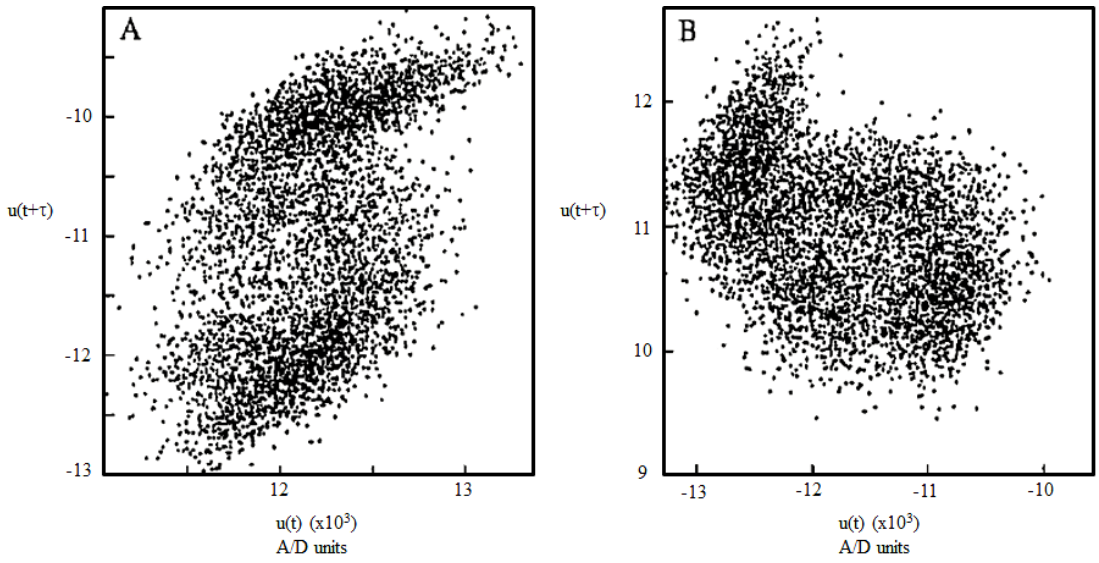


Figure A.4 2D projection of the positive (A) and negative (B) crossings in the QCA Poincaré section from an upstream velocity signal.

### A.3 Determining Upstream Perturbations for UPO

As argued before, the feedback from downstream pairing dynamics, i.e., spatial coupling, guarantees that an upstream velocity signal (at the jet exit) contains footprints of all the periodic states, i.e., the UPOs. Thus, analyses of close returns in the upstream signal, sampled simultaneously with the downstream signal, should reveal (unstable) periodic

orbits as well. The following two methods were described in Chapter 3 as well, and the key ideas and results are interpreted here using the DS approach.

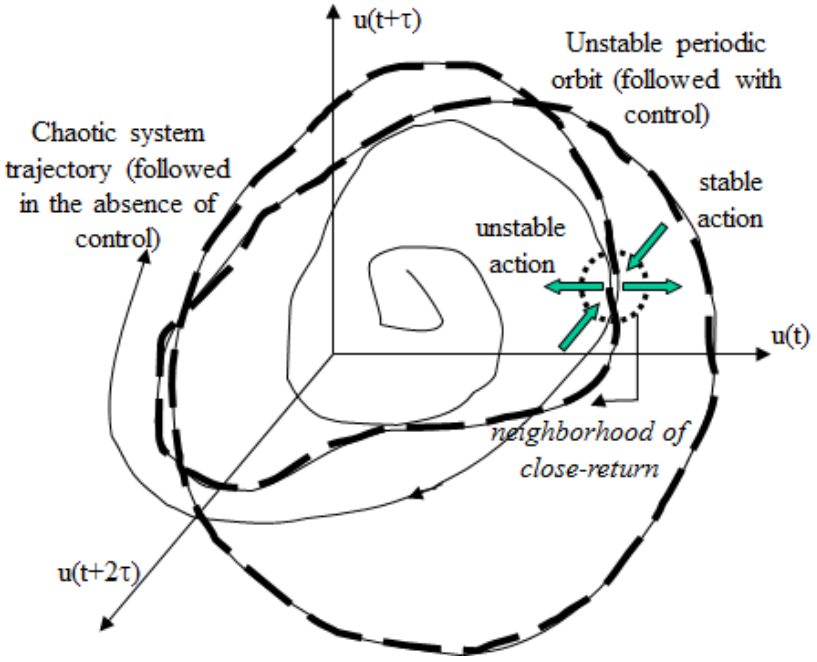


Figure A.5 Schematic of time delayed embedding of a low-dimensional chaotic attractor, highlighting unstable periodic orbits embedded within.

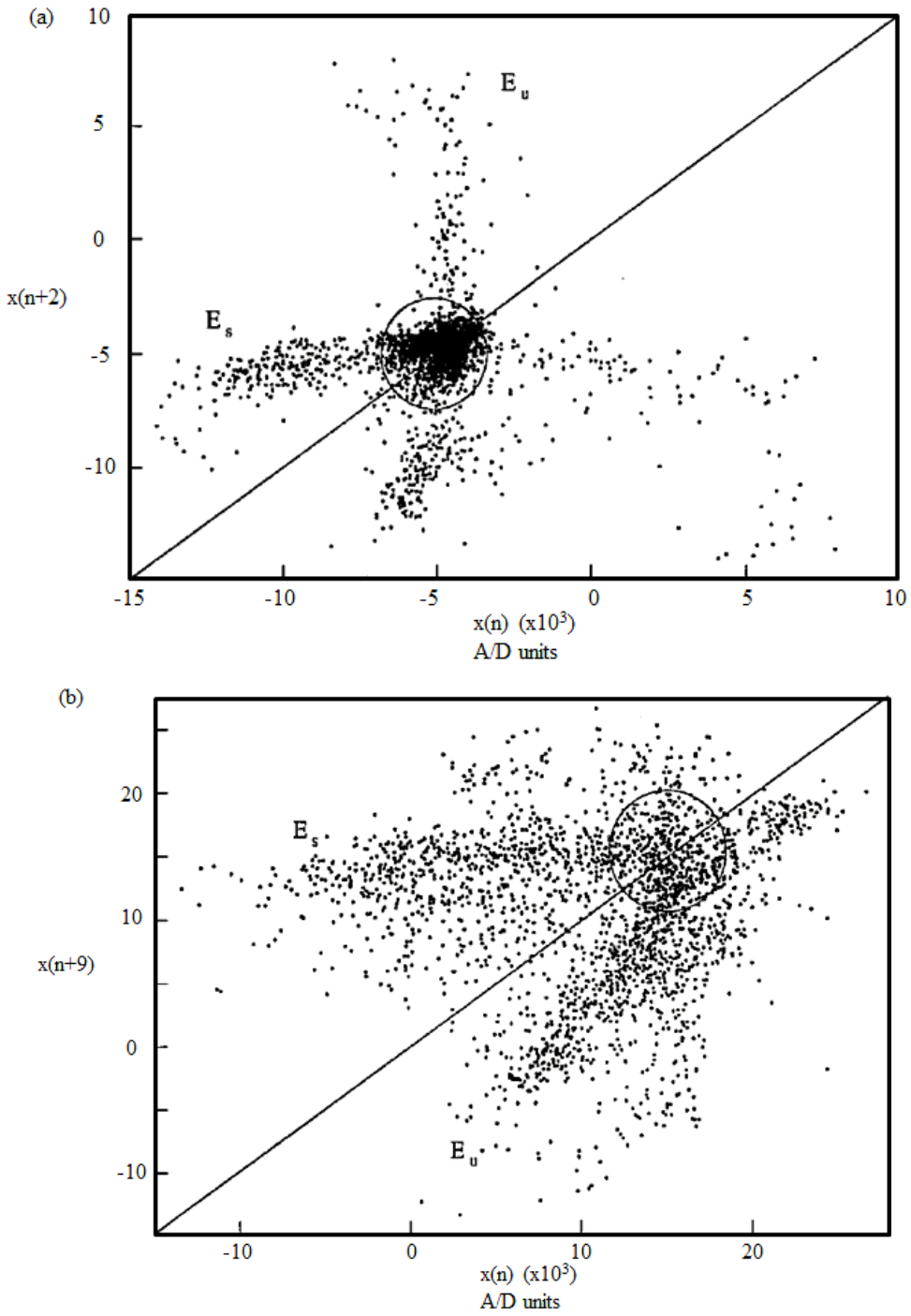


Figure A.6 (a) Unstable fixed point corresponding to crossing of period-2 UPO; $E_u$ and $E_s$ denote the unstable and stable manifolds. The encircled region denotes the approximate fixed point location; (b) Unstable fixed point corresponding to crossing of period-9 UPO; $E_u$ and $E_s$ denote the unstable and stable manifolds. The encircled region denotes the approximate fixed point location.

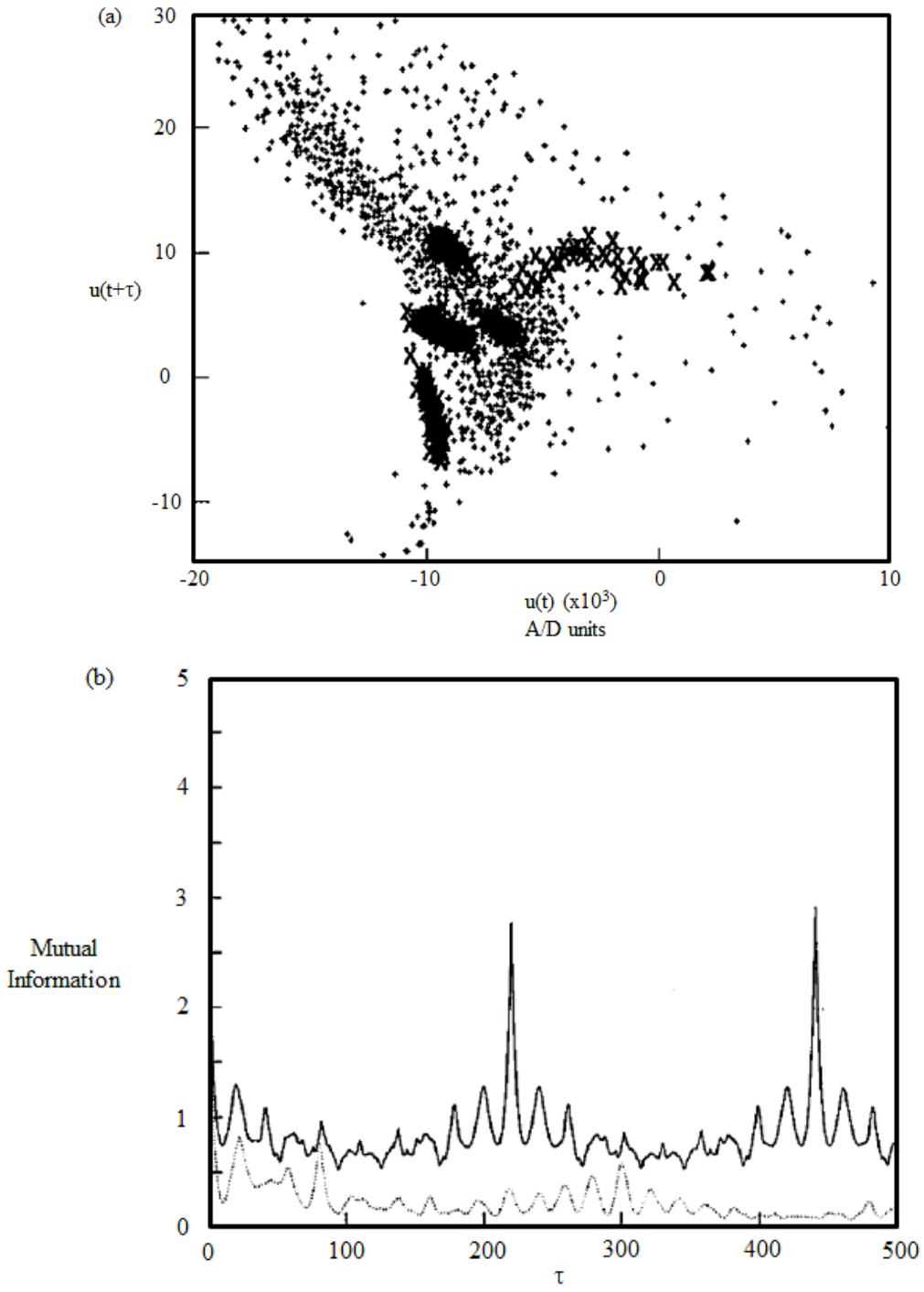


Figure A.7 (a) Poincaré section of the controlled signal ('x'-shaped symbols) overlaid on that for uncontrolled flow ('+' shaped symbols); (b) Mutual information of controlled and uncontrolled flow signals with a peak corresponding to a time delay for period-11 UPO.

*Direct analyses of upstream signals*. The distribution of UPO signatures at the nozzle exit plane (using $\varepsilon_1$ = 5%) shown in Figure 3.7 resembles that in Figure 3.4 (for the downstream signal). The positive and negative crossings in the corresponding Poincarè section are shown in Figure A.4; the extent of scatter is greatly reduced compared to that for QCA at x/D ≅ 2 (see Figure A.2), but the uneven distribution of the crossings is indicative of the underlying deterministic chaotic dynamics. When displayed together, the positive and negative crossings give the appearance of crossings from a "noisy" limit cycle, since the fundamental frequency component dominates the dynamics at this location. The dominance of some frequency components at this upstream location causes the number of UPOs detected for a certain period to be different in Figure 3.7 (compared to Figure 3.4). Clusters (as well as trajectory bundles), like those analyzed in the previous sections, are found for this upstream signal as well. Figures 3.8(a, b) displayed instantaneous realizations of period-11 orbits crossing two different Poincarè section clusters. The small relative variations in the peak-to-peak amplitudes of the dominant fundamental periods are footprints of the downstream UPOs. Notice that, due to the sensitivity of chaotic dynamics, the two similar realizations in Figures 3.8(a, b) in entirely different downstream UPOs [see Figures 3.6(b, c)]. The reason for not choosing to analyze UPOs in these upstream signals before is that it is unclear what goal states are desirable for control; this is because periodicity from the dominant fundamental frequency component overshadows the low-dimensional dynamics associated with the sub-/quarter-harmonic frequencies (associated with vortical interactions of interest).

To identify the upstream signal segment corresponding to a UPO found downstream,

signals sampled simultaneously at two points were analyzed. Whenever a UPO crosses a chosen Poincarè section cluster recorded downstream, a realization from the upstream signal for the UPO period is extracted, assuming that feedback is instantaneous and is dominant compared to background disturbances. These realizations from the upstream signal were then averaged to obtain a perturbation that will guide the downstream attractor dynamics to the vicinity of the desired downstream UPO. For control, this perturbation must be provided continuously (with sufficient amplitude) at the flow origin.

*Adaptive filtering*. The adaptive filtering technique was used to approximate the relationship between a pair of simultaneously sampled signals [x(t), y(t)] (shown schematically in Figure 3.9a) for flows where spatial coupling is not as strong as in the jet. The least-mean-square algorithm to determine the weights is described in Appendix D. Using the estimated adaptive filter and the known averaged downstream UPO to be controlled $x_{UPO}(t)$, the corresponding upstream perturbation $x_{origin}(t)$ is evaluated (see Figure 3.9b). Since the UPOs are all within the chaotic attractor, we use QCA signals (of at least 300, 000 data points) for evaluating the filter weights, taking simultaneously sampled data at the nozzle exit plane and at x/D = 2. Further details were provided in Chapter 3 and Appendix D. The upstream perturbation evaluated is then averaged over the desired UPO period (ignoring initial transients during convergence). The averaged perturbation in Figure 3.10 was determined using adaptive filtering on a downstream period-11 UPO (from cluster-I in Figure A.3b). Its close resemblance to the averaged perturbation obtained directly from an upstream signal (see Figure 3.8b) demonstrated successful "adaptation."

We now describe the new concept to control chaotic dynamics in a (convectively un-

stable) open flow that was experimentally demonstrated in Chapter 4. Prior to the control approach and results discussion, we briefly review the progress and challenges in the emerging area of the control of complex (but low-dimensional) dynamical systems.

*Background. Chaos control* is a recent development in the use of the DS approach. The goal of chaos control is to track periodic states embedded in a *chaotic* dynamical system. This approach typically requires "small" parameter changes for control and is particularly appealing because of its ability to target (potentially useful) unstable states, unattainable by conventional control methods. Chaos control has found applications in diverse fields such as chemical reaction, electronic communication, and lasers (where low-dimensional chaos has been found); see reviews in (Chen & Dong 1993, Shinbrot 1995). For example, using chaos control, the input power for a multimode laser could be increased to levels that enable significantly higher steady output power (Gills et al. 1992); without control, such high levels of input power induce (undesirable) unsteady laser output. Recent findings of low-dimensional chaos in some open flows, such as cylinder wakes (Sreenivasan 1985), plane mixing layer (Narayanan & Hussain 1996), axisymmetric jet (Broze & Hussain 1994), suggest that technologically significant hydrodynamic, in particular turbulence, phenomena such as jet noise, drag, mixing and chemical reaction, as well as flow-induced structural vibrations can also be manipulated via *chaos control*.

Prior chaos control methods have been applied to simple temporal dynamical systems of a few coupled ordinary differential equations, one-/two--dimensional maps, or closed flows (Ott et al. 1990, Singer et al. 1991). Control of spatiotemporal chaos was attempted in homogeneous systems (Auerbach 1994, Aranson et al. 1994). Virtually all

practical flow systems are inhomogeneous, e.g., spatially developing; in these flows, even findings of low-dimensional dynamics, let alone their nonlinear control, have been scarce. Keefe's demonstration of control (with the strategy suggested in Ott et al. 1990) using simulations of the spatially homogeneous Ginzburg-Landau equation necessitates spatiotemporal velocity field information at numerous locations (see Keefe 1993). Consequently, such approaches will face significant (perhaps insurmountable) problems in practical implementation. In fact, an experimental demonstration of chaos control in an open flow system is still lacking.

All advanced control schemes (adaptive neural net, chaos control) rely (at least implicitly) on a dynamical model. In some cases (e.g., standard adaptive control), the model is *linear*, obviously invalid in an open flow system and more generally in commonly encountered dynamical systems. Since nonlinearity can produce *multiple solutions* for the same forcing, the selection of a specific goal state using a linear control method may not always be possible. This signifies that robust control schemes are likely to necessarily nonlinear. The following discussion presents the pros and cons of two commonly used concepts in the control of complex nonlinear dynamical systems.

Two control approaches are prevalent: feedback-based and open-loop. The merit of feedback-based methods (e.g., see Ott et al. 1990, Pyragas 1992) lies in their use of simple models and their success in the presence of multiple solutions. In contrast, open-loop control techniques need accurate models, may not achieve the desired goal dynamics when multiple solutions exist, and are ineffective in non-stationary system conditions (Lüscher & Hübler 1989, Shermer et al. 1991). However, they do not involve cumber-

some sensing/actuation and real-time processing, which are essential for feedback control. Furthermore, feedback-based control may not be feasible in spatially developing dynamical systems. Since real-time sensing of a local variable is used to modify the future input of control perturbations, sensing must accompany nearly instantaneous actuation. For this, high-speed control algorithms (for real-time data acquisition and modeling/control computations) and sophisticated sensor/actuator response are required. Even so, the additional time delays associated with the spatial development of system disturbances are unavoidable. The total delay in providing control makes a (convectively unstable) flow system susceptible to undesirable ambient disturbances, which can cause the flow system to deviate from a goal state for control. Since no simple approach to overcome the problems associated with time delays is evident, we first develop an open-loop control strategy that uses relatively a simple, empirical model of the chaotic dynamics.

### A.4 Conceptual Control Approach for the Jet Flow – Chaos Control

The schematic in Figure A.5 displays the chaotic evolution of orbits in a low-dimensional attractor reconstructed with time-delay phase space coordinates. Having chosen the goal state (i.e., a downstream UPO) to be stabilized, we propose to achieve its control by providing the appropriate perturbations at the flow origin to maintain the attractor dynamics observed downstream near the selected UPO. Since a chaotic trajectory visits all UPOs, in a long enough time interval the attractor dynamics will come near each UPO; the "dominant" UPOs are visited frequently. Figure A.6 also sketches a naturally occurring periodic orbit in the chaotic system (denoted as a bold dashed line) with stable and unstable eigenvalues that influence the future evolution of the orbit. Since this trajec-

tory returns very close to its initial condition in phase space, it is termed a UPO. Evolutions of orbits close to a UPO being similar (see Chapter 3 and section A.3), in the absence of "noise," the desired dynamics are expected to be sustained for at least one orbital period, after which the orbit wanders into other phase-space neighborhoods (denoted by the line with arrows). To remain close to the selected (intrinsically unstable) periodic state indefinitely (thereby maintaining a nearly periodic state), low-level control perturbations are needed to prevent the dynamics from wandering away. Continuous control is needed to overpower ambient perturbations, since the growth and advection of disturbances leaves the flow origin susceptible to "noise." The control provides additional energy at the appropriate frequency components to enhance preexisting feedback and enable locking to a specified UPO.

Figure A.6(a, b) displays return maps from the chaotic jet flow for period-2 and period-9 flow states, denoting the stable and unstable directions for the periodic orbit intersection on the two-dimensional plane extracted from a time delayed velocity signal embedding; these are the essential unstable fixed points underlying the periodic orbit in the chaotic dynamical system. To control the downstream dynamics (i.e., a UPO), appropriate upstream perturbations needed at the receptivity point are determined as described in Chapter 3 and section A.3.

### A.5 Discussions of Control Experiments and Results

The chaos control experimental demonstration results from the jet shown in Chapter 4 are now discussed. The control effectiveness was evaluated by comparing centerline, longitudinal velocity signals u(t) from the controlled and the desired flows.

We begin by describing the control of the period-11 flow state. The motivation for selecting the period-11 UPOs from cluster-I in Figure A.3(b) was discussed in Chapter 4. Single-frequency bulk-forcing is first employed to obtain the chaotic attractor. The control signal is synthesized from realizations similar to that shown Figure 3.8(b) and low-pass filtered to minimize the dominant fundamental component. The bulk excitation signal and that provided at the exit are phase locked at the fundamental frequency. The control signal is then continuously applied at the nozzle lip with an external gain which is increased until the desired UPO is sustained, observed by a downstream centerline probe (as in Figure 3.1). The flow was seen to lock on to the selected UPO after a transient during which the attractor dynamics seem to wander from other UPOs to the selected orbit. For much larger control signal amplitude, a period-11 state was observed which does not resemble the desired UPO; i.e., an undesired goal state is obtained. As expected, ceasing control causes the flow to revert back to the chaotic dynamics of QCA, showing that the low-level control perturbations merely direct the dynamics to the vicinity of the selected UPO but do not cause the bifurcation to a new (stable) state. Note that, the desired UPOs (e.g., a period-11 flow state) are observed for one or at most a couple of consecutive orbital periods in the chaotic flow, while it is sustained indefinitely (with weak modulations) in the controlled flow.

Figure A.7(a) displays a 2D projection of the positive crossings from a 3D QCA Poincarè section (constructed similar to Figure A.2), with the crossings from the controlled period-11 dynamics overlaid (with “x”-shaped symbols); we used a 1500 fundamental period long sample from the controlled flow. The presence of about 5 clusters (as

opposed to 11, expected for a period-11 orbit) is due to the dominant subharmonic component in the signal and the lack of distinct fundamental periods. The spread within a cluster due to slight aperiodicities in the controlled flow is discussed later in this section. Also shown (see Figure A.7b) are the mutual information from QCA (dotted line) and the controlled flow, displaying the rapid loss of information in the chaotic flow and the recovery of information, at a delay corresponding to the period-11 orbit, in the controlled flow, in addition to an increase of the floor to almost 1 bit (as expected for a periodic flow state). Similar results (of period-11 control) were also obtained by using the upstream control perturbation estimated by an adaptive filter approximation (see Chapter 3). To test the controllability when multiple phase-space bundles of the same period exist, a period-11 UPO like that shown in Figure 3.6(c), from cluster-II in Figure A.3(b), was also chosen and its control was shown (see Figure 4.2). Thus, open-loop chaos control was shown to be effective even in the presence of more than one type of UPO with the same period in the attractor.

As mentioned in Chapter 4, the control of a period-13 UPO from the second cluster with dominant quarterharmonic (see Figure A.3c)) was unsuccessful: the flow frequently wandered away from the selected UPO to the flow state shown in Figure 4.3 (which corresponds to a different cluster in Figure A.3c). This loss of control seems to be caused by the relative stability of the orbits in the neighboring cluster (with orbits corresponding to the realizations in Figure 4.3, having a smaller magnitude of the unstable eigenvalue. Moreover, the clusters for period-13 UPO crossings are less distinct than those for the period-11 UPO [see Figures A.3(b,c)]. “Adaptive” control would be needed to resolve

this problem of failure to target a periodic orbit when it occurs close to other periodic orbit bundles.

In addition to ambient perturbations and uncertainty in determining control perturbations, the discrepancies between the controlled flow and the desired UPO [see spread in the five Poincarè section clusters (Figure A.7a)] – indicating the occasional drift of the dynamics away from the desired UPO – seem to result from the variations among orbits in a UPO bundle. The study in §A.2 revealed some scattered UPO crossings in the vicinity of distinguishable clusters. The orbits close to a certain UPO are similar, but not identical, having variations in amplitude/phase (see Figure 3.6c). Thus, drift of the controlled flow is unavoidable. For example, the period-11 UPO found in cluster-I in Figure A.3(b) resemble each other in most details except the amplitude and relative phase (with respect to the subharmonic) of the isolated fundamental period (also see Figure 3.6c). Consequently, the Poincarè section cluster for the controlled flow (see Figure A.7a) associated with the isolated fundamental is spread the most.

In particular, for UPOs of larger periods (≥ period-15), the less distinct clustering of their crossings renders control quite difficult, resulting in frequent excursions from the desired flow. As mentioned in Chapter 4, errors in computing appropriate upstream perturbations can also make it difficult to achieve "perfect" control of a UPO, since small changes in initial conditions, i.e., upstream dynamics, for this chaotic flow will cause noticeable differences farther downstream. These errors arise from our averaging of UPOs in upstream signals or as random errors in the adaptive filtering method.

In summary, simple (empirical) representations of the dominant UPOs in a chaotic attractor are used to obtain perturbations for controlling specified (periodic) dynamical states in the chaotic jet. Successful chaos control was shown experimentally by verifying the close match between the controlled orbit and the desired UPO. Use of such an open-loop chaos control method to sustain otherwise unachievable (i.e., unstable) states is evident from the pairing suppression demonstrated here for $St_D > 1$, wherein second vortex pairing is unavoidable. Control seems to be effective even in the presence of several types of UPOs, although this is not always guaranteed.

The open loop chaos control method presented is sensitive to ambient flow disturbances and empirical modeling errors. As noted earlier in Chapter 4, a feedback control strategy, having real-time input about the flow conditions during control, is expected to be more "robust." In particular, the control of UPOs with large periods (e.g., greater than period-15) using our open loop method was ineffective in that frequent excursions from the selected flow state were noticed; the lack of distinct clusters associated with UPO crossings seems to be the cause for this frequent loss of control. It is expected that control using feedback will prevent such deviations from the selected (periodic) goal state; appropriate changes for maintaining the chosen goal state can be made to the controller (which provides the control perturbations) in real time by sensing the departure of the controlled orbit away from the desired orbit.

The presence of internal feedback in the jet implies that measurements anywhere within the spatially coupled domain will reflect the "global" dynamics. Thus, a centerline feedback sensor at the flow origin was used to sense the controlled flow in real time and

feedback changes to the controller at the flow origin. As a result of spatial coupling, there exists a nominally unique relationship between UPOs found in the downstream chaotic attractor and those from the attractors analyzed at the flow origin (viz., the nozzle exit plane). The flow response to the changes in the control signal will be slightly delayed; however, these delays (e.g., for propagation of acoustic perturbations within the excitation system) will be much smaller than the period of the UPO we wish to control.

The simplest form of (linear) feedback control was used to feed a signal proportional to the difference between the controlled flow state (in phase space) and the desired flow state. Pyragas (1992) demonstrated similar control in a simple temporal DS. The control perturbation, to be provided at the nozzle lip, has the form: $u_{control}(t) = \alpha*[u_{UPO}(t) - u(t)]$, where $u_{control}(t)$ is provided as excitation at the nozzle lip, $\alpha$ is some adjustable gain, $u_{UPO}(t)$ is the upstream footprint of a selected UPO (obtained *a priori* from a downstream signal) and u(t) is the real-time signal from a probe placed close to the jet centerline in the nozzle exit plane. This is analogous to feeding back a "tracking error" (between the controlled trajectories and the desired orbit). Prior analysis of the downstream attractor is essential for goal state identification (in particular, when multiple types of UPOs are present). Using the above-mentioned method, two UPOs with relatively large periods (viz., period-15, 17) in QCA were controlled, which the open loop chaos control method failed to stabilize. In the following section, the dynamical systems tools used in the prior sections to describe and analyze the chaotic attractors are explained briefly.

### A.6 Dynamical Systems Tools

Dimension and Lyapunov exponent calculations were performed on Cray Y-MP at

the NASA Ames Research Center. Primarily, three measures were used to describe a flow state in phase space. Long time series, about 200,000 points, sampled at sufficiently high sampling rates (40 times the significant frequency component) to yield well resolved Poincaré sections were used for computing the following,

(i) Mutual information (MI): MI is given by

$$I(S,Q) = \sum_{ij} P_{sq}(s_i,q_j) \log \{ \frac{P_{sq}(s_i,q_j)}{P_s(s_i)\, P_q(q_j)} \} \text{ (for discrete signals)}, \qquad (A.1)$$

where $P_{sq}$, $P_s$, $P_q$ are the probability density functions of the two signals. This quantifies the correlation between two time traces. In accordance with suggestions of Fraser & Swinney (1986) we have used $\tau$, the first minimum of MI, for time-delay reconstruction of the phase space from time traces. We used sample sizes larger than 30,000 points with 32 bins for all our datasets. Further computational details are discussed by Broze (1992).

(ii) Correlation dimension ($\nu$): This provides us with a measure of the geometry of the attractor. For a self-similar object, power law scaling, $C(r) \sim r^{\nu}$, is expected, and

$$C(r) = \lim_{N \to \infty} \frac{1}{N^2} \sum_{i\, j=1}^{N} \theta(r - |X_i - X_j|), \qquad (A.2)$$

where $\theta$ is the Heaviside function, and r is the radius of the sphere in an m-dimensional phase-space (Grassberger & Procaccia 1983). Details of the procedure for evaluating $\nu$, computation validation, and choice of the minimum embedding dimension (note, C(r) is evaluated for several m) for reporting a value of $\nu$ are documented in Broze (1992).

(iii) Largest Lyapunov exponent ($\lambda$): The exponent quantifies the rate of exponential convergence/divergence of trajectories in phase space. A necessary and sufficient condition for a system to be chaotic is at least one positive Lyapunov exponent, i.e., a direction in which the distance between neighboring trajectories increases exponentially. The exponent is given by

$$\lambda = \lim_{N \to \infty} \frac{1}{t} \frac{d(t)}{d(0)} \quad , \tag{A.3}$$

where d is the distance between two neighboring trajectories in phase-space. The algorithm developed by Wolf et al. (1985) was used to estimate the largest Lyapunov exponent, in units of bits/sec; normalizing $\lambda$ by the time period corresponding to the dynamically significant frequency provides $\lambda$ in units of bits/orbit. At least 50,000 points on the attractor were used for all $\nu$ and $\lambda$ computations.

# APPENDIX B

## APPLICATION OF CONTROL APPROACH TO A TRANSITIONAL PLANE MIXING LAYER

The investigation of chaos control in a plane mixing layer is of general interest because this is a simple prototypical open shear flow (Ho & Huerre 1984). Detailed studies of a forced mixing layer revealed low-dimensional chaotic attractors that are strikingly similar to those observed in the jet (Narayanan & Hussain 1996). The mechanism of spatial coupling (viz., feedback from vortex pairings) and the local convective instabilities are similar to that found in the jet too. The spatiotemporal mixing layer dynamics extend from the lip to about $x/\theta_e \cong 300$, wherein nominally two-dimensional vortices transition to fine-scale turbulence; $\theta_e$ is the exit momentum thickness of the initially laminar boundary layer. The transition region is subject to several linear and nonlinear instabilities (see Figure B.1), closely resembling the jet dynamics shown in Figure 1.1. Such similarities in the "global" dynamics strongly support the idea that the nonlinear control method developed and earlier demonstrated in the transitional region of an axisymmetric jet can be effective in the transitional region of the mixing layer as well.

By combining temporal dynamical systems methods with a newly proposed spatial coupling measure (viz., *coherence*), low-dimensional dynamics in a forced plane mixing layer were identified and described (Narayanan & Hussain 1996). The previous experiments were performed inside an *anechoic* chamber (at the UH ATL) in an initially laminar plane mixing layer using forcing of the fundamental instability only; the forcing fre-

quency and amplitude were used as control parameters. Single-frequency forcing was provided (acoustically) at the ML lip. Dynamical invariant estimates show that vortex roll-up and the feedback-driven first two pairing dynamics are well described by one periodic and at least two low-dimensional chaotic attractors; a phase diagram delineating such dynamical states in the control parameter space was presented in Narayanan & Hussain (1996). The large spatial extents of these feedback-sustained states (verified using coherence and cross-bicoherence), spanning many instability wavelengths downstream, indicate spatial coupling. It was concluded that the transitional plane mixing layer (although locally convectively unstable) behaves as a temporal dynamical system.

### B.1 Plane Mixing Layer Facility

A plane mixing layer facility (schematic shown in Figure B.2) is attached to a 15.25 cm diameter nozzle of an air jet facility in the air room of ATL. Details of the air room jet facility, including documentation of its settling chamber characteristics are provided in Husain (1982). The centrifugal blower is driven by a 20 HP Powertron DC motor and a Polyspede motor controller. The extended plane mixing layer facility, comprising a circular-to-square section, a diffuser, a settling chamber, and a 5 cm wide and 50 cm tall rectangular nozzle, is described in Narayanan (1994) and Narayanan & Hussain (1996); a 38.1 cm long wall extends on one side of the nozzle exit. An enclosed shear layer excitation system (three 4 in, 10 W woofer speakers) was installed close to the shear layer lip (see inset in Figure B.2), with sharp-edged aluminum blocks at the exit to enable adjustment for a uniform excitation slit width ($\cong$ 1 mm). The excitation box walls were padded inside with synthetic wool to minimize the acoustic perturbations that escape from the

back of the box, thereby providing effective excitation at the nozzle lip; upon acoustic excitation, the fluctuation levels recorded by a probe displaced transversely away from the lip were found to be an order of magnitude lower those for a probe placed at the lip (next to the excitation slit). The excitation frequency was chosen to be 512 Hz to achieve the desired $St_{\theta e}$ range (0.012 – 0.02) with $U_e \leq 12$ m/s (for which the exit boundary layer is laminar). The transfer function of the settling chamber and the contraction was also inspected, and no abnormal resonances were detected.

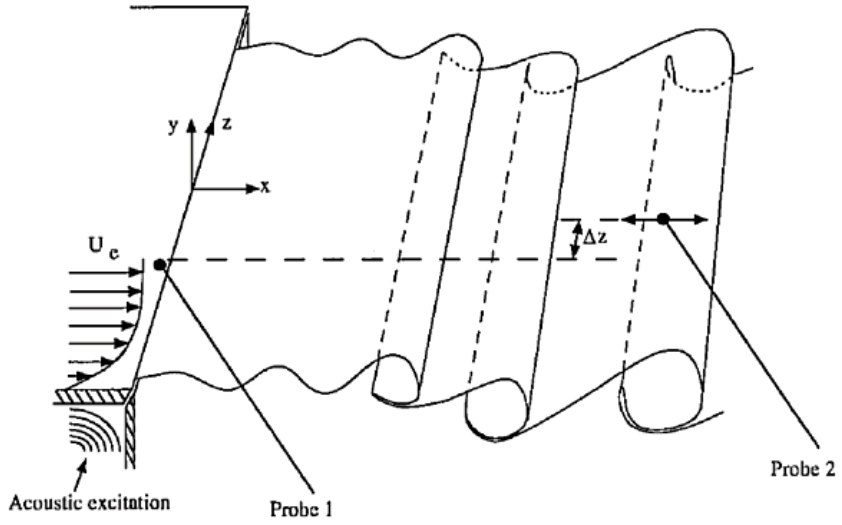


Figure B.1 Schematic of plane mixing layer, displaying nominally 2D vortex dynamics and probe locations.

The exit boundary layer characteristics (see Fig. B.3) indicate "nominally laminar" boundary layers (Hussain 1983) for velocities up to 12 m/s, i.e., a shape factor in the range 2.5–2.75, low peak turbulence intensity ($u'_{max}/U_e \leq 2\%$), and no discrete frequencies seen in the spectrum recorded in the boundary layer except peaks near 7 Hz (associated with blower oscillations) and 30 Hz (presumably a room acoustic mode). Note

that, the peak turbulence intensity levels in the boundary layer are higher during the air room experiments when compared to those measured in the mixing layer when housed in an anechoic chamber (Narayanan & Hussain 1996). Measurements of the mean and rms-fluctuation velocity profiles across the exit boundary layer over a range of flow velocities, and conditional two-point measurements (revealing minimal interaction between the free shear layer and the boundary layer on the wall-side) are reported in Narayanan & Hussain (1996).

In the following, the results from analyzing the chaotic dynamics in a plane mixing layer, attached to a large jet facility in the air room of ATL, are presented. Analyses of the chaotic dynamics and of the spatial evolution of the flow are similar to that for the jet.

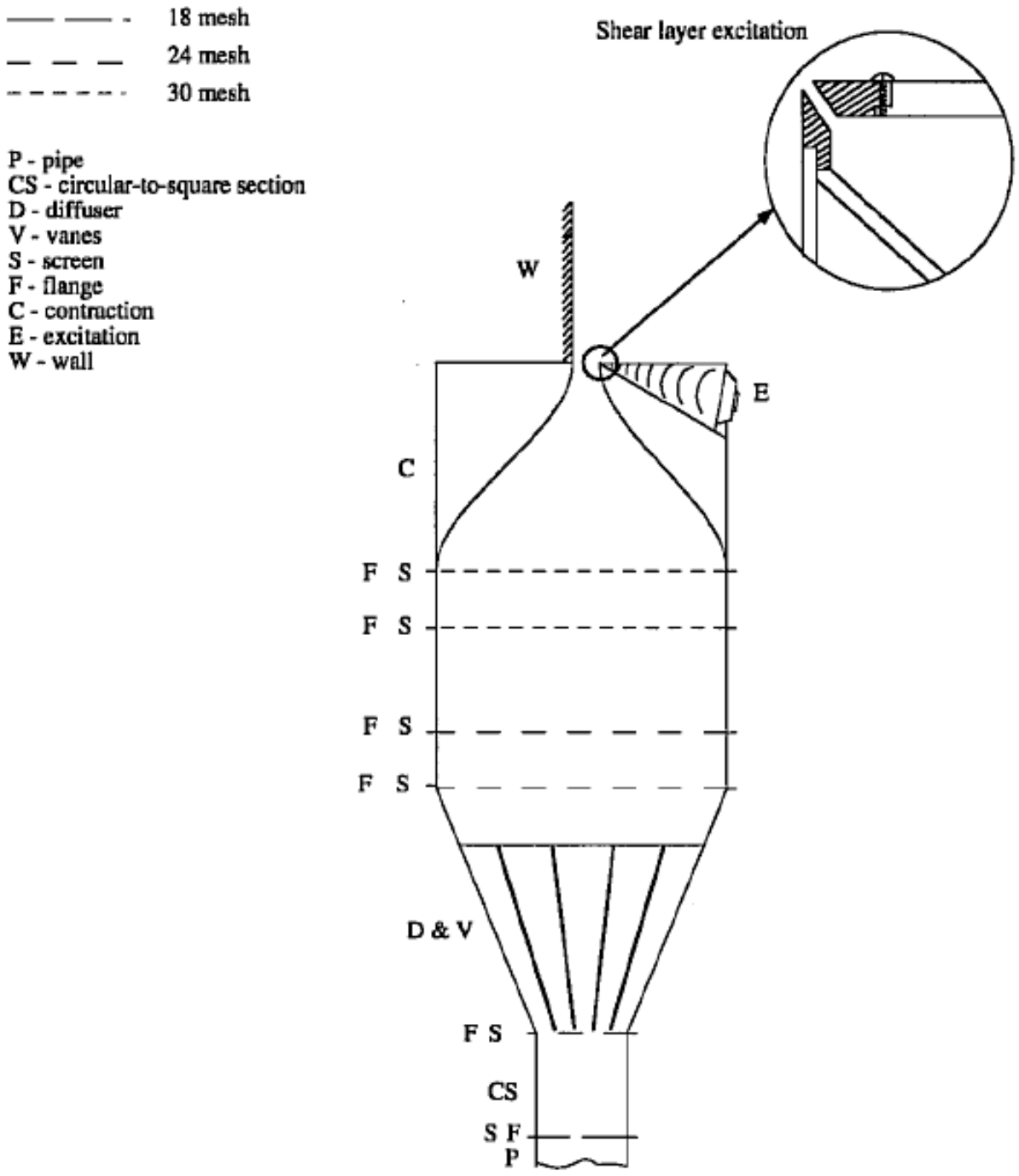


Figure B.2 Plane mixing layer facility with shear layer excitation.

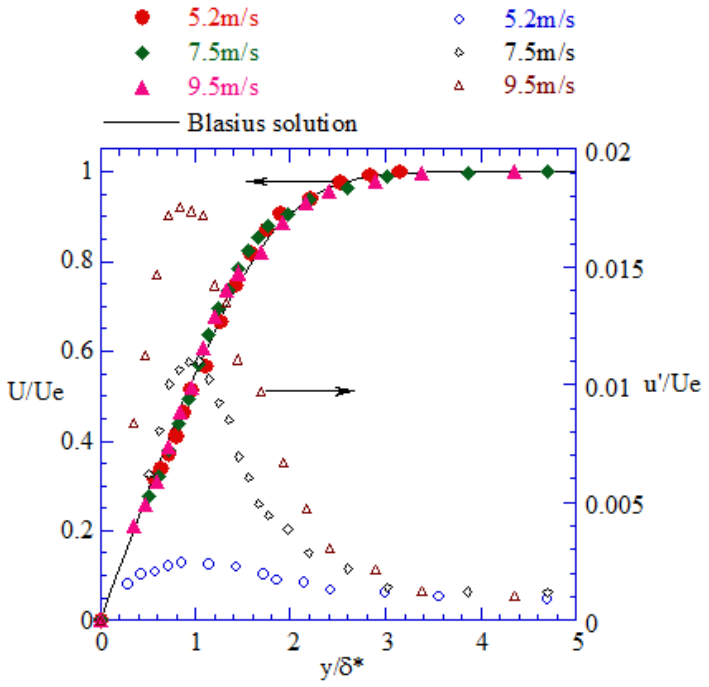


Figure. B.3 Exit boundary layer characteristics for plane mixing layer.

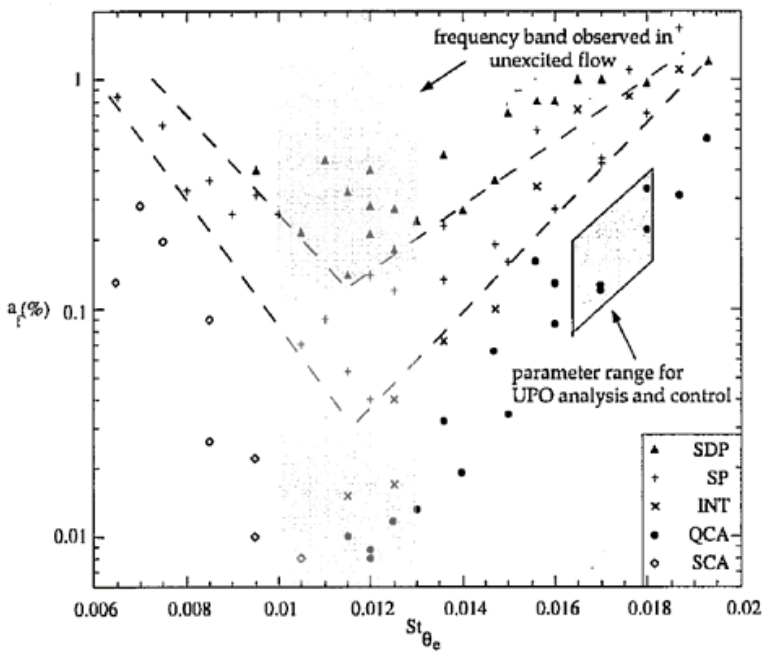


Figure B.4 Phase diagram for forced mixing layer (reproduced from Narayanan & Hussain 1996); area marked with a box denotes parameter space location for present study.

## B.2 Chaotic Dynamics in the Mixing Layer

A measurement location ($x \cong 130\ \theta_e$) where the probe senses footprints of all important events was chosen. These events are: vortex roll-up ($x \cong 50\text{-}60\ \theta_e$), first pairing ($x \cong 110\text{-}130\ \theta_e$) and second pairing ($x \cong 200\text{-}220\ \theta_e$); the precise roll-up and pairing locations depend upon the forcing frequency and amplitude. The probe's transverse location corresponds to $U(y)/U_e \cong 95\%$, where a clear imprint of large-scale events is obtained but effects due to small scales or internal vorticity laminations are essentially avoided; a long-prong single-wire probe was used to minimize probe interference (Hussain & Zaman 1978). The Reynolds number was varied in the range $100 < Re_{\theta e} < 150$, for which the initial boundary layer is "nominally laminar." The control parameters used are: the Strouhal number $St_{\theta e}$ ($\equiv \frac{f_{ex}\,\theta_e}{U_e}$, $U_e$ = exit velocity and $f_{ex}$ = excitation frequency) and the nondimensional forcing amplitude $a_f$; $U_e$ was varied to change $St_{\theta e}$. The phase diagram, the attractors' invariants and transitions between dynamical states are extensively discussed in Narayanan & Hussain (1996).

The spectral dynamics in the transitional mixing layer are similar to those in the jet, wherein saturation of the fundamental frequency (being forced externally) is physically realized by vortex rollup and saturation of successive subharmonic frequencies indicate vortex pairings (following subharmonic resonance). Feedback from vortex pairings is the primary mechanism for spatial coupling in the mixing layer; this was verified from exit velocity signals (Narayanan & Hussain 1996). The present use of single-point velocity

measurements to describe the mixing layer as a low-dimensional DS was justified using spatial coupling measurements. Coherence and cross-bicoherence were used to verify the existence of coupling in the flow for substantial spatial extents, viz., $x/\lambda_f \cong 7$, (Narayanan & Hussain 1996). (Note that $\frac{x}{\lambda_f} \cong 2\ St_{\theta e}\ \frac{x}{\theta_e}$, where $\lambda_f$ is the fundamental instability wavelength.) Thus, even though the flow is *physically open*, the dynamics are coupled over several instability wavelengths; i.e., the flow is spatially coupled and hence *dynamically closed*.

A periodic state, stable double pairing (SDP), is found for *all* $St_{\theta e}$ studied, for sufficiently high $a_f$ ($\geq 0.15\%$); Figure B.4 displays the phase diagram for the forced plane mixing layer, reproduced from Narayanan & Hussain (1996). A brief investigation in the mixing layer facility installed in the air room also reveals a similar distribution of periodic and chaotic attractors for the same $St_{\theta e}$ range but slightly higher $a_f$ compared to that required for the anechoic facility, due to the higher background disturbance levels. The vortex dynamics involve forced periodic roll-up and self-excited periodic first pairing (of rolled-up vortices) and second pairing (of once-paired vortices). Another low-dimensional attractor, termed stable pairing, is found for lower $a_f$ (than for SDP), wherein periodic first pairings and chaotic second pairings occur. As $a_f$ is decreased from that required for SP, two different chaotic states occur for $St_{\theta e} \geq 0.012$ (QCA) and $St_{\theta e} < 0.012$ (SCA) (see Figure B.4). The two chaotic states are the quarterharmonic chaotic attractor (QCA) and the subharmonic chaotic attractor (SCA). We choose the former attractor, i.e., QCA, for further analysis since it captures low-dimensional dynamics of multiple

vortex pairings in the flow. The shaded area in Figure B.4 denotes the dominant instability frequency band ($0.01 \leq St_{\theta e} \leq 0.013$) in an unforced ML.

*QCA*. A representative signal and spectrum of the chaotic state for $a_f \cong 0.2\%$, $St_{\theta e} \cong 0.017$ are shown in Figures B.5(a,b); the similarity with QCA found in the jet is evident (see Figure 3.3). Such chaotic dynamics are found in a contiguous neighborhood, i.e., QCA appears uniformly anywhere for $0.09\% < a_f < 0.4\%$ and $0.0165 < St_{\theta e} < 0.018$ (see area marked by a box in Figure B.4). The spectrum has sharp sidebands around the subharmonic (marked with a dashed line) indicating nearly periodic modulations of the first pairing, due to nearly periodic shifts in the pairing locations upstream and downstream (caused by periodic changes in the feedback phase), and a broadband quarterharmonic indicating chaotic shifts in the second pairing location. Amplitude modulations in the time trace reflect nearly quasiperiodic variations in the induced velocity from pairing or once-paired vortices. Vortex roll up occurs after $x/\theta_e \cong 55$, followed by a modulated first pairing in the region $x/\theta_e \cong 90\text{-}110$, and a chaotic second pairing near $x/\theta_e \cong 200$. Correlation dimension calculations (from time-delay reconstruction) revealed $\nu \cong 2.43$ ($m = 4$), reasonable scaling region (factor of 2-3) and convergence. Similar calculations using singular value decomposition-based reconstruction (Narayanan et al. 1997) revealed $\nu \cong 3.1$ ($m = 4$), a larger scaling region (factor of 4-5) and better convergence. The largest Lyapunov exponent is positive ($\lambda \cong 0.32$ bpo), indicating chaos.

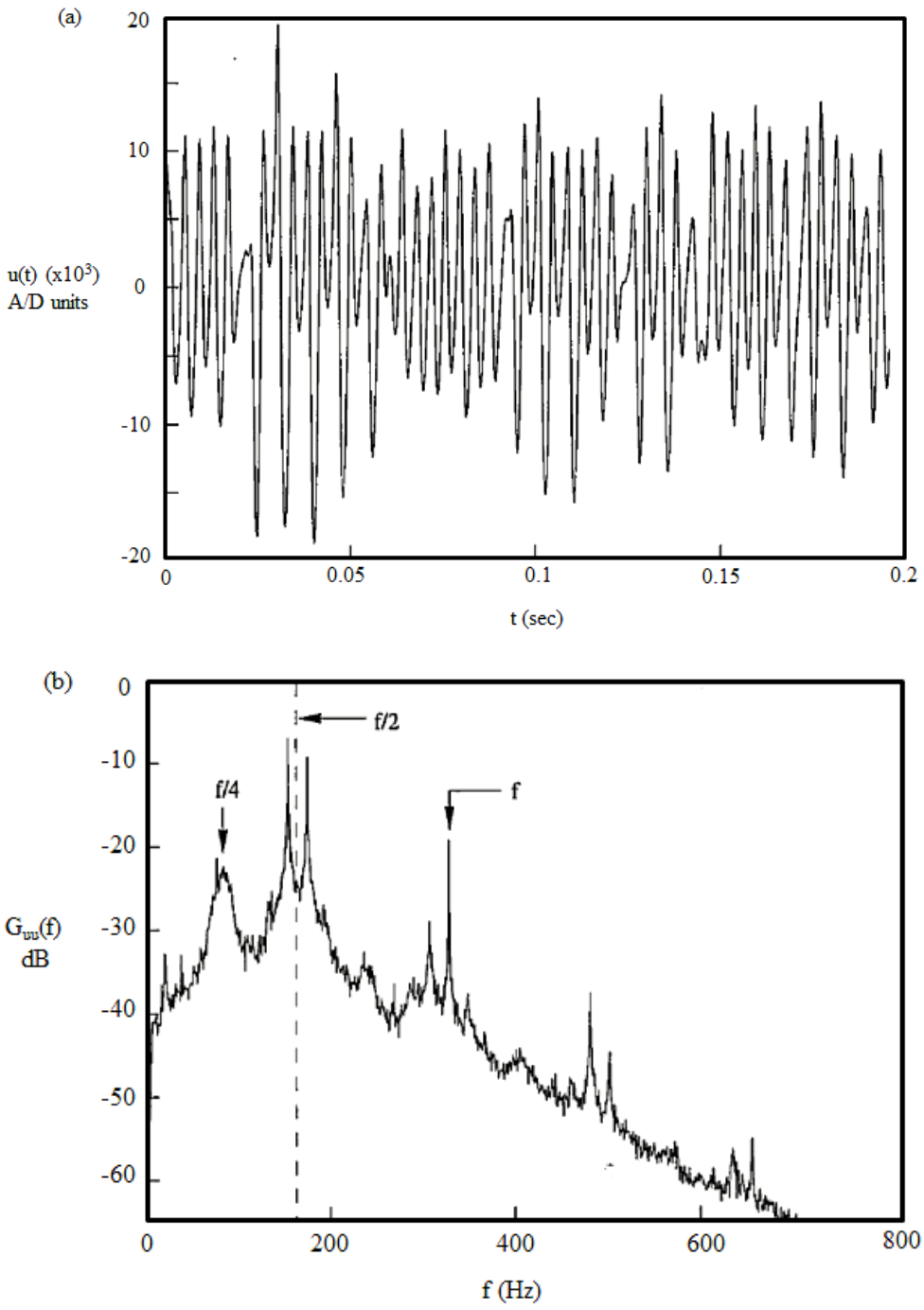


Figure B.5 (a) Velocity time trace for chaotic state (QCA) from plane mixing layer; (b) Power spectrum for chaotic state (QCA) from plane mixing layer.

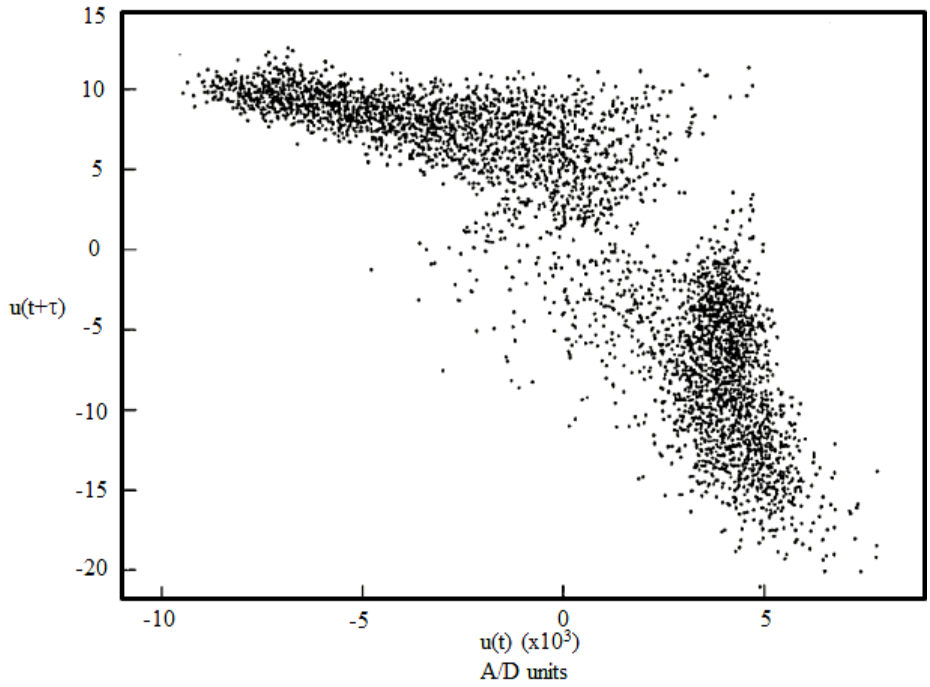


Figure B.6 Two-dimensional projection of Poincaré section for QCA.

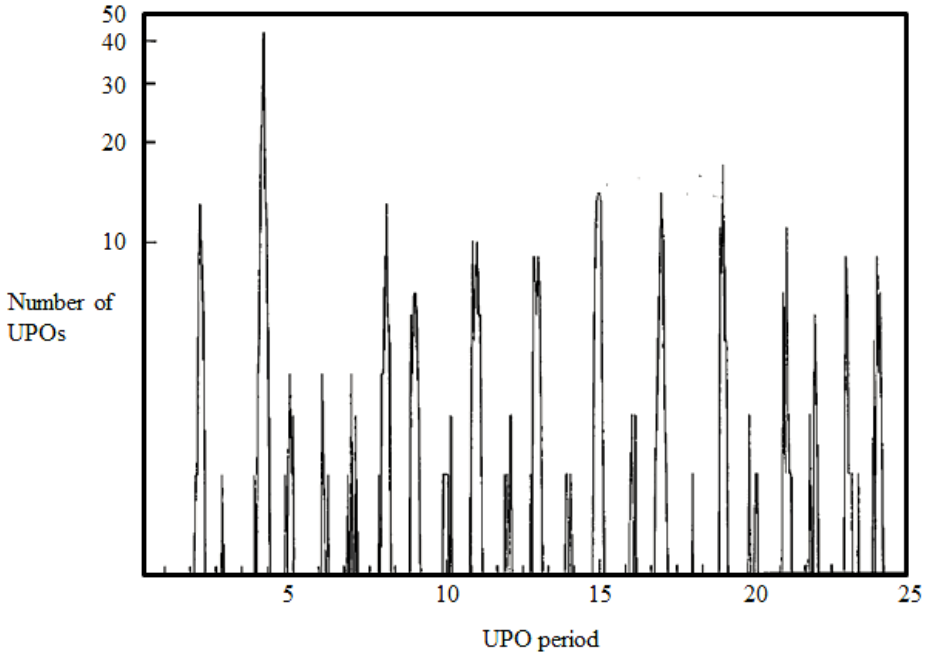


Figure B.7 UPO histogram from QCA.

### B.3 Unstable Periodic Orbit (UPO) Dynamics

The UPO identification procedure is the same as for the jet. The chaotic attactor (QCA) is reconstructed in the minimum embedding dimension using signal time delays and a Poincarè section is chosen to record the UPOs. The $u(t+2\tau) = u(t) + u(t+\tau)$ plane was used to obtain the 3D Poincarè section; the time series was 300, 000 data points long and was sampled at 20 times the fundamental frequency. Figure B.6 displays the 2D projection of such a Poincarè section. The histogram of UPOs in Figure B.7 was determined from the above Poincarè section with $\varepsilon_1 \cong 5\%$, the fraction of the Poincarè section coordinates' range. The recurrence times were normalized by the fundamental period.

As observed in the jet, for a selected period-n orbit, Poincarè section crossings were found to cluster, indicating the dominance of certain types of UPOs. The clusters were identified using the pdf for the number of UPO crossings in the Poincarè section. Clusters of crossings for UPOs with large periods are found to be smeared and scattered, as in the jet. However, such smearing occurs even for lower period UPOs, and clustering diminishes for UPOs with periods higher than 11. This seems to result from influence of (extrinsic) low-frequency modulations (arising from wind tunnel acoustics and blower oscillations in the mixing layer facility) on the intrinsic low-dimensional dynamics of the mixing layer. Increasing the embedding dimension of the chaotic attractor could enable clearer identification of clusters, which appear smeared in a lower dimensional projection.

The transitional mixing layer CS dynamics can also be interpreted in terms of the

UPOs found from centerline velocity signals (similar to the jet analyses), assuming nominally 2D vortex dynamics; i.e., the spatial sequence of the vortex dynamics is inferred from the velocity trace in the spirit of Taylor's hypothesis.

Figures B.8(a-e) display UPOs of several periods extracted from QCA found in the mixing layer. The realizations corresponding to period-2 UPOs in Figure B.8(a) display dominant subharmonic components in the induced velocity from advecting once-paired vortices; the multiple realizations reveal similar UPOs belonging to a Poincarè section cluster. The period-4 UPOs in Figure B.8(b) have dominant subharmonic and quarter-harmonic components from advecting once-paired vortices and vortices undergoing a second pairing. The second pairing process is inferred from the alternating peak-to-peak amplitudes of adjacent subharmonic period segments in the induced velocity signal. Similar inferences can be drawn for the period-9, 11, 13 UPOs in Figures B.8(c-e). The differences among UPOs belonging to a cluster become pronounced for the period-11, 13 UPOs; this is most apparent close to the isolated fundamental period, marked using '*' on Figures B.8(d,e). We speculate the physical mechanism for such mismatches to be similar to that for the jet (see Chapter 3), involving an unstable configuration of paired and unpaired vortices.

In summary, chaotic dynamics in the mixing layer sweep through several unstable, nearly periodic, states. The above results also support the expectation that orbits neighboring low-order UPOs evolve similarly (in trajectory "bundles"). The presence of UPO "bundles" signifies preferential occurrence of certain sequences of CS formation and interactions, which can be controlled using low forcing levels. Orbits crossing distinct clus-

ters are averaged, removing slight variations in amplitude/phase, to reveal the underlying UPO. In the following section, such averaged representations of selected UPOs will be used to determine appropriate upstream control perturbations.

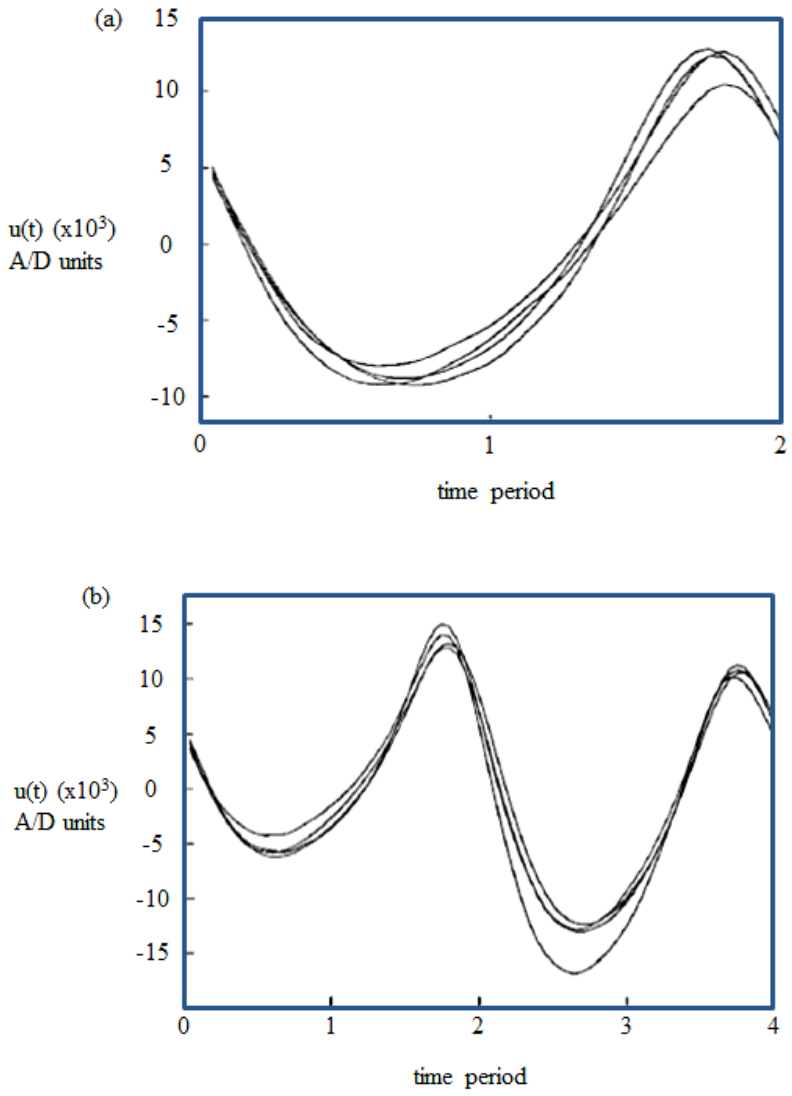


Figure B.8 (a) Period-2 UPO from a QCA Poincare section cluster; (b) Period-4 UPOs from a QCA Poincaré section cluster.

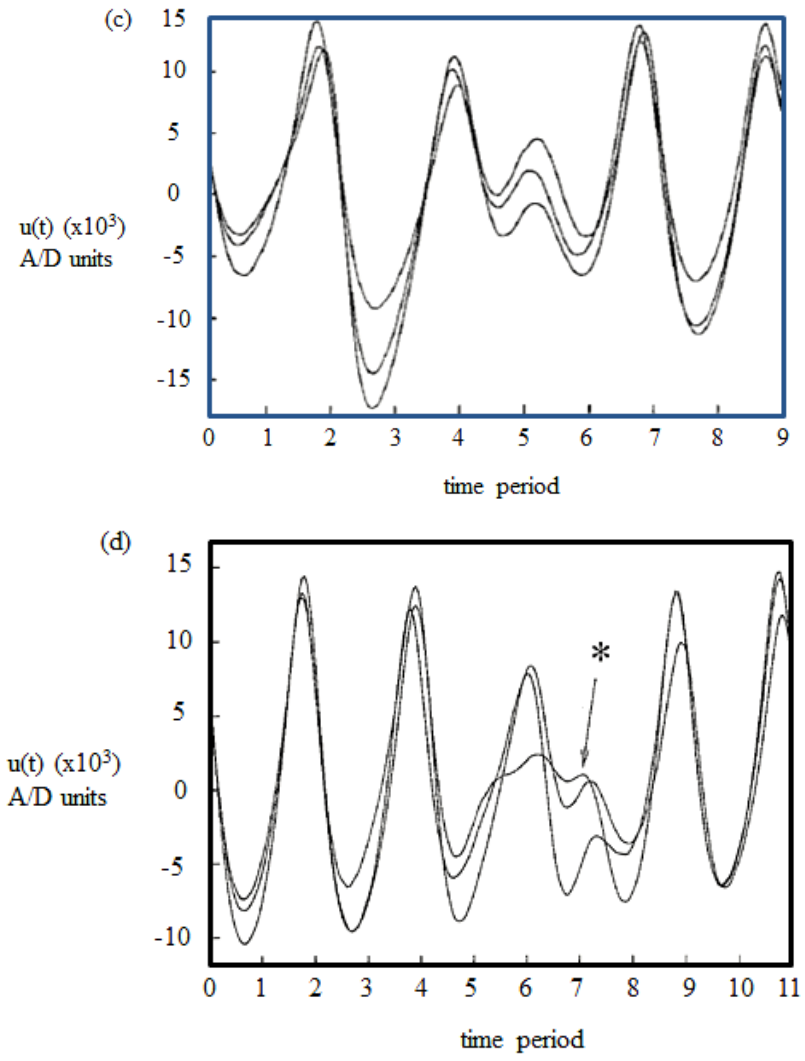


Figure B.8 (c) Period-9 UPO's from a QCA Poincaré section cluster; (d) Period-11 UPO's from a QCA Poincaré section cluster.

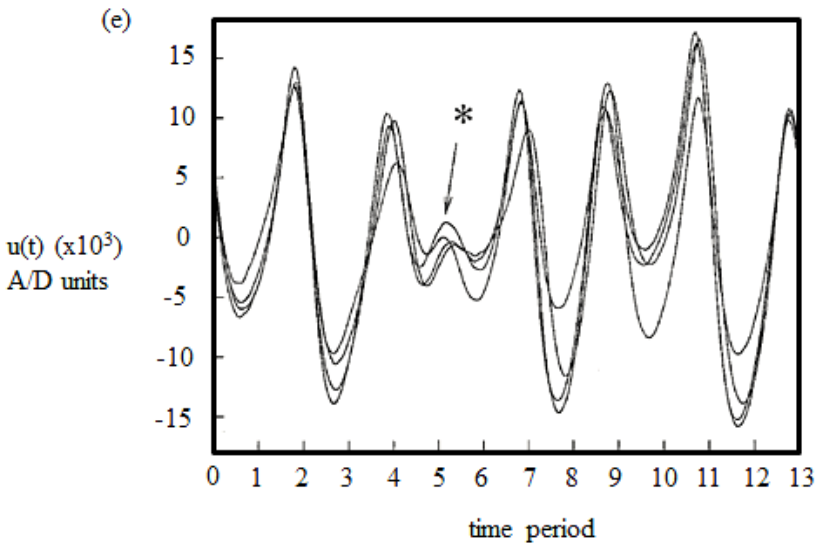


Figure B.8 (e) Period-13 UPO's from a QCA Poincaré section cluster.

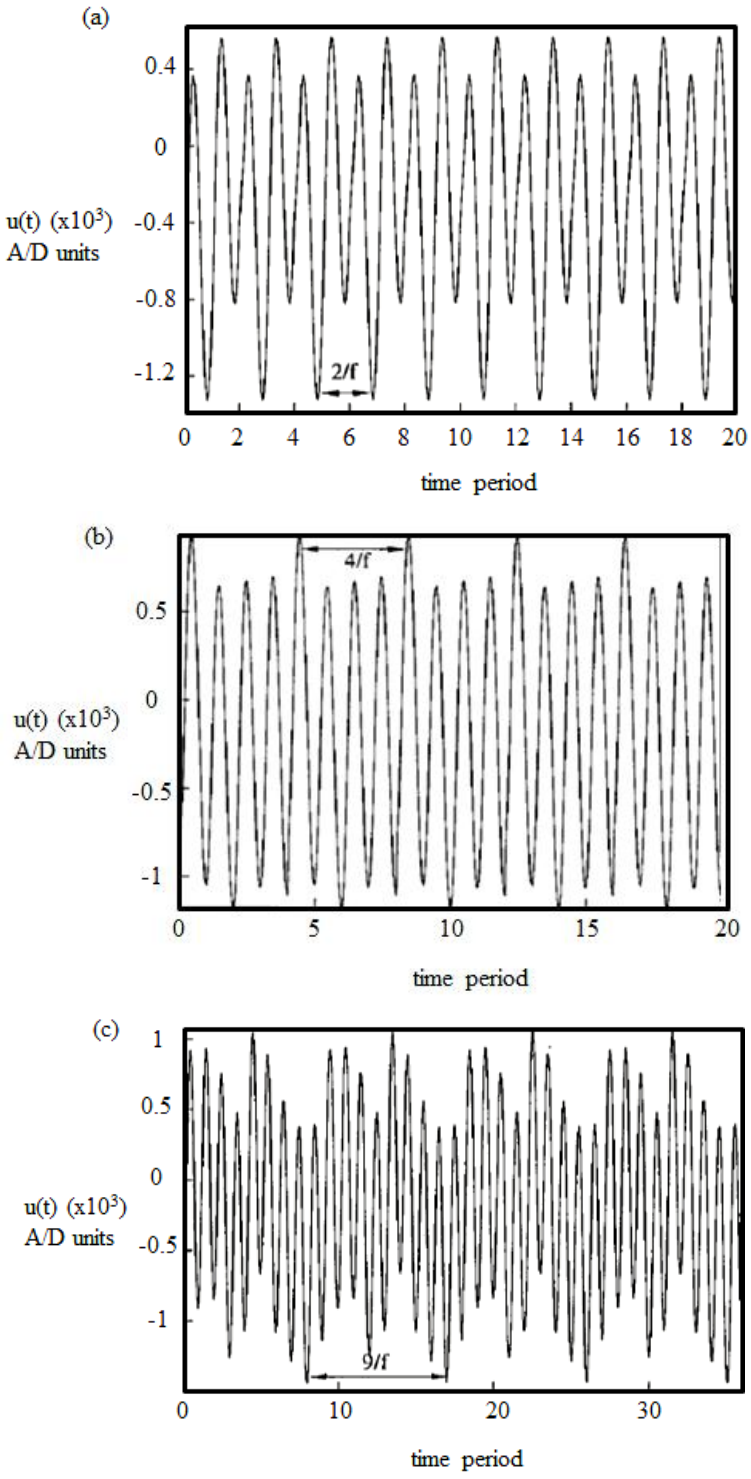


Figure B.9 (a) Upstream perturbations for controlling period-2 UPO's; (b) Upstream perturbations for controlling period-4 UPO's; (c) Upstream perturbations for controlling period-9 UPO's.

### B.4 Method for Determining Control Perturbation

The feedback from downstream pairing dynamics, i.e., spatial coupling, implies that an upstream velocity signal at the mixing layer origin will contain footprints of all the UPOs detected in the downstream chaotic attractor. Thus, "direct" analyses of close-returns in the upstream signal, sampled simultaneously with the downstream signal, should reveal (unstable) periodic orbits; this procedure for identifying upstream footprints of downstream dynamics is the same as that used in the jet. For the two-point velocity measurements discussed below, a hot-wire probe is positioned at an angle at the nozzle exit on the high speed side of the exit shear layer, and a second long prong probe is stationed (also positioned at an angle to minimize probe interference effects) on the high speed side of the mixing layer at $x/\theta_e \cong 130$.

The distribution of UPO signatures at the nozzle exit plane (not shown) resembles that in Figure B.7 (for the downstream signal). Clusters (as well as trajectory bundles), like those analyzed in the previous sections, are found for this upstream signal as well. To identify the upstream signal segment corresponding to a UPO detected downstream, signals sampled simultaneously at two points are analyzed. Whenever a UPO crosses a chosen Poincarè section cluster recorded downstream, a realization from the upstream signal for the UPO period is extracted, assuming that feedback is instantaneous and is dominant compared to background disturbances (evidenced by strong spatial coupling). These realizations from the upstream signal are then averaged to obtain a perturbation that will guide the downstream attractor dynamics to the vicinity of the desired downstream UPO. Figures B.9(a-c) display *repeated* realizations (to better illustrate the underlying periodic-

ity) of induced velocity perturbations associated with period-2,4,9 orbits in the upstream signal. The variations in the peak-to-peak amplitudes of the dominant fundamental periods are footprints of the downstream CS dynamics. The low frequency modulations, evident in the upstream footprint for period-9 UPOs (see Figure B.9c), is responsible for the smearing of Poincarè section clusters downstream.

For control, this perturbation is provided continuously (with sufficient amplitude) at the nozzle lip. Since shear layer excitation (by single frequency forcing) is already provided to establish QCA, the fundamental frequency component must be eliminated from the modeled upstream perturbation for control.

### B.5 Experimental Results from Control of Mixing Layer

To control selected (unstable) periodic states underlying the mixing layer chaotic dynamics, the control method used in the jet is applied, utilizing the presence of UPOs and their "bundles". Control is achieved by maintaining the dynamics near the selected UPO after the chaotic trajectory comes near the selected UPO. The appropriate upstream perturbations needed to maintain the downstream dynamics near a UPO were determined in the previous section. Since a chaotic trajectory visits all UPOs, in a long enough time interval the attractor dynamics will come near each UPO; in particular, the "dominant" UPOs are visited frequently. Evolutions of orbits close to a UPO being similar, the desired dynamics would be self-sustained for at least one orbital period. Low-level control perturbations are then needed to prevent the dynamics from wandering away due to the unstable nature of the selected orbit. For a chaotic state, although UPO perturbations (primarily from pairings) are fed back to the origin, none of them are strong enough to

sustain phase-locking. The control provides additional energy at the appropriate frequency components to enhance preexisting feedback and enable phase-locking to a specified UPO.

Period-2,4,9,11 UPOs (see Figures B.10(a-d)) were selected to demonstrate the chaos control method in the plane mixing layer. The control signal is synthesized from realizations similar to those shown Figures B.9(a-c), and low-pass filtered to minimize the otherwise dominant fundamental component. The single frequency excitation signal and the control signal provided at the exit are phase-locked at the fundamental frequency. Single-frequency forcing is first employed (at $a_f \cong 0.2\%$ and $St_{\theta e} \cong 0.017$) to obtain QCA. The control signal is then continuously applied at the nozzle lip with an external gain which is increased until the desired UPO is sustained, observed by the downstream probe (as in Figure B.1); the flow is seen to lock on to the selected UPO after a transient during which the attractor dynamics wanders among other UPOs. Ceasing control causes the flow to revert back to the chaotic dynamics of QCA, showing that the low-level control perturbations only maintain the dynamics near the selected UPO and do not excite a new (stable) periodic state.

Figure B.10(a) displays a velocity time trace from controlling the period-2 UPO at $x/\theta_e = 130$; the inset above also displays the period-2 UPO from the uncontrolled (chaotic) flow (denoted by a solid line) matching well with the a segment (denoted using symbols) from the controlled flow velocity signal. Note that, the desired period-2 UPO (in the inset) is observed only for one orbital period in the chaotic flow, while it is sustained indefinitely (with weak modulations) in the controlled flow. The low-level control energy

provided is seen in the upstream control signal used (see Figure B.9a), with a dominant fundamental component and relatively smaller subharmonic perturbations. With the exception of weak modulations, the controlled flow is periodic (Figure B.10a). Similarly, the control of period-4 and period-9 UPOs is seen in Figures B.10(b,c), which show signals from the controlled flow and comparisons with the desired flow states. (Note that, the period-4 flow state controlled here appears in the phase diagram as a periodic attractor (SDP in Figure B.3) for 5-10 times higher $a_f$.) The control of the period-2 UPO has implications for turbulence suppression via inhibition of the second pairing. Such pairing suppression may be used to control flow separation during slot injection over airfoil (to improve aircraft maneuverability); near-wall separation, induced by energetic large-scale vortices, can be delayed by inhibiting shear layer interactions. Controlling vortex pairings in free shear flows may also permit control of small-scale transition to turbulence for mixing control (Schoppa et al. 1995). The use of chaos control for turbulence suppression in the jet was discussed in Chapter 5.

The control of the period-11 UPO was unsuccessful in that the flow frequently wandered away from the selected UPO to chaotic behavior. The inability to control period-11 or higher order UPOs seems to be caused by the increasing influence of ambient perturbations (in particular, low frequency modulations from the facility), producing higher dimensional modulations. Note that, the clusters for period-11 UPO crossings are less distinct than those for the period-2,4,9 UPOs. "Adaptive" control may be needed to resolve this problem of failure to target such goal states of high order periodicity. UPOs with periods larger than 11 have significant spectral content at low frequencies, for which

the corresponding three-dimensional modes can be as unstable as their two-dimensional counterparts. Thus, three-dimensionality can become dominant earlier in x, causing aperiodic modulations that cannot be controlled by low-level two-dimensional perturbations.

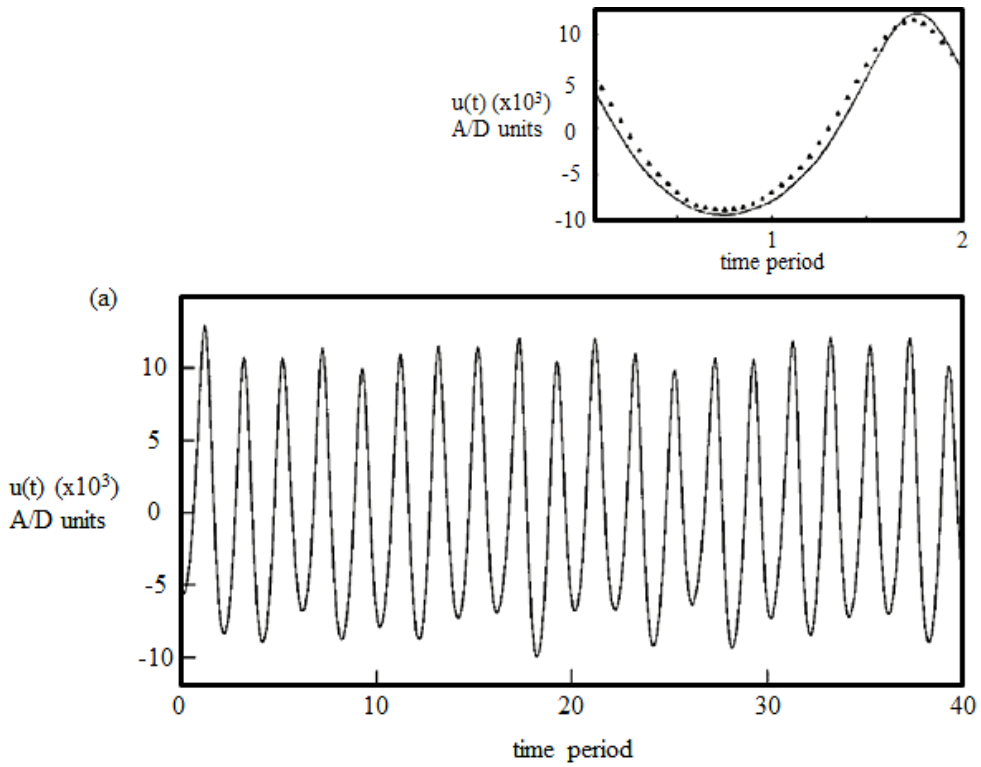


Figure B.10 (a) Velocity signal for a controlled period-2 flow state; inset shows comparison with period-2 UPO in chaotic flow (solid line).

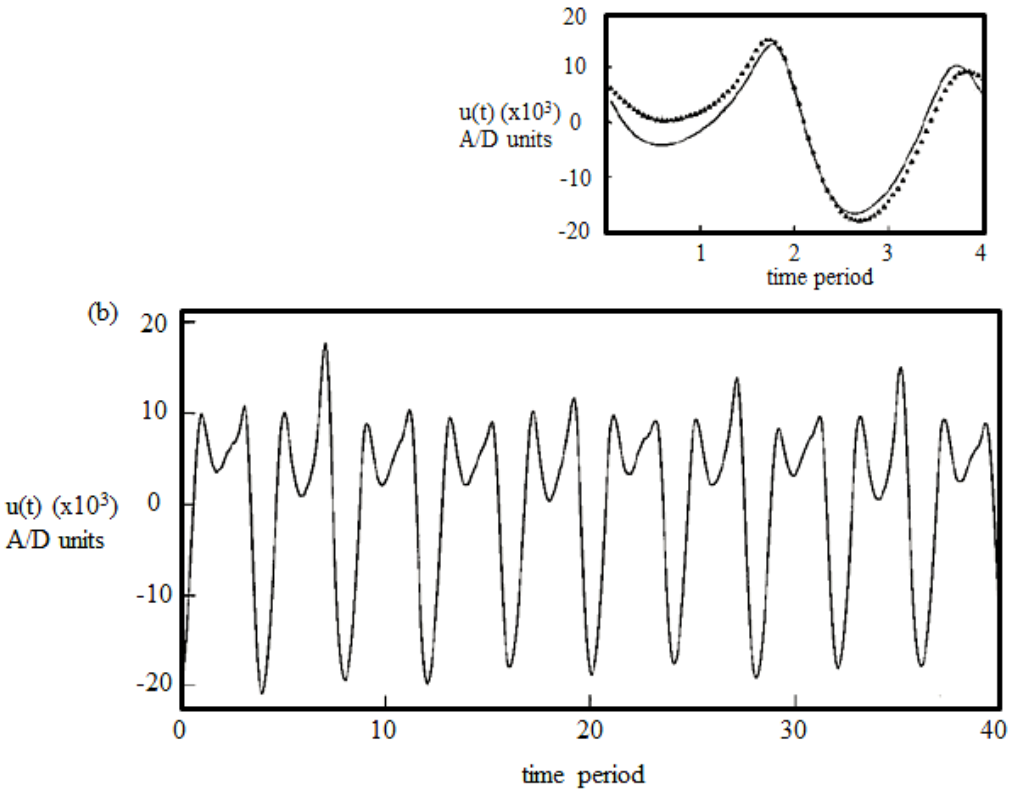


Figure B.10 (b) Velocity signal for a controlled period-4 flow state; inset shows comparison with period-4 UPO in chaotic flow (solid line).

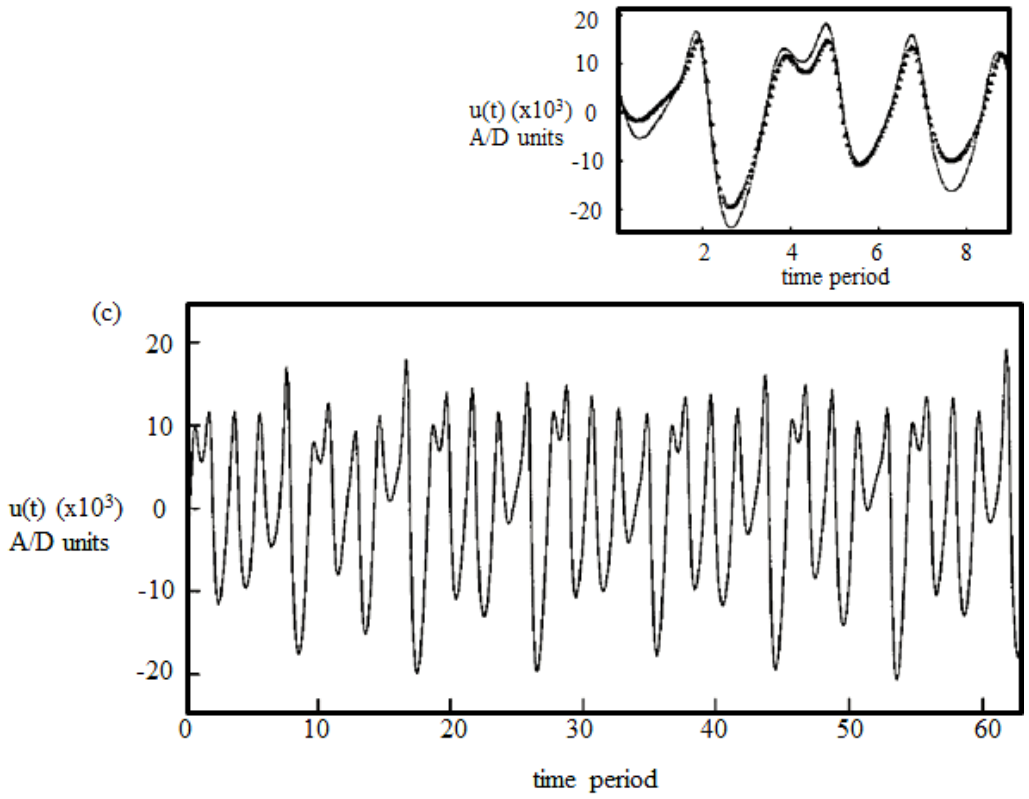


Figure B.10 (c) Velocity signal for a controlled period-9 flow state; inset shows comparison with period-9 UPO in chaotic flow (solid line).

To summarize, the chaos control method developed for the jet was successfully demonstrated in a mixing layer. Low-level perturbations were used to control selected (unstable) periodic flow states underlying a low-dimensional chaotic attractor. Success in the mixing layer control experiments provides hope that a similar chaos control method may be used in other open shear flows (e.g., wakes, wall jets, boundary layers).

# APPENDIX C

# SPATIAL COUPLING MEASURE FOR INHOMOGENEOUS DYNAMICAL SYSTEMS

Coherence was proposed as a tool to quantify spatiotemporal dynamics, in particular, in spatially inhomogeneous dynamical systems (Broze et al. 1997). Coherence was demonstrated to be an appropriate measure of predictability and, hence, spatial coupling in nonlinear systems, using analysis and via experimental results from a circular jet flow. Coherence measurements reveal sizable regions of strong spatial coupling in this spatially developing open flow, in contrast to much smaller coupling regions indicated by conventional correlation. Decaying coherence, indicating spatiotemporal dynamics, is also found in the jet, and possible mechanisms are discussed. In addition, the causes for coherence decay are explained analytically. The following analytical formulation, computation and demonstration results have been extracted from Broze et al. (1997).

## C.1 Coherence Analytical Formulation

Experimental studies of spatially extended dynamical systems (Cross & Hohenberg 1993) utilize the idea of *spatial coupling*. Coupling throughout the domain indicates temporal dynamics (permitting the capture of dynamics through single-point measurements), while its spatial decay indicates spatiotemporal dynamics (requiring simultaneous measurements at multiple locations). The number and locations of probes required to describe the dynamics adequately depend on the spatial extent of coupling and the domain size, thus necessitating spatial coupling measurements. Devising an appropriate measure of

spatial coupling is the goal of this study.

Inhomogeneous systems are typified by spatially varying dynamical quantities, e.g., modal amplitude and phase. Single-mode systems can be described by a single frequency, mode shape, and phase speed, or, phase envelope. In contrast, multimode systems have a spectrum of mode shapes and phase speeds, making the dynamics, particularly complex mode interactions, much more difficult to describe. In this study, we address the spatio-temporal dynamics of inhomogeneous multimode systems. Such systems are common and of major scientific and technological interest, e.g., in open-flow hydrodynamics.

Measures often used in homogeneous spatiotemporal systems, e.g., correlation length (Cross & Hohenberg 1993, Gollub & Ramshankar 1991) and dimension density (Mayer-Kress & Kurz 1987), may be inapplicable to inhomogeneous systems due to their spatially varying length and time scales. Ordinary coherence and cross bicoherence were used to infer spatial coupling in a plane mixing layer, an inhomogeneous open flow (Narayanan & Hussain 1996). Spectra and bispectra (from which coherence is derived) were previsouly used to describe energy transfer among frequencies (accompanying transition to turbulence) in plasmas (Ritz & Powers 1986), in free shear layers (Miksad et al. 1983) and in a Poiseuille-profile jet (Bonnetti & Boon 1989). However, for the first time, coherence is shown here to be a reliable measure of spatial coupling.

The following is organized as follows. First, coherence is shown to be a measure of "predictability" and of spatial coupling in dynamical systems. Coherence is compared with conventionally used correlation, and the causes of its spatial decay are analytically illustrated. A coupling measure for quadratically nonlinear systems is formulated (which

can be extended to higher-order, e.g., cubic and quartic, systems). Following this, experimental measurements of coherence and correlation are used to analyze spatiotemporal dynamics in an open flow (viz., a circular jet), and possible physical mechanisms for the observed coherence decay are analyzed.

*Coupling in linear and nonlinear systems*. By spatial coupling we mean that the dynamics at one location can be predicted using measurements at another. This implies the existence of an underlying predictive function or a dynamical system (perhaps low dimensional).

*Linear Model.* For a linear system, the *transfer function* H(f) is used for prediction (Figure C.1). Here, we employ standard signal processing formulations with one important distinction: the input x(t) and output y(t) signals are from *spatially separated* probes. It is indeed this distinction which permits the interpretation of coherence as a measure of the spatiotemporal dynamics.

In an ideal (i.e., single-input, noise-free, linear) system with known H(f) and input, one can predict the output signal, Fourier transform and power spectrum respectively:

$$y(t) = h(t) * x(t), \tag{C.1a}$$

$$Y(f) = H(f)\, X(f), \tag{C.1b}$$

and

$$G_{yy}(f) = |H(f)|^2\, G_{xx}(f), \tag{.C1c}$$

where h(t) is the impulse response, $H(f) = G_{xy}(f)/G_{xx}(f)$, $G_{xy}$ is the cross-spectrum, and

$G_{xx}$ and $G_{yy}$ are the autospectra. Inserting H(f) into (C1c) and normalizing by $G_{yy}(f)$, one obtains the coherence spectrum (called "coherence" or "ordinary coherence"):

$$\gamma^2_{xy}(f) = \frac{|G_{xy}(f)|^2}{G_{xx}(f)\, G_{yy}(f)} \equiv 1. \qquad \text{(C.2)}$$

Given H(f), an ideal system is completely predictable and hence has unity coherence.

*Coherence and Predicted Energy*. In experiments, spectral quantities are estimated (denoted by "^") from ensemble averages. The *estimated* $\hat{G}_{xx}$ and $\hat{G}_{xy}$ can be used to *predict* the output spectrum ("~" indicates prediction): $\tilde{G}_{yy} = |\hat{H}|^2 \hat{G}_{xx} = \frac{|\hat{G}_{xy}|^2}{\hat{G}_{xx}}$, yielding the *coherence estimator*:

$$\hat{\gamma}^2_{xy} = \frac{\tilde{G}_{yy}}{\hat{G}_{yy}} = \frac{|\hat{G}_{xy}|^2}{\hat{G}_{xx}\, \hat{G}_{yy}} . \qquad \text{(C.3)}$$

Thus, the estimated coherence is a frequency-by-frequency ratio of the predicted to the measured output energies. Moreover, since $\tilde{G}_{yy}$ is evaluated from $\hat{G}_{xx}$ measurements a *different* location, coherence is a measure of *spatial coupling*. High coherence (≈ 1) indicates strong coupling, while its difference from unity indicates the fraction of unpredictable output energy, i.e., the loss of coupling. Further, since $|\hat{H}|^2 = \hat{\gamma}^2_{xy}\ \hat{G}_{yy} / \hat{G}_{xx}$, time series prediction also depends on coherence. Note that the estimation errors can be arbitrarily reduced given sufficiently large datasets (Bendat & Piersol 1986) and need not contribute significantly to coherence decay. (Henceforth, we will drop the caret

" ^ " since all spectra discussed are estimated.)

*Comparison of Coherence and Correlation Function.* Correlation length $\xi$ was used (Cross & Hohenberg 1990) to categorize dynamical systems as "large" (*viz.*, spatiotemporal) or "small" (*viz.*, spatially coupled) when $\xi/\lambda \sim 1$ or $\xi/\lambda >> 1$ respectively (where $\lambda$ is some dynamically significant length scale). However, in spatially inhomogeneous systems (e.g., free shear flows), spatial growth rates and phase speeds of the various instability modes differ, making correlation inadequate for coupling measurements. Consider the simple example of a completely predictable one-dimensional spatiotemporal system with input u(x,t) and output v(x,t):

$$u(0,t) = a \cos \omega_1 t + b \cos \omega_2 t, \text{ and } v(x,t) = c(x) \cos \omega_1 t + d(x) \cos \omega_2 t. \qquad (C.4)$$

Since u is at the origin x = 0 and u = v for zero spatial separation, the coefficients a = c(0) and b = d(0). Using any input u, and H(f) derived from (C4), v can be predicted exactly. Applying (C3) to (C4) yields $\gamma^2_{uv}(\omega_1) = \frac{(ac)^2}{a^2 c^2} = 1$ and $\gamma^2_{uv}(\omega_2) = \frac{(bd)^2}{b^2 d^2} = 1$, irrespective of the spatial variation of c and d. Thus, coherence is unity at the relevant frequencies and, as expected, the spatial coupling extends as far as the evolution in (C4) is obeyed (i.e., to infinity, in principle). Note that even correlation will correctly indicate spatial coupling in a multimode system provided modal amplitude ratios and phase differences do not vary in space (not the general case).

Using the cross-correlation coefficient defined as $\rho_{uv}(\tau) = [R_{uv}(\tau)/\sigma_u \sigma_v]$ (where $R_{uv}(\tau)$ is the cross correlation, $\sigma$ are the standard deviations, and signals u and v have ze-

ro mean), we obtain: $\rho_{uv_{max}} = \frac{R_{uv}(0)}{\sigma_u \sigma_v} = \frac{(ac+bd)}{[(a^2+b^2)(c^2+d^2)]^{1/2}} \leq 1$. Thus, $\rho_{uv_{max}} \equiv 1$ only if c/a = d/b, i.e., each frequency is (spatially) amplified identically. Note that, although $G_{uv}(f) = 2 \int_{-\infty}^{\infty} R_{uv}(\tau)\, e^{-j\, 2\pi f \tau}\, d\tau$, (i.e., the cross-correlation and the cross-spectrum are a Fourier pair), additional information is obtained from $\gamma^2_{uv}(f)$ due to its normalization by spectra (which differ at each frequency) rather than by constants as in $\rho_{uv}(\tau)$. A frequently used measure of spatial coupling – correlation length – is based on correlation, which is expected to decay as $\rho_{uv_{max}}(x) \sim e^{-x/\xi}$; i.e., over a distance x=ξ, ρ decays to $e^{-1}$ (≈ 37%) of its original value. At what correlation value, and, hence, what value of x/ξ, can two signals still be considered coupled? This being an unresolved issue, comparisons of coherence is restricted to correlations only.

As a simple example, consider the amplitude evolution of c(x) and d(x) to be exponential and omit spatially dependent phases. Such exponentially growing amplitudes are commonly found in the initial (instability-dominated) regions of shear flows such as mixing layers and jets (Narayanan & Hussain 1996). Consider coherence for spatially growing waves (Figure C.1) with a/b = 10 and c/d = 0.5 at x/λ = 2, typical of amplitude ratios (of a fundamental frequency and its subharmonic) observed in free shear flows (Husain & Hussain 1995). Again, coherences at both frequencies remain unity throughout the domain, while $\rho_{uv_{max}}$ rapidly decays, with ξ/λ ≈ 1, suggesting a limited spatial extent of coupling even when the dynamics are completely predictable.

Downstream (relative) shift among frequency component waves of different fre-

quencies in dispersive systems also causes low correlation at all time delays. However, since coherence only depends on phase variations (from one realization to another) at each frequency, it can accurately detect spatial coupling in such systems.

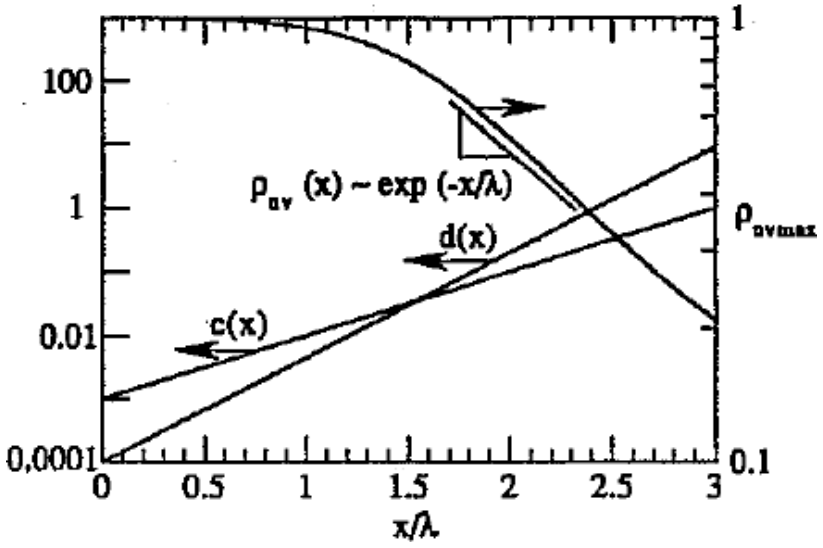


Figure C.1 Correlation decay for a fully coupled spatially developing system.

*Coherence Decay.* Coherence can be less than unity due to measurement noise, unmeasured uncorrelated additional inputs, or nonlinearity (Bendat & Piersol 1986); since measurement noise can be minimized, its effects will not be considered here. Expanding (C3) in terms of ensemble-averaged Fourier spectra and substituting amplitude and phase decompositions of the form $X_k = x_k \exp(i\phi_{x_k})$, $Y_k = y_k \exp(i\phi_{y_k})$ and $\phi_k = \phi_{y_k} - \phi_{x_k}$, we can isolate the effects of amplitude and phase jitter on coherence. (By "jitter" we mean random variations of a dynamical variable.)

To study amplitude jitter, we fix phase difference $\phi_k$ in all realizations and obtain

$$\gamma^2_{xy} = \frac{< x_k\ y_k >^2}{< x^2_k > < y^2_k >} \leq 1, \qquad \text{(C.5)}$$

where the ensemble-averages are defined by $< u_k > = \frac{1}{N} \sum_{k=1}^{N} u_k$, k is the realization number and N is the ensemble size. This becomes an equality if $y_k = r\ x_k$ for all k; i.e., the ratio r of the output to input amplitudes can vary with frequency but must be fixed for all realizations (in contrast to the requirement that r = constant *for all frequencies* for $\rho_{uv_{max}} \equiv 1$). As a simple example, assuming that $y_k = r_k\ x_k$ and $r_k$ is distributed uniformly on the interval [0,1], uncorrelated with $x_k$, with mean $\mu_r$ and variance $\sigma_r^2$, we get $\gamma^2_{xy} = \mu_r^2 / (\mu_r^2 + \sigma_r^2)$, which decays with increasing $\sigma_r^2$.

To examine phase jitter, we hold amplitudes $x_k$ and $y_k$ fixed and obtain

$$\gamma^2_{xy} = |< e^{i\phi_k} >|^2 = |< \cos\phi_k + i \sin\phi_k >|^2 \leq 1. \qquad \text{(C.6)}$$

Note that it is the *difference* $\phi_k$, not the individual phases $\phi_{y_k}$ or $\phi_{x_k}$, which affects coherence. Coherence is unity only if $\phi_k$ is constant in all realizations. Consider $\phi_k = \phi + s\ \theta_k$, with constant $\phi$ and a random variable $\theta_k$ distributed uniformly on the interval $[0, 2\pi]$. Here, $\gamma^2_{xy} = \sin^2 \pi s / (\pi s)^2$, which decays to zero as $s \rightarrow 1$.

*Nonlinear Model*. For nonlinear systems, ordinary coherence $\gamma^2_{xy}$ may fall below unity, but this does not necessarily imply that the dynamics are less predictable. Coupling can be measured using a nonlinear system model (Figure C.2) and its coherences (Ritz &

Powers 1986). The procedure outlined below is applicable to systems of arbitrary order; after constructing the system model, sufficient moments and inner products can be taken to extract transfer functions and/or coherence. However, the mathematical complexity and computational expense grow drastically with increasing order. The discussions will be restricted to second-order (i.e., to triad interactions); higher-order computations are justified only if (i) knowledge about the dynamics indicates their presence or (ii) second-order results are substantially different from linear coherence.

The quadratic system model is

$$Y(f) = L(f)\,X(f) + \sum_{f_1 \geq f_2} Q(f_1,f_2)\,X(f_1)\,X(f_2) \;\; ; \;\; f_1 + f_2 = f. \qquad (C.7)$$

It is represented in terms of the linear and quadratic transfer functions L(f) and $Q(f_1, f_2)$ respectively; the first term on the right side represents linear energy transfer to the output at f, and the second term represents the cumulative contribution of all triad interactions to the output at f. Due to symmetry with respect to $f_1$ and $f_2$, the summation in (C7) is restricted to $f_1 \geq f_2$.

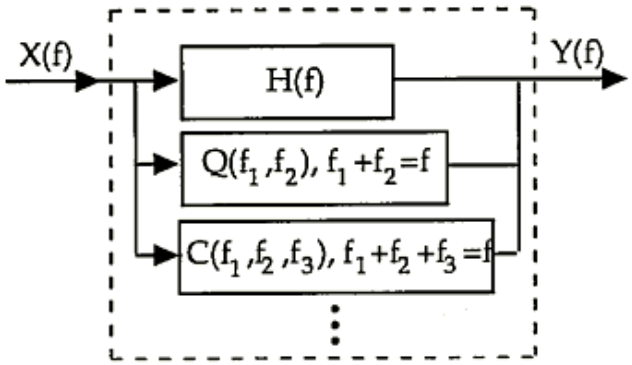


Figure C.2 Schematic of nonlinear system model.

Multiplying (C7) by its complex conjugate, ensemble-averaging and then normalizing by $G_{yy}(f)$ yields the *total coherence*:

$$\gamma^2_T(f) = \frac{1}{G_{yy}(f)} \left[ |L(f)|^2 G_{xx}(f) + \sum_{f_1 \geq f_2} |Q(f_1,f_2)|^2 D(f_1,f_2) + 2 \text{ Re} \left\{ L(f) \sum_{f_1 \geq f_2} Q^*(f_1,f_2) A^*(f_1,f_2) \right\} \right] \leq 1, \quad (C.8)$$

where $A(f_1,f_2) = \langle X_k(f_1) X_k(f_2) X^*_k(f) \rangle$ (the auto-bispectrum) and $D(f_1,f_2) = \langle |X_k(f_1) X_k(f_2)|^2 \rangle$; this assumes negligible fourth-order moments $\langle X_k(f_1) X_k(f_2) X_k^*(f_1') X_k^*(f_2') \rangle$ (with $f_1 + f_2 = f_1' + f_2' = f$), unless $f_1 = f_1'$ (Ritz & Powers 1986). Estimation errors are neglected for large ensembles.

Although each term in (C8) is subject to (possibly misleading) physical interpretation, to measure spatial coupling we need only $\gamma^2_T(f)$. As in the linear system, total coherence indicates the predictability of output energy using measured input energy; when the input and output measurements are spatially separated, *total coherence is a measure of spatial coupling*.

Taking moments of (C7) with respect to $X^*(f)$ and $X^*(f_1') X^*(f_2')$, and ensemble-averaging gives two coupled equations for L and Q respectively (Ritz & Powers 1986), which can be substituted into (C8) to obtain the following new *explicit* formula for total coherence:

$$\gamma^2_T(f) = \gamma^2(f) \frac{\left| 1 - \sum_{f_1 \geq f_2} \eta(f_1,f_2) \right|^2}{1 - \sum_{f_1 \geq f_2} \alpha^2(f_1,f_2)} + \sum_{f_1 \geq f_2} \beta^2(f_1,f_2) \quad , \qquad (C.9)$$

where $\gamma^2(f)$ is the ordinary coherence, $\alpha^2(f_1,f_2) = \frac{|A(f_1,f_2)|^2}{D(f_1,f_2)\, G_{xx}(f)}$ (the auto-bicoherence),

$\eta(f_1,f_2) = \frac{C^*(f_1,f_2)\ A(f_1,f_2)}{D(f_1,f_2)\, G_{xy}(f)}$, $C(f_1,f_2) = \langle X_k(f_1)\ X_k(f_2)\ Y^*_k(f) \rangle$ (the cross-bispectrum), and $\beta^2(f_1,f_2) = \frac{|C(f_1,f_2)|^2}{D(f_1,f_2)\, G_{yy}(f)}$ is the cross-bicoherence. Note that this new result does not require computationally intensive L or Q calculations to evaluate $\gamma^2_T(f)$ (Ritz & Powers 1986, Kim & Powers 1988). Further, if $A(f_1,f_2) \equiv 0$, $\gamma^2_T(f)$ reduces to the sum of $\gamma^2(f)$ and $\Sigma\, \beta^2(f_1,f_2)$ (simplifying computations considerably). In fact, even in the presence of substantial $A(f_1,f_2)$, further (heuristic) analyses suggest that a sufficient condition for high $\gamma^2_T(f)$ is high values of both $\gamma^2(f)$ and $\Sigma\, \beta^2(f_1,f_2)$.

For negligible auto-bicoherence, analytical results for total coherence decay can be obtained, analogous to the linear case: fixed amplitude ratios and phase differences give high values of total coherence, and amplitude/phase jitter cause its decay. Similar results are expected when auto-bicoherence is high, but analysis is difficult; this was verified by examining some synthetically generated examples as shown below.

This completes the formulation of a spatial coupling measure (viz., $\gamma^2_T$) for a quad-

ratically nonlinear system. In contrast to prior methods, we provide an explicit and easily calculable formula for $\gamma^2_T$.

The causes of coherence decay are difficult to interpret when auto-bicoherence is high. To investigate this, we used synthetic input and output signals (e.g., from spatially separated probes) of the following form.

$$u(t)|_{x=x1} = a_k\cos(\omega_1 t + \phi_{ak}) + b_k\cos(\omega_2 t + \phi_{bk}) + c_k\cos(\omega t + \phi_{ck}) + d_k\cos(\omega t + \phi_{dk}) + n_u(t)$$

$$v(t)|_{x=x2} = e_k\cos(\omega t + \phi_{ek}) + f_k\cos(\omega t + \phi_{fk}) + n_v(t),$$

where $\omega = 2\pi f$, and $n_u(t)$ and $n_v(t)$ are low-amplitude band-limited white noise (at least 50 dB below $\omega_1$, $\omega_2$, and $\omega$ peaks). For simplicity, the two signals are provided significant energy only at three frequencies.

The key effects we expect to capture in these signals are (i) linear energy transfer at $\omega$ between the $d_k$ and $f_k$ terms, (ii) auto-bicoherence at $\omega_1 + \omega_2 = \omega$ using the $a_k$, $b_k$ and $c_k$ terms, and (iii) quadratic energy transfer to w using the $a_k$, $b_k$ and $e_k$ terms. To ensure high auto-bicoherence, the amplitude ratio akbk/ck and the phase difference $\phi_{ck} - \phi_{ak} - \phi_{bk}$ are kept constant; $\alpha^2(f_1,f_2) \approx 0.99$ for all cases. Pseudo-random number generators produced amplitudes and phases with uniform distribution in the ranges [0,1] and [0,2$\pi$], respectively. At least 200 records of 1024 samples were averaged with a 2 Hz frequency resolution.

We consider three cases: full coupling, amplitude jitter, and phase jitter. For full coupling (see case I, Table I), we eliminate jitter by holding phase differences ($\phi_{fk} - \phi_{dk}$ and

$\phi_{ek} - \phi_{ak} - \phi_{bk}$) and amplitude ratios constant ($d_k/f_k$ and $a_k b_k/e_k$) for each realization. As expected, $\gamma^2_T(f) \approx 1$, indicating strong coupling and hence nearly complete predictability of v(t). To investigate amplitude jitter (case II, Table I), we hold the phase differences constant, while the amplitude ratios have independent, random variations on the interval [0,1]. The drop in $\gamma^2_T(f)$ indicates a loss of coupling. For phase jitter (case III, Table I), we hold amplitude ratios constant, and qk, hence, the phase differences $\phi_k = s\ \theta_k$, are allowed random variations in the range $[0,2\pi]$, where s = 0.6. (As shown before, s = 1 yields 0 for all coherences.) The low $\gamma^2_T(f)$ indicates coupling decay, hence, poor predictability of v(t). For high $\gamma^2_T(f)$, notice that both $\gamma^2(f)$ and $\beta^2(f_1,f_2)$ are high, while low $\gamma^2_T(f)$ is associated with low $\gamma^2(f)$ and $\beta^2(f_1,f_2)$.

Table I. Effects of amplitude and phase jitter on coherences.

| Case No. | Case type | $\gamma^2_T(f)$ | $\gamma^2(f)$ | $\beta^2(f_1,f_2)$ |
|---|---|---|---|---|
| I | Fully coupled | 0.999 | 0.999 | 0.999 |
| II | Amplitude jitter | 0.715 | 0.460 | 0.389 |
| III | Phase jitter | 0.386 | 0.322 | 0.285 |

**C.2 Coherence Computations**

The $\gamma^2_T(f)$ estimation using (C9) is made quite difficult by two problems: noise and spectral leakage. The summations in (C9) contain many terms (up to 512 here), depending on the frequency resolution. Noise and random estimation errors at all frequencies

cause residual values whose accumulation yield poor estimates of $\gamma^2_T(f)$. Since the random error for spectral estimation scales as $N^{-1/2}$ (where N is the ensemble size), the cumulative error can be significant even when N is large (e.g., $10^2 - 10^4$); to minimize these errors, we used a threshold of $(2/N)^{1/2}$ on all spectra/bispectra. Data windowing causes leakage of coherent energy into frequencies neighboring significant coherence/bicoherence peaks, causing summations including these frequencies to be erroneously high. After testing different windows, we found rectangular windows (suggested by E.J. Powers, private communication) to have minimal coherent sideband leakage.

Auto-bicoherence was computed using 200 realizations of a synthetic signal with significant energy at a single triad, $f_1 + f_2 = f$, and low-amplitude random noise. The auto-bicoherence sum $S = \Sigma_{f1 \geq f2} \alpha^2(f_1,f_2)$ is ideally equal to unity. This sum was evaluated after applying rectangular (R) and Hanning (H) windows, yielding $S_H = 4.21$ and $S_R = 2.04$ [with $\alpha^2(f_1,f_2)_H \sim 1$ at two frequencies around the true peak]. After applying thresholds, $S_H = 3.00$ and $S_R = 1.00$. Although the noise contribution is reduced, $S_H$ is clearly still in error (due to spectral leakage).

In processing the experimental data, it was found that using a relatively small number of realizations (e.g., 100 records) for spectral averaging resulted in $\gamma^2_T(f)$ exceeding 1 (its theoretical upper bound). In fact, even after the number of realizations was increased to 400, such excursions were not completely eliminated (evident in results from the jet experiments shown later). These errors can be attributed to noise. In practice, it may not

always be possible to select a threshold which eliminates all noise while preserving all signal contributions. In general, increasing the number of realizations should diminish these excursions. For the stable double pairing flow state at x/D ≅ 3.75, calculations yielded $\gamma^2_T(f/2) \approx 1.14$ using 100 realizations, but $\gamma^2_T(f/2) \approx 1.07$ using 400 realizations. Also for the stable double pairing state, at x/D ≅ 3.25, $\gamma^2_T(f/4) \approx 1.14$ using 100 realizations, but $\gamma^2_T(f/4) \approx 0.992$ using 400 realizations.

### C.3 Physical Mechanisms of Coherence Decay in Free Shear Flows

As addressed before, coherence decay (indicative of coupling loss) can result from amplitude and/or phase jitter. However, the physical mechanism for such jitter may differ among dynamical systems. In the following, some such mechanisms are discussed in the context of jet flows; similar arguments may apply to other open shear flow as well, such as wakes and mixing layers.

*Amplitude jitter*. An example of how amplitude jitter may occur in a jet is illustrated in Figure C.3, where the spatial development of the amplitude of an instability mode (viz., Kelvin-Helmholtz) is sketched for two realizations from an ensemble of different initial amplitudes; the saturation amplitudes of these modes are known to relatively insensitive to the initial amplitudes (Husain & Hussain 1995). The input amplitude $u_k$ at f is measured at the origin $x_o$. In the first case, the output fundamental spectral amplitude $v_k$ is measured at $x_l$ in the linear range; hence, the ordinary coherence $\gamma^2_{uv} = 1$ (assuming constant phase shift at f between $x_o$ and $x_l$) since the amplitude ratio $v_k/u_k$ is constant is each

realization [see (C5)]. In the second case, the output spectrum is measured at $x_{nl}$ in the nonlinear range, where u has reached its saturated value $u_{sat}$. Here, the amplitude ratio $u_{sat}/u_k$ varies from one realization to another, and $\gamma^2_{uv} < 1$. Similar effects may occur for the subharmonic and the quarterharmonic as well.

*Phase jitter*. Coherence can be affected by variations of the phase *difference* (between individual frequency components) in several ways; here, two such effects are illustrated by examining the spatial development of a resonant subharmonic wave (Figure C.4) in a jet flow. When the fundamental wave (not shown) reaches a critical amplitude at $x_o$, it resonates nonlinearly with and reinforces the subharmonic, thus modifying the subharmonic spatial growth rate (depending on $\theta$, the phase difference between the two waves) (Husain & Hussain 1995). First, consider the coherence at f/2 between the signals at $x_o$ and $x_1$: phase jitter will be absent if the subharmonic phase speed is independent of $\theta$. Nevertheless, $\theta$ variations (due to detuned feedback) result in amplitude jitter at $x_1$ and, hence, coherence decay. In contrast, there is no amplitude jitter between $x_o$ and $x_2$, but the phase after saturation (i.e., at $x_2$) may not be linearly related to the phase prior to the onset of resonance (i.e., at $x_o$). This phase jitter will also result in coherence loss. Phase jitter may also be caused by the development of three dimensionality. The three-dimensional effect sketched in Figure C.5 (showing two realizations of advecting rectilinear vortices) is analogous to azimuthal instabilities of ring vortices, but is more easily understood in a planar configuration. In both realizations, the trailing vortex is rectilinear (or nearly so), but a spanwise instability (of fixed wavenumber but arbitrary phase) has grown on the leading vortex as it moved downstream. Coherence at the vortex passage

frequency will fall below unity since the phase shift $\phi_k$ between u(t) and v(t) varies from one realization to the next. Not that, in this case, the phase jitter is due to an unknown input (viz., the disturbances which trigger the three-dimensionality). If the spanwise disturbance is present on the upstream vortex, even at low amplitudes, additional spawise-separated probes at the upstream location might provide sufficient information to make the downstream distortion predictable (using multi and partial coherences, Bendat & Piersol 1986).

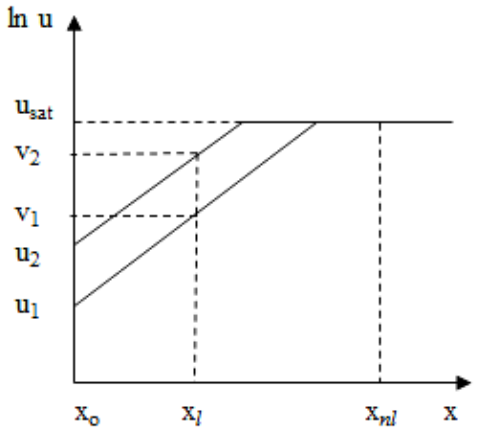


Figure C.3 Spatial development of an instability amplitude for a pair of realizations, illustrating an amplitude jitter mechanism in free shear flows.

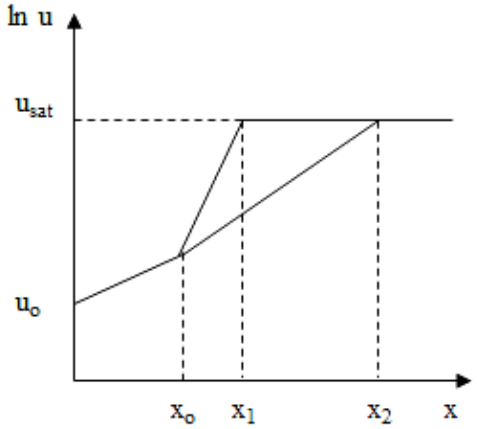


Figure C.4 Spatial development of the amplitude of a resonant subharmonic wave for different phases $\theta_i$, illustrating mechanisms for amplitude and phase jitter in free shear flows.

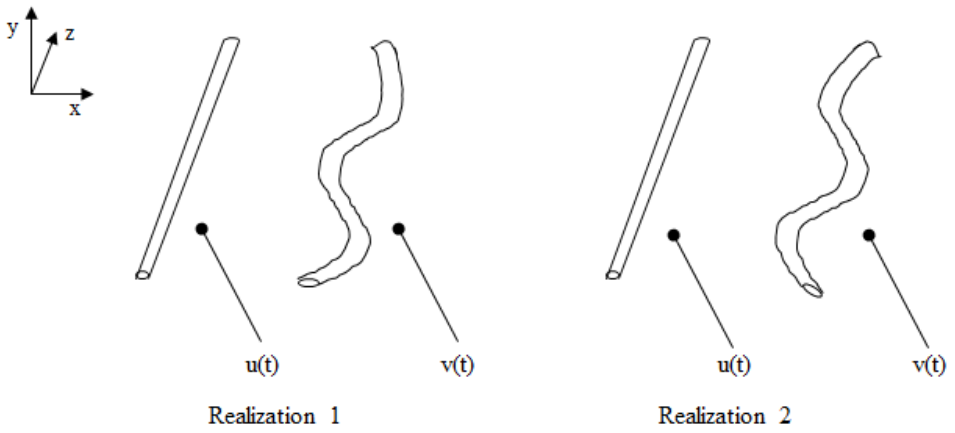


Figure C.5 Illustration of phase jitter due to random three-dimensional disturbances on rectilinear vortices in a place free shear flow; the downstream phase at the vortex passage frequency [in v(t)] is different in the two realizations.

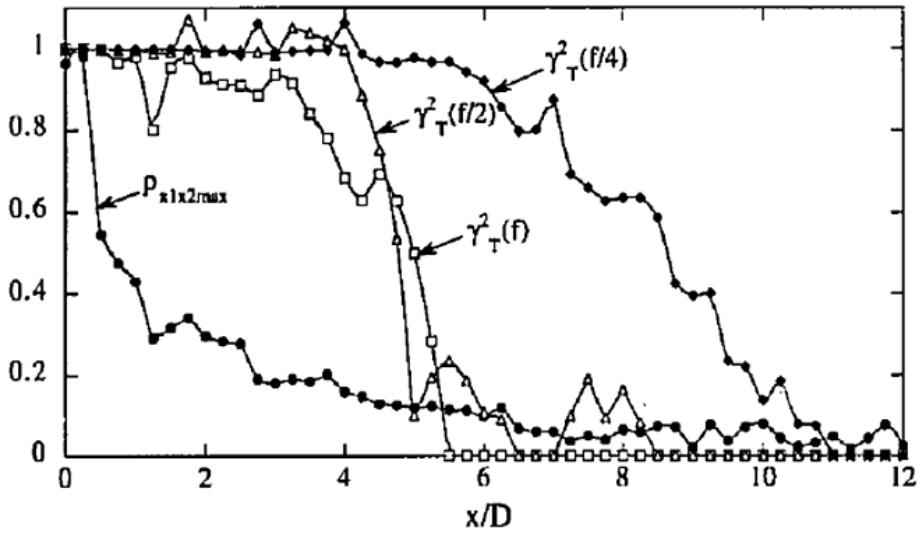


Figure C.6 Spatial evolution of total coherence $\gamma^2(f)$ and peak correlation coefficient $\rho_{x1x2max}$ for SDP; high $\gamma^2(f)$ at all f indicates strong spatial coupling for x/D < 4.

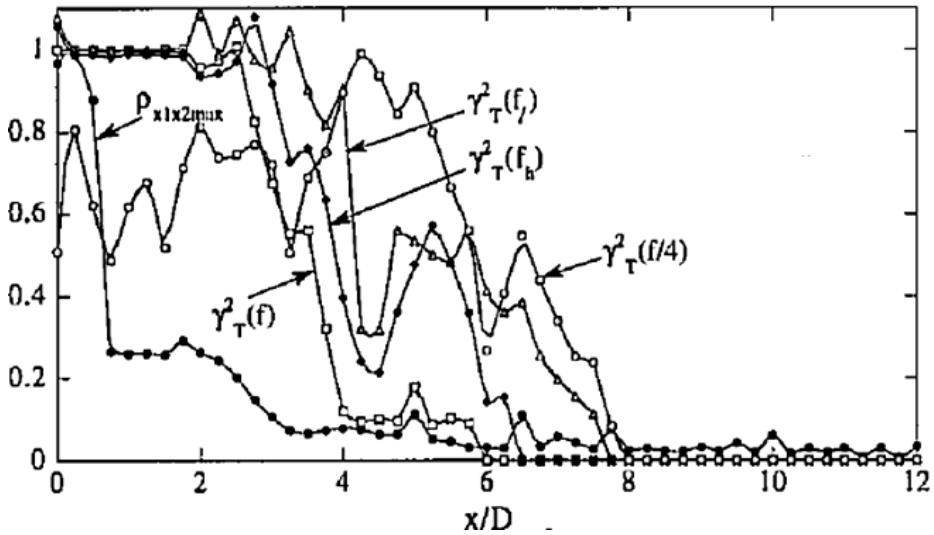


Figure C.7 Spatial evolution of total coherence $\gamma^2(f)$ and peak correlation coefficient $\rho_{x1x2max}$ for QCA; strong coupling is evident (from high $\gamma^2(f)$) for $x/D < 4$.

**C.4 Measurements of Spatial Coupling in the Jet**

We now present cross-correlation and total coherence for a periodic flow state stable double pairing SDP (at $a_f \cong 2.4\%$, $St_D \cong 1.2$) and a chaotic flow state quarterharmonic chaotic attractor QCA (at $a_f \cong 1.4\%$, $St_D \cong 1.2$), measured using hot-wire probes; data-acquisition was performed using a 12-bit A/D converter on a Masscomp MC6650 computer. The periodic and chaotic states were described in Chapter 3 and Appendix A. The reference probe was positioned near the jet exit ($x/D \cong 0$) and displaced radially by 0.2 D, with long prongs to keep the probe body out of the jet core minimizing probe interference and wakes (Hussain & Zaman 1978); a second probe (aligned with the jet centerline) was traversed downstream at intervals of $\Delta x/D \cong 0.25$.

*Cross-correlation.* The peak cross-correlation coefficient $\rho_{x_1 x_2 max}$ for both attractors decay rapidly (Figures C.6 and C.7), falling below 0.5 by $x/D = 1$. This decay is primarily

due to rapid spatial variation of the ratio of the fundamental and the subharmonic amplitudes (as argued in the previous section). Correlation diminishes well before the minimum expected coupling distance of x/D ≅ 2.5 (i.e., the second pairing location).

*Total Coherence.* To analyze total coherence $\gamma^2_T(f)$ for the dynamically significant frequencies noted in the power spectra of SDP and QCA, 400 records of 1024 samples were averaged with a frequency resolution of 2 Hz. Since the sources of f/2 and f/4 at the jet exit are presumably feedback from pairings, it is reasonable to expect that spatial coupling will extend at least as far as the pairing locations (and perhaps beyond, unless there are significant effects from new instabilities whose origins were not measured).

*SDP*. Total coherences at f, f/2 and f/4 remain high (≤ 0.8) as far as x/D ≅ 4, 5 and 7 respectively (Figure C.6), indicating *spatial coupling* well beyond the second pairing location. As previously noted, this is not surprising provided new unmeasured events do not occur, i.e., events whose origins are under resolved or undetected at the first location (e.g., three-dimensional secondary instabilities). Although theoretically bound by unity, $\gamma^2_T(f/2)$ and $\gamma^2_T(f/4)$ slightly exceed unity at a few locations (e.g., at x/D = 4), apparently because of insufficient spectral averaging. The most significant quadratic interactions were found to be between the fundamental and the subharmonic (i.e., f + (-f/2) = f/2) and between the subharmonic and the quarterharmonic (i.e., f/2 + (- f/4) = f/4), culminating in the first and second vortex pairings respectively.

*QCA.* Total coherences at f, the lower sideband $f_l$, and the higher sideband $f_h$ frequencies (see Figure C.7) remain above 0.8 as far as 3 ≤ x/D ≤ 5, the region where chaotic second

pairing is usually completed (Broze & Hussain 1996). Again, there are slight excursions above unity in the values of $\gamma^2_T(f_l)$ and $\gamma^2_T(f_h)$. The dynamically significant quadratic interactions here are those of (i) f and $f_h$ (i.e., $f - f_h = f_l$), (ii) f and $f_l$ (i.e., $f - f_l = f_h$), and (iii) $f_l$ and $f_h$ with frequencies in the broadband surrounding f/4 (e.g., $f_l - f/4 = f/4 - \Delta f$ or $f_h - f/4 = f/4 + \Delta f$); owing to the broadband surrounding f/4, a coarser frequency resolution of 9 Hz was chosen around that frequency for computations. High $\gamma^2_T$ at all significant frequencies up to $x/D \cong 4$ indicate strong spatial coupling, even as the flow behaves chaotically.

High values of $\gamma^2_T$ over a large region (at least 4-6 jet diameters) indicate that the transitional jet displays *temporal*, rather than spatiotemporal, dynamics. Since spatial coupling implies the predictability of dynamics at one location from observables at another, single-point measurements suffice to describe the low-dimensional dynamics in the jet near field. In the jet, the physical mechanism for coupling was verified to be "feedback" from characteristic events, specifically, vortex pairings, caused by upstream propagating pressure perturbations. Evidence of such coupling justifies the use of single-/two-point, centerline, longitudinal velocity signals in this study. The rapid drop of $\gamma^2_T$ downstream (past the end of the time-averaged jet potential core end) is evidence of spatiotemporal dynamics. As addressed before, coherence decay (indicative of coupling loss) can result from amplitude and/or phase "jitter."

In summary, total coherence $\gamma^2_T(f)$ is shown to accurately identify coupling in spatio-temporal dynamical systems, particularly inhomogeneous ones. Coherence is applicable to homogeneous systems as well; when dynamics are dominated by a single frequency, coherence and correlation results are identical; with multiple modes, coherence can identify frequencies and interactions responsible for coupling decay. Since coherence can be interpreted as the predictable energy fraction, this appears to be the first method for measuring predictability in multimode spatiotemporal systems. Consequently, this result is an important step in addressing the challenging problem of modeling and controlling technologically relevant spatiotemporal (*open*) flows.

To demonstrate the practical feasibility of coherence, as aspatial coupling measure, total coherence was measured in a circular jet (as shown in previous sections). The results indicated large spatially coupled regions (extending from 4 to 7 jet diameters), implying high predictability of dynamics (using single-point measurements) in these flow regions. On the other hand, misleading estimates of spatial coupling can be inferred from correlation-based measures.

Diminished coherence comes from additional unmeasured inputs (or interactions), higher-order nonlinearity or measurement noise; these manifest as jitter in amplitudes and phases of the measured dynamical variable. Mechanisms for such jitter depend on the physical system under consideration, e.g., the onset of secondary instabilities in Rayleigh-Bénard convection (Ahlers et al. 1985), transverse instabilities in film flows (Liu et al. 1992), three-dimensionality in open shear flows (Lasheras & Choi 1988), higher-order nonlinearities, or transition to turbulence. In the first three cases, the apparent loss of pre-

dictability can, in principle, be recovered by judicious placement of additional sensors; increasing the order of the system model will capture higher-order nonlinearities. In deterministic systems, the only "true" sources of unpredictability (given an adequate system model) are unmeasured or under resolved inputs, specifically, small fluctuations (e.g., changes in initial conditions) amplified by instabilities and/or chaos.

# APPENDIX D

## LEAST MEAN SQUARES ALGORITHM FOR ADAPTIVE FILTERING

We compute the adaptive filter weights to approximate the relationship between a pair of upstream and downstream jet signals (see Chapter 3) using a least-mean-square algorithm (Widrow & Stearns 1985). These weights were then used to evaluate upstream control perturbations associated with desirable downstream dynamics, *i.e.*, as an "inverse" model. The simplest gradient estimate for the $k^{th}$ iteration of this steepest descent type algorithm is: $W_{k+1} = W_k + 2\ \mu\ \varepsilon_k\ X_k$, where $\mu$ is the gain constant that regulates the speed and stability of the adaptation, $\varepsilon_k$ is the error ($\varepsilon_k = d_k - X^T_k\ W_k$), $W_k$ is the weight vector with elements $\{w_1, w_2, .... , w_{Nw}\}$, $X_k$ is the input vector, $d_k$ is the actual (output) response for testing the adaptive filter prediction, and $N_w$ is the number of weights. The two major criteria to evaluate the reliability of an adaptive filter are: (i) convergence of the envelope of $\varepsilon_k$ (within ±10% of peak-to-peak signal amplitude), and (ii) convergence of the rms of all the weights $(\Sigma\ w_i^2)_k$. We also inspect the adaptive filter prediction (expected to be periodic for each UPO) to ensure that no major changes occur in its envelope. To continue refining the approximated weights, the input/output pair of signals are provided to the algorithm even after achieving acceptable convergence of the weights. We also compare (not shown) an actual upstream signal (from a second set of two-point data) with that predicted using the adaptive filter weights (computed using the originally sampled two-point QCA data) to verify reliable adaptive filter predictions.